The Austenite $\rightleftharpoons$ Ferrite Transformations in Low-Alloy Steels

by

NIGEL CAREY LAW

DARWIN COLLEGE

CAMBRIDGE

A dissertation submitted for the Degree of Doctor of Philosophy in the University of Cambridge, November, 1977

PREFACE

This dissertation, which is submitted for the degree of Doctor of Philosophy in the University of Cambridge, describes work carried out in the Department of Metallurgy and Materials Science under the supervision of Dr D. V. Edmonds between October 1974 and September 1977. Except where acknowledgement and reference to previous work has been made, the work described is original and has been done without collaboration. The dissertation does not exceed 60,000 words and no part has been, or is being, submitted for a degree, diploma or any other qualification at any other University.

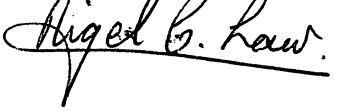

Nigel C. Law

ACKNOWLEDGEMENTS

I would like to thank Dr D. V. Edmonds for his continued interest and encouragement during the course of this project. I am also grateful to Professor R. W. K. Honeycombe for the provision of laboratory facilities and to the other members of the Alloy Steels Research Group for their companionship and for many valuable discussions. In particular, thanks are due to Dr P. R. Howell and to the Abbott for their unfailing stimulus throughout the course of the work.

I am also indebted to the Assistant Staff, in particular, Mr J. Leader and Mr D. Ackland for their invaluable practical help.

My thanks are also due to Denise for her careful typing of this dissertation and to Anne for help with the photographs.

To My Parents

SUMMARY

The dissertation describes a structural investigation of the austenite⇄ferrite transformations in alloys based upon Fe-IV-0.2C, and includes a detailed examination of the martensite structure in this alloy. The conditions under which fine grained ferritic structures may be produced by heat treatment, and an investigation into the mechanical properties of these fine grained steels is also reported.

Electron microscopy of the martensite structures revealed thin films of interlath and interpacket retained austenite. These films were shown to obey either a Kurdjumov-Sachs or a Nishiyama-Wasserman orientation relationship with the martensite laths. The laths themselves occupied a {110} martensite habit plane, and it was found that groups of laths within a martensite packet were separated by small angle boundaries, while the groups themselves were often twin related.

The austenite to ferrite reaction was investigated in the range 650°C-800°C, and it was found that the ferrite nuclei were Kurdjumov-Sachs related to one or other of the austenite grains at the prior austenite boundary. At low temperatures growth was predominantly into the austenite grain to which the ferrite was related and was accompanied by the deposition of aligned vanadium carbide. The vanadium carbide was shown to be related to the ferrite by the Baker-Nutting orientation relationship and the aligned rows of precipitates were shown to occupy a {110} ferrite

habit plane.

The ferrite morphology was of an angular nature and the aligned precipitates were found to be parallel to the advancing ferrite interface. Work on a chromium-vanadium steel showed that this interface was stepped and it was concluded that growth occurred by a ledge mechanism. The single habit plane selected by the precipitates was shown to occur as a result of the three-phase orientation relationships obeyed by the ferrite, austenite and vanadium carbide at the interphase boundary.

At higher transformation temperatures growth became more predominant into the austenite grain to which the ferrite was not crystallographically related and was found to be accompanied by precipitation of fibrous vanadium carbide. It was concluded that the fibrous precipitation was associated with an incoherent interface.

The formation of austenite from ferritic, bainitic and martensitic structures was found to occur exclusively by a nucleation and growth process. At low degrees of superheat nuclei were concentrated at prior austenite boundaries in the bainite and martensite structures and at grain boundaries in the ferrite structure. Intragranular nucleation occurred at higher degrees of superheat. Nucleation was found to be most profuse in the martensite, followed by the bainite and finally the ferrite structure.

Austenite nucleated on ferrite grain boundaries was found to be Kurdjumov-Sachs related to the grain into which significant growth did not occur. Austenite nucleated on sub-grain boundaries was found to be Kurdjumov-

Sachs related to the surrounding matrix. Dissolution of the vanadium carbide precipitates occurred at the advancing austenite/ferrite interface followed by reprecipitation of a coarser nature in the austenite, with a cube/cube orientation relationship.

By employing rapid austenitisation heat treatments to directly transformed ferrite, grain sizes of approximately 5 μm were produced with a single cycle and approximately 3.5 μm using a multi-cycle treatment. Under optimum conditions the impact transition temperature was reduced by over 300°C and tensile strength levels of approximately 1600MNm^{-2} were achieved.

CONTENTS

CHAPTER ONE

INTRODUCTION

This dissertation describes an investigation into the transformation characteristics of alloys based on the composition Fe-IV-0.2C. Such alloys have been used previously to study precipitation reactions in low alloy steels, notably the so-called "interphase" precipitation reaction (Batte and Honeycombe, 1973). The steel is particularly suited to such investigations as the vanadium and carbon are stoichiometrically combined and therefore, the structures isothermally transformed between approximately 650°C and 800°C are void of pearlite and "clean" ferrite, and consist only of ferrite grains bearing a dispersion of vanadium carbide. Furthermore, the volume fraction of precipitate is particularly high, which facilitates examination of the dispersion characteristics.

The alloy also provides a convenient means of comparing similar steels on a structural basis, in that by adjustment of the initial heat-treatment conditions, it is possible to produce structures consisting entirely of ferrite, upper or lower bainite, or martensite.

Despite extensive work on the morphological and kinetic aspects of the ferrite reaction as modified by the in situ precipitation of alloy carbide in low alloy steels, (Davenport and Honeycombe (1971), Heikkinen (1973a/b), Campbell and Honeycombe (1974), Edmonds and Honeycombe (1973)), controversy remains as to the exact mechanism by which precipitation can occur. The alloy carbide has been shown to

display either a fibrous morphology or to be aligned as sheets of discrete precipitates. The precipitation occurs as the ferrite/austenite phase boundary advances and as such is a form of discontinuous precipitation. Therefore, it is considered likely that the mechanism by which such precipitate morphologies arise is closely associated with the ferrite reaction itself and cannot be completely described unless the mechanism of formation of the ferrite phase is understood. This requires not only a morphological and kinetic description of the reaction but also a crystallographic one, as this identifies the nature of the interphase boundaries and consequently the mechanisms by which they are mobile. This was considered to be particularly important when examining these precipitation reactions, as the alloy carbide has been shown to be precipitated in close association with the interphase boundary (Berry, 1968). Establishment of the orientation relationship governing a reaction can only be achieved through the preservation of the parent phase, in this case the high temperature austenite. Traditionally this has been effected by depression of the martensite start temperature and stabilisation of the austenite using alloy additions. However, this may influence the nature of the transformation, and to date, attempts to retain the parent austenite, while sustaining an "interphase" type of precipitation reaction, have proved unsuccessful (De Ardo (1972), Beaven (1975)).

A number of alternative routes may be considered, in that high temperature X-ray and electron diffraction tech-

niques have been devised, whereby crystallographic information can be recorded as a transformation occurs. In general these techniques suffer from poor resolution because of difficulty in maintaining static conditions during a phase transformation. Oxidation effects and varying magnetic characteristics of the specimen also prove disruptive to high temperation, high resolution investigations. However, it has been shown that under certain conditions, austenite may be retained in quenched martensites, even in low-alloy steels (Thomas, 1973), although a full morphological and crystallographic description has not been documented. It was thought that a complete characterisation of austenite retained in this way might provide a means of studying the crystallography of transformations occurring in low alloy steels. This is of course dependant upon the ability to relate the orientation of the retained austenite to that of the parent austenite.

The precipitation of aligned alloy carbides in commercial ferritic steels has been recognised for some time (Leslie, 1963), particularly in the area of control-rolled steels, where carbide forming elements have been used as a means of grain refinement yet are found to provide added increments of strength through precipitation of fine alloy carbide dispersions. This has revolutionised the production of rolled strip and plate in what are generally called micro-alloyed steels, but as yet, steels of higher alloy content, strengthened by a similar mechanism, have not been extensively studied or developed for commer-

cial application. This may be due to the inferior toughness behaviour of these steels compared to conventional quenched and tempered structures. This results from the high solution treatment temperatures, which are necessary to dissolve sufficient alloy carbide to be precipitated on retransformation. A large austenite grain size results, which is inherited by the transformation product to give a large ferrite grain size. In conjunction with the very potent strengthening effect of the alloy carbide dispersion, the large ferrite grain size results in poor toughness*.

However, if adequate toughness could be achieved, directly transformed, heat treatable steels could have many advantages over quenched and tempered brands. These advantages lie mainly in the more direct processing route to produce a ferritic structure strengthened by a fine carbide dispersion. Conventional steels require a multi-stage treatment involving:-

(i) A quench into water or oil from elevated temperature. This induces severe thermal and transformation strains and frequently results in the cracking of expensive components. Alternatively alloy additions can be used to supress austenite decomposition by diffusional processes and allow martensite structures to be produced on an air cool. Such additions (e.g. Ni, Mn, Cr, Mo) are expensive and usually require relatively large concentrations to

---

* Work is currently being carried out (Benson, 1977), to investigate the possibility that the aligned nature of the carbide dispersion itself may be deleterious to toughness.

produce the required hardenability.

(ii) A tempering treatment to relieve some of the internal stresses associated with the martensite structure, and to promote precipitation of a carbide dispersion. This may involve lengthy heat treatments and can result in embrittlement should the process be performed at an unsuitable temperature.

By careful control of the alloy composition, similar structures and strengths can be achieved on either a continuous cool or by isothermal transformation. The advantages of such a one stage treatment are very attractive to the manufacturer as quench cracks and tempering problems are avoided while processing time is kept to a minimum, and cheaper compositions can be employed.

The inferior toughness of directly transformed steels is, however, a considerable hindrance to their widespread application. A number of possible means of improving this are available based on the established relationships which describe the mechanical properties of steels. These include either grain refinement or a reduction in the precipitation hardening component to strength. The latter may be effected simply by reducing the volume fraction of precipitate, but is the least favourable alternative as although toughness is improved it is accompanied by a decrease in strength. However, it is well known that a reduction in grain size not only improves toughness but also provides an added strength increment.

There are many possible means by which the grain size may be reduced, some of the more successful methods

involving thermomechanical treatment. This can be discounted in the context of the present study as mechanical deformation during the final stages of processing of a heat treatable component would usually be inconvenient. Other methods include the use of innoculants to increase nucleation rates, and the pinning of grain boundaries using stable precipitates. While these methods provide useful means of reducing grain size, they have received some attention in the past and so it was decided to concentrate on rapid heat treatment methods, where it was thought that more dramatic reductions might be achieved, and for which there is as yet limited data in the literature.

Traditional heat treatment cycles often begin with a slow rate of heating to the austenitising temperature, followed by a prolonged soak. Grange (1971) attributes this to poor furnace temperature control in former years, where prolonged heating was necessary to avoid incomplete reaustenitisation. However, such treatments eliminate a powerful method of microstructural control in that the characteristics of the austenite produced on heating can influence subsequent austenite decomposition.

Development in furnace technology now enables far greater temperature control and flexibility in heat treatment cycles. Rapid heat treatment utilises this and involves accelerated heating into the austenite range followed by a short duration anneal. A fine grained austenite is produced and grain growth is kept to a minimum prior to retransformation. The optimum conditions under

which fine grained structures are produced will clearly be related to the mechanism of austenite formation in the particular steel. It is essential, therefore, that these processes be understood before the full potential of rapid heat treatment can be realised.

Chapter Two

The Occurrence of Retained Austenite in Some Quenched Low-Alloy Steels

2.1 Introduction

The presence of retained austenite in quenched steels has been known for some time (Menter, Tsou and Nutting, 1952), but it has received little attention in the area of low-alloy steels. This is because volume fractions are usually low, and consequently were not considered to have any major bearing on the mechanical performance of the steel. However, more recent work by Thomas (1973) has intimated that interlath films in quenched chromium steels, have a beneficial influence on toughness, but a complete characterisation of such films is not given.

The alloy concentration necessary to retain austenite is in fact very small, as demonstrated in the early work of Menter et al. (1952) and Tsou, Nutting and Menter (1952). They detected austenite as grain boundary films in quenched α-iron using X-ray techniques.

It seems likely, therefore, that austenite may be retained in a number of quenched low-alloy steels, and the work reported in this chapter attempts to examine this more closely. A more thorough understanding of this phenomenon of retained austenite was considered necessary for the following reasons:

(i) The only way by which a phase transformation can be completely described, is through the establishment of the

orientation relationships governing that reaction. In the case of the austenite to ferrite or the reverse ferrite to austenite reactions, this necessitates the retention of the high temperature austenite phase. It has proved unsuccessful to effect this through austenite stabilisation using alloy additions and a possible solution to the problem may be by the retention of interlath austenite.

(ii) The processes involved in the reaustenitisation of martensite are not clear as there is some controversy over the mechanism of nucleation of the austenite. The occurrence of retained austenite may well influence this, and could depend on the thermal stability of interlath austenite films.

(iii) Thomas (1973) has suggested that toughness may be improved by the presence of austenite as interlath films. In order to optimise toughness by this phenomenon, the factors influencing austenite retention must be clearly defined.

2.2 Commercial Significance and Detection of Retained Austenite

Work on the influence of retained austenite on the mechanical properties of low-alloy steels is limited. Thomas (1973) describes the presence of retained austenite as a "special effect" and suggests that it may contribute to the high toughness values associated with quenched chromium steels. The mechanism by which this improved toughness is obtained is not reported by Thomas.

Work by Seal and Honeycombe (1958), also on chromium steels, notes the absence of embrittling interlath carbides on tempering, and attributes this to the presence of stable films of retained austenite up to 400°C.

In high-alloy steels, however, where large quantities of retained austenite may be present, much industrially orientated research has been carried out. These studies centre largely on the influence of retained austenite upon the mechanical performance of the steel. Problems can arise due to the thermal and mechanical instability of the austenite. A 4% volume expansion accompanies any subsequent austenite decomposition and as a result, very high localised stresses may be generated, possibly inducing microcracks in a service component over a number of years or under conditions of shock loading.

Work has been carried out particularly in the area of fatigue, where retained austenite may have a considerable influence on the advancement of fatigue cracks. The mechanisms involved, however, are not well understood and results often conflict. For instance, it is cited by Debuyschere (1975) that the fatigue life of a 0.2C-Cr-Ni steel is drastically reduced by the presence of retained austenite. However, work by Yajima, Miyazaki, Sugiyama and Tenajima (1974), on the fatigue life of ball bearing steels, suggests that retained austenite can have a beneficial effect, in some instances, by blunting the advancing crack tip. They point out that the fatigue process in the presence of retained austenite, is a complex one and it seems likely that the stability of the retained austenite

and the operating stress system are important parameters.

Because of the influence of the retained austenite on mechanical behaviour, it is necessary to be able to detect its presence and also to measure accurately the volume fraction present. The most common methods employ X-ray diffraction, although magnetic measuring techniques also exist, which are more rapid but less sensitive.

Early X-ray determinations of retained austenite (Gardner, Cohen and Antia, 1943) analysed relative peak heights as a measure of intensity, relating this directly to the volume fraction of austenite in the steel. This method is subject to large errors, however, as the morphology of the austenite can lead to peak broadening and a reduction in peak heights. A more accurate method, reviewed by Miller (1964), employs measurements of the area under the peak, or integrated intensity.

As Miller indicates, all X-ray methods are subject to inaccuracies caused by preferred orientation or texture, and a range of angles must be scanned in order to establish if such inaccuracies are present.

2.3 Scope of Chapter

The retention of austenite in low-alloy steel appears to be closely related to the mechanism of martensite formation and hence its subsequent morphology. The literature relating to plate and lath martensite has therefore been reviewed in sections 2.4.1 and 2.4.2 respectively. The section on plate martensite is included, as some parallels can be drawn between martensite formation with plate

and lath morphologies. Section 2.5 deals with theories which attempt to explain the retention of austenite in terms of the characteristics of the martensite reaction.

The results and discussion of investigations on quenched, low-alloy, vanadium bearing steels are presented in section 2.6.

Section 2.7 provides a summary of the chapter and includes conclusions of the results where applicable.

2.4 Literature Review

Steels cooled from the austenitic condition fast enough to avoid decomposition by diffusional processes, transform to martensite at low temperatures by a process of formative shear. The reaction involves the co-operative movement of atoms over small distances and has been described by Christian (1965) as a "military transformation".

Two distinct types of martensite have been shown to exist depending largely upon the chemical composition of the steel, particularly the carbon content. These will be considered separately.

2.4.1 Plate Martensites

High carbon martensites are typically platelike in shape and incorporate a heavily twinned substructure, (Kelly and Nutting, 1960). These twins lie on $\{122\}_{\alpha'}$ planes and provide effective barriers to dislocation movement, as few slip systems are operative on both sides of a twin boundary. This has been shown to result in an increase in strength but a decrease in both ductility and

toughness, (Kelly and Nutting, 1961; Das and Thomas,1969).

Plate martensites can be further subdivided into those exhibiting the Kurdjumov-Sachs, (K-S), (1930)* and those exhibiting the Greninger-Troiano, (G-T), (1949) orientation relationships. Mehl and Van Winkle (1953) showed that plates formed at lower temperatures tended to obey the G-T relationship and occupy a $\{259\}_\gamma$ habit, while higher temperature transformations favour the K-S relationship with a $\{225\}_\gamma$ habit.

As a consequence of the many available habit planes, plate martensites often appear as an interlocked arrangement of lenticular plates although under certain conditions the plates may accommodate the shear stresses associated with the reaction and form co-operative arrangements, (Maksimova and Nikonorova, 1955).

2.4.2 Lath Martensites

Low carbon martensites, in contrast to plate martensites, have a less random appearance both optically and in the electron microscope. This is attributed to the grouping of the basic martensite units into what are usually described as packets (Marder and Marder, 1969), although other terminologies such as blocks, sheaves or bundles have been used.

The basic martensite unit, from which the packets are comprised, has been described using many terms, for

---

* Stereograms describing all the orientation relationships used in this thesis are given in Appendix II.

example, needles (Kelly and Nutting, 1960), cells (Speich and Swann, 1965), platelets (Marder and Krauss, 1967). However, it is now generally agreed that the unit is so shaped that if a, b and c are the principal dimensions then $a \gg b > c$ and that the unit be termed a lath (Krauss and Marder, 1971).

The mechanism of nucleation and growth of the laths to form complete packets it not well understood, largely because the speed of the martensite transformation in low-alloy steels hinders effective partial transformation studies. However, work by Krauss and Marder (1971) on an Fe-2% Mo alloy, isolated two specific growth modes by the use of hot stage cinephotomicroscopy. These were found to be:

(i) The independent nucleation of laths within one packet with parallel growth directions. The intervening austenite then transforms by the nucleation and growth of further parallel sided laths to consume the remaining austenite and form the packet.

(ii) The repeated nucleation of laths adjacent to those already formed. The packet thus forms by the successive, sideways nucleation of laths until impingement with other packets restricts its further development.

A prior austenite grain thus transforms to many packets of martensite of various orientations. Adjacent laths within any one packet tend to be misorientated to some degree although regions of high dislocation density, with no apparent lath structure, have also been observed, (Chilton, Barton and Speich, 1970).

Electron microscopy studies of the relative orientations of adjacent laths within single packets have shown that three specific types of interlath boundary can be described:

(i) Adjacent laths are separated by high-angle boundaries;

(ii) Adjacent laths are separated by low-angle boundaries;

(iii) Adjacent laths are twin related.

Speich and Swann (1965) explain this in terms of adjacent laths occupying the lowest strain energy configuration. They propose that the laths occupy the particular K-S orientation which results in the minimum shape change, and that by selection of different variants in adjacent laths, all three of the above types of interlath boundary can be created as shown below.

If the K-S orientation relationship is applied to the austenite/martensite transformation one possibility is that:

$$(111)_\gamma // (011)_{\alpha'}$$

From this it is possible to generate six variants of the relationship by choosing the two different $\langle 111 \rangle_{\alpha'}$ directions that lie in the $(111)_\gamma$ plane:

(a) $[\bar{1}10]_\gamma // [\bar{1}\bar{1}1]_{\alpha'}$

(b) $[\bar{1}10]_\gamma // [\bar{1}1\bar{1}]_{\alpha'}$

(c) $[\bar{1}01]_\gamma // [\bar{1}\bar{1}1]_{\alpha'}$

(d) $[\bar{1}01]_\gamma // [\bar{1}1\bar{1}]_{\alpha'}$

(e) $[0\bar{1}1]_\gamma // [\bar{1}\bar{1}1]_{\alpha'}$

(f) $[0\bar{1}1]_\gamma // [\bar{1}1\bar{1}]_{\alpha'}$

In the same way, six variants are associated with the other three equivalent $\{111\}_\gamma$ planes to give a total

of twenty-four variants. By taking the variants in pairs it is possible to generate either high-angle, low-angle or twin boundaries as shown in table 2.1.

From the table it is evident that if adjacent laths occupy different K-S variants on a purely random basis, then analysis should reveal 20% to be separated by low-angle, 60% by high-angle and 20% by twin boundaries. However, Speich and Swann (1965) produced evidence that adjacent laths were often found to be twin related (or within 5 degrees of a twin variant). Work by Biswas and Codd (1968) on Fe-N martensites supports the work of Speich and Swann in that they also found twin variants to be a common occurrence.

A more quantitative approach was adopted by Chilton et al.(1970) working on an Fe-20Ni-C martensite. Comparing experimental data with the expected incidence of high-angle, low-angle and twin boundaries, as shown above, they investigated the possibility of certain K-S variants being favoured. This might be expected if adjacent laths had a tendency towards self-accommodation, that is, forming with an orientation which minimises the nett homogenous shears introduced during transformation.

Kelly (1965) showed that twin related variants have shears of equal magnitude, but opposite sign, and hence it might be expected that an increased incidence of twin related laths would be observed. The work of Chilton et al.(1970) shows that evidence for this is inconclusive. Recent work by Bozic and Lucic (1977) has also shown that there appears to be no tendency towards predominantly

twin related laths in a number of Fe-As alloys.

Other work has found no evidence at all of twin related laths. Goodenow and Hehemann (1965), working on similar Fe-Ni alloys to those used by Speich and Swann, described comparable lath morphologies but found no evidence of twin related laths. Their results suggest that laths within any one packet are separated by low-angle boundaries. Further work by Marder and Krauss (1967) on a 0.2% plain carbon steel, also demonstrated that the majority of laths were separated by low-angle boundaries and that twin related laths were not seen.

In general, the apparent absence of retained austenite in these steels has precluded the establishment of a complete crystallographic description of the austenite/martensite reaction. This is necessary if the controversy concerning lath misorientations is to be resolved unambiguously.

As described earlier, much work on the relative orientations of laths within a packet suggests that the laths obey the K-S orientation relationship with the austenite (Speich and Swann, 1965). However, work by Owen, Shoen and Srinivasan (1970) disputes this, as they claim that electron diffraction techniques are not of sufficient accuracy to resolve the small differences between the Kurdjumov-Sachs (1930) and Nishiyama (1934)-Wassermann (1935), (N-W), orientation relationships. They performed experiments on a single crystal of an Fe-Ni binary alloy where the nickel content of the crystal varied between 4% and 28% along its length. A single crystal diffracto-

meter was then used to examine the crystal after quenching to produce regions of martensite, austenite and a region where austenite is retained between the martensite laths. This revealed evidence which was inconsistent with the martensite adopting the K-S relationship, but which gave good agreement when analysed in terms of the N-W relationship. Twin variants are not possible with the N-W relationship and hence they claim the work of Speich and Swann (1965) to be untenable. However, twin related laths have been observed by a number of workers and so it seems likely that neither orientation relationship is obeyed in all cases.

2.4.3. Habit Plane and Major Growth Direction

In plate martensites, the habit plane can be determined in terms of either the martensite or the austenite crystallography because of the abundance of retained austenite.

The habit plane in lath martensites can normally only be related to the martensite crystallography because of the apparent general absence of retained austenite. A number of investigators have used single surface trace analysis to show that lath martensites occupy a $\{110\}_{\alpha'}$ habit plane (Kelly and Nutting (1960), Biswas and Codd (1968), Chilton et al. (1970), Krauss and Marder (1971), Bozic and Lucic (1977)). Assuming the martensite obeys a K-S or N-W relationship with the parent austenite, then the lath will form with a $\{111\}_{\gamma}$ habit plane.

Similar work has attempted to define a major growth direction for the laths, also using single surface trace analysis. Results have been interpreted in terms of a $\langle 111 \rangle_{\alpha'}$ major growth direction although this requires assumptions concerning the basic lath morphology which may not be justified. This aspect of the work will be investigated more thoroughly in Section 2.6.

2.5 Theories of Austenite Retention

At room temperature austenite will be retained in steels under specific instances:

(i) If the Mf temperature of the steel has been depressed by alloy additions to below room temperature, a thermodynamically stable volume fraction of austenite will be present.

(ii) If the Mf temperature is above room temperature, but the thermodynamic driving force is insufficient to transform any remaining austenite to martensite.

The ability to propagate a martensite plate or lath through the austenite depends on two factors: the magnitude of the thermodynamic driving force; and the resistance of the austenite to transformation. The driving force will be a function of the temperature difference between the quenching medium and the Ms and Mf temperatures.

Studies of the resistance of the parent austenite to transformation have been carried out by Davies and Magee (1971) who show that the ease with which the austenite transforms is a function of the relative flow stresses

of the austenite and the martensite. They conclude that variations in these relative values could be effected by alloy additions and suggest that this may influence habit plane selection.

Mechanical stabilisation of austenite has been shown to occur as a result of the shape and volume changes associated with the formation of a martensite unit (Yershov, 1973). In the early stages of transformation, austenite adjacent to a martensite lath is subjected to tensile coherency stresses. However, as the reaction proceeds, the stresses become compressive owing to the constraint of the martensite frame on any remaining austenite. This can inhibit further martensite formation.

A further consideration regarding the transformation of small amounts of austenite is the energy considerations associated with the creation of further boundary surface. The reaction will become less favourable as the units of transformation become smaller, because the surface area to volume ratio increases as the size decreases. In the later stages of transformation, the introduction of a small martensite unit will be accompanied by the formation of a relatively large amount of boundary surface. The free energy for the reaction will thus decrease until it is insufficient to propagate the reaction further.

2.5.1 Application to Plate Martensites

Austenite retention in plate martensites can be explained in terms of two main factors:

(i) The high solute concentrations associated with steels

exhibiting a platelike martensite structure results in a lowering of the Ms and Mf temperatures. Thus, on quenching, the thermodynamic driving force for the reaction may be insufficient to complete the transformation.
(ii) Fisher (1953) investigated the mechanism and kinetics of the nucleation of martensite plates within individual austenite grains. He observed that as the martensite plates formed, they tended to partition the austenite into increasingly smaller units. Plates formed early in the reaction are therefore larger than those formed at a later stage. As the regions of remaining austenite decrease in size then the constraining influence of the surrounding martensite frame increases, inhibiting any further shape or volume change. The creation of smaller martensite units as the reaction proceeds also increases the surface area to volume ratio, hence becoming energetically less favourable.

Fisher's approach to nucleation in plate martensites is shown by Magee (1970) to be an oversimplification. Magee shows that martensite plates are not necessarily randomly nucleated but tend to cluster to some extent, as the shear stresses introduced during the formation of one plate may encourage the nucleation of a plate nearby. This phenomenon is termed autocatalysis.

2.5.2 Application to Lath Martensites

Some of the principles governing austenite retention in plate martensites can be extended to lath martensites, in that the mechanisms governing transformation are sim-

ilar. However, in contrast to plate martensites, which display a structure of interlocked plates, lath martensites consist of impinging packets, each packet containing many parallel laths. From the work of Thomas (1973) it is evident that any retained austenite is present as interlath films. This suggests that the processes by which the austenite is retained is more closely associated with the mechanism of the martensite transformation itself.

The very presence of interlath austenite suggests that individual martensite laths grow into the prior austenite grains to leave regions of untransformed austenite between them (Krauss and Marder, 1971). If this situation is assumed to exist, where a region of austenite separates two martensite laths of similar orientation, then the conditions under which the remaining austenite will transform can be considered.

Owing to the shear nature of the martensite transformation, the austenite adjacent to a particular martensite lath will be subjected to a shear system which is equal and opposite to that associated with the formation of the lath. Kelly (1965) has shown that twin variants have shear components which have equal magnitude but opposite sign. Bhadesia (1977) has pointed out that the formation of a twin related martensite lath would therefore provide complete self-accommodation of the transformation shears and appears to be a favourable condition for the transformation of the interposed austenite. The fact that a number of workers have observed twin related laths (Speich and Swann (1965), Biswas and Codd (1968), Chilton

et al.(1970), Bozic and Lucic (1977)), yet have not reported the presence of retained austenite, gives some credence to this theory.

For twin related variants to be possible it is necessary that the martensite laths obey a K-S orientation relationship with the austenite, as twin variants are not permitted if the operating relationship is N-W. This has led Bhadesia (1977) to suggest that austenite will only be retained when the N-W relationship is operating and hence the formation of twin related laths is not possible. This would otherwise necessitate the formation of martensite units at an angle to the major growth direction of the existing laths, if self-accommodation was to occur. These units would be extremely small and hence have a high surface area to volume ratio. Clearly this would be energetically unfavourable.

2.6 Experimental Results and Discussion

2.6.1 Alloys and Heat Treatments

(i) Alloys:

The basic alloy for these studies was a simple ternary steel of nominal composition Fe-1V-0.2C. The influence of quaternary additions on the quenched structure was also investigated. The three alloys used were as follows:

A1 Fe-1V-0.2C

A2 Fe-1V-0.2C + 2Ni

A3 Fe-1V-0.2C + 2Mn*

---

* Actual compositions of all alloys used are given in Appendix I. All concentrations are quoted in wt%.

The three alloys produced very similar results and only under circumstances where one of the parameters investigated has been influenced by alloy addition will specific attention be given to them individually.

(ii) Heat Treatment:

There has been some dispute in the past as to the austenitising treatment required to dissolve completely the alloy carbide. Work by Darbyshire (1972) claims that even for an Fe-0.5V-0.1C alloy, complete dissolution is only achieved after treatment at 1250°C for 45 mins. It seems likely, however, that in his material the initial carbide dispersion was particularly coarse, as much work since this time has revealed that 1200°C for 30 mins. is quite sufficient (Dunlop (1974), Benson (1976), Wilyman (1976)).

A solution treatment temperature of 1200°C for 30 mins. was therefore used and found to be adequate, as shown by the electron microscopy of quenched specimens.

The ferrite and bainite reactions in the system are very rapid, nucleation occurring in times as short as 5 secs.; consequently an iced brine quench was used in all cases to avoid any partial transformation at prior austenite boundaries by diffusional processes.

2.6.2 Structural Characteristics of the Martensite

(i) Optical Metallography:

The optical microstructure was typical lath martensite. The individual laths could not be resolved optically, but the packets themselves had a characteristic acicular

morphology (figure 2.1). Owing to the large grain size produced by solution treatment at 1200°C, the prior austenite grain boundaries were readily visible, as the crystallographic nature of the martensite reaction precludes the propagation of laths or plates across grain boundaries.

(ii) Electron Metallography:

A predominantly lath structure, typical of low carbon martensites, was generally revealed by electron microscopy. However, closer examination identified three distinct lath morphologies.

(a) The principal structure encountered, comprising about 80% area fraction, consisted of an irregular lath structure (figure 2.2). The lath boundaries were not always planar and often terminated with a lenticular appearance (figure 2.2). Pascover (1968) describes this structure as "interwoven" lath martensite and attributes its formation, in preference to a more regular lath morphology, to changes in the apparent Ms caused by alloy additions or a high quench rate.

(b) About 15-20% of the structure consisted of a very regular lath morphology within the martensite packets (figure 2.2). The laths themselves displayed very planar boundaries and were characterised by a high dislocation density.

(c) Occasionally the lath martensite structure would be interrupted by particularly large laths. Figure 2.2 shows that these were heavily autotempered, which suggests that they formed at an early stage in the transformation.

Adjacent Variants	Boundary Type	Relative Rotation about 011 '
a-b, c-d, e-f	Twin	70° 32'
a-d, b-e, c-f	Small Angle	10°
a-c, a-e, b-d b-f, c-e, d-f	Large Angle	60°
a-f, b-c, d-e	Large Angle	49°

Table 2.1:

Boundary types generated between different variants of the Kurdjamov-Sachs orientation relationship.

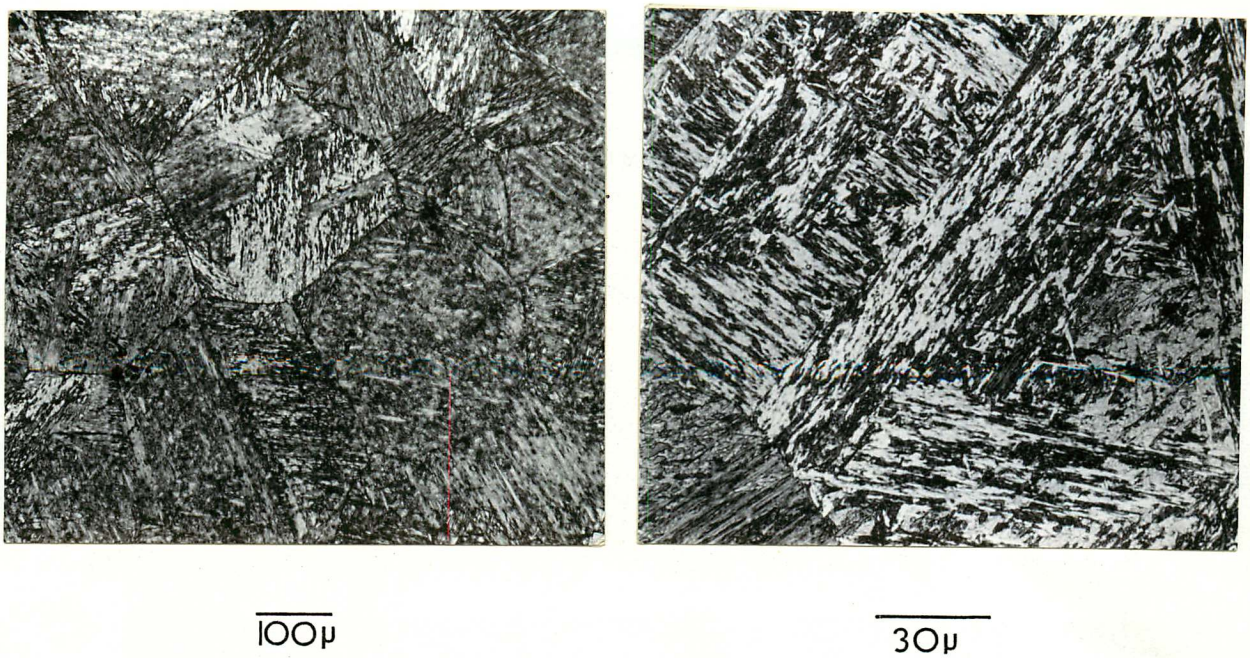

Fig. 2.1:

Optical micrographs of the martensite structure. Fe-IV-0.2C austenitised at 1200°C for 30 mins. and quenched.

Electron diffraction evidence identified the autotempered phase as cementite and showed that it displayed the Bagaryatski (1950) orientation relationship with the martensite (figure 2.2).

These large laths also exhibited twinning, the twins being generally associated with the lath boundaries (figure 2.3). The exact cause of the twinning is unclear but two possible explanations can be considered.

The first possibility is that these are straightforward accommodation or transformation twins introduced during the formative shear reaction. However, this interpretation is open to question. A consequence of the homogenous nature of the martensite transformation is that any accommodation twins have a regular spacing. No such strict regularity was observed in these steels.

A second and more likely explanation is that these laths, having been the first to form, are then subjected to stresses resulting from the formation of adjacent packets. Therefore, the twins are likely to be simple deformation twins, formed under the influence of these external stresses.

(iii) Habit Plane and Growth Direction:

Single surface trace analysis was carried out on all the observed types of lath martensite. As shown in figure 2.4a the analysis proved consistent with a $\{110\}_{\alpha'}$ habit and is therefore in agreement with previous work (Kelly and Nutting (1960), Krauss and Marder (1971)).

A major growth direction in lath martensites has been defined by previous studies (Kelly and Nutting (1961),

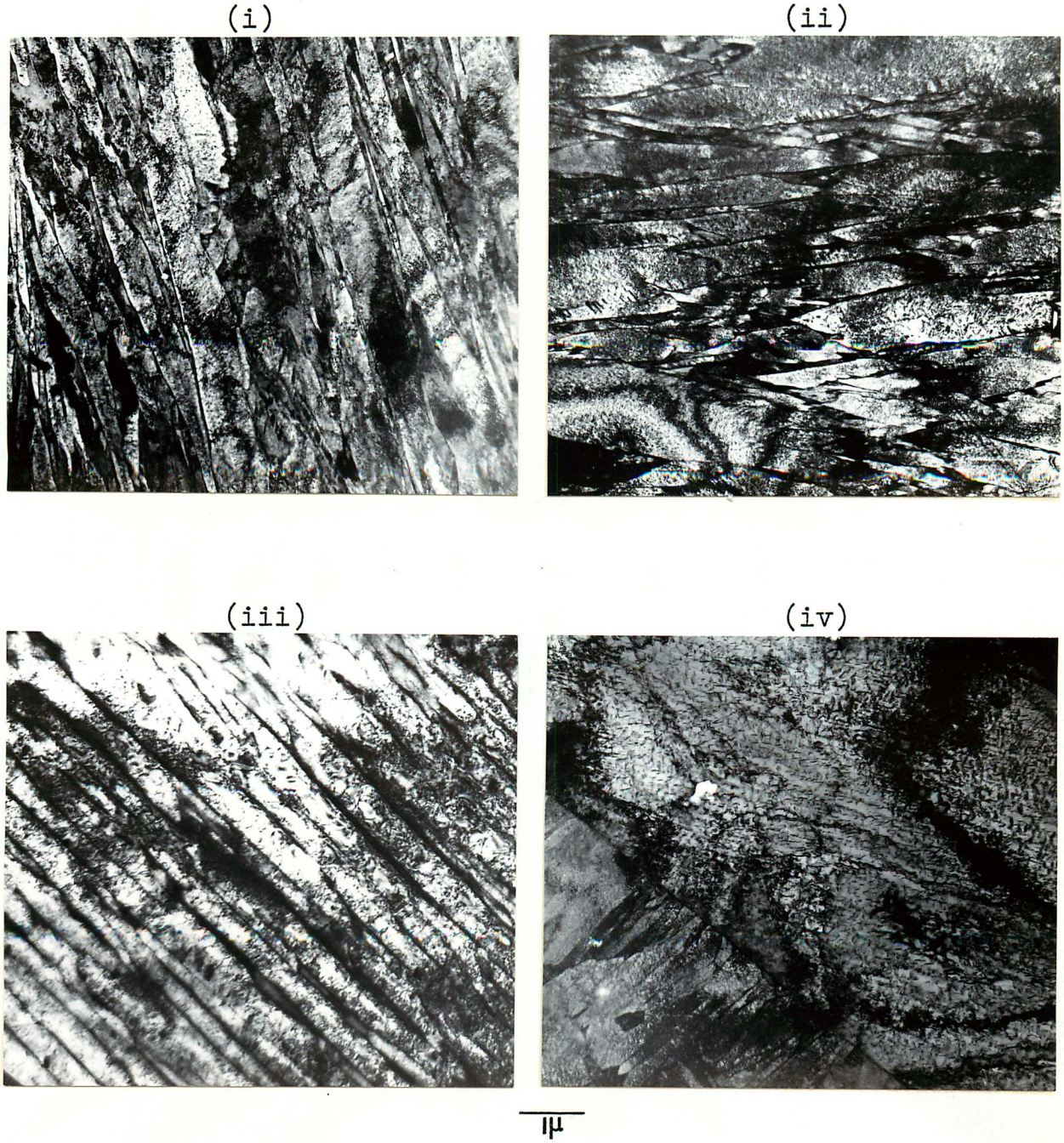

Fig. 2.2a:
(i) and (ii) Interwoven martensite.
(iii) Regular martensite.
(lv) A large autotempered lath.

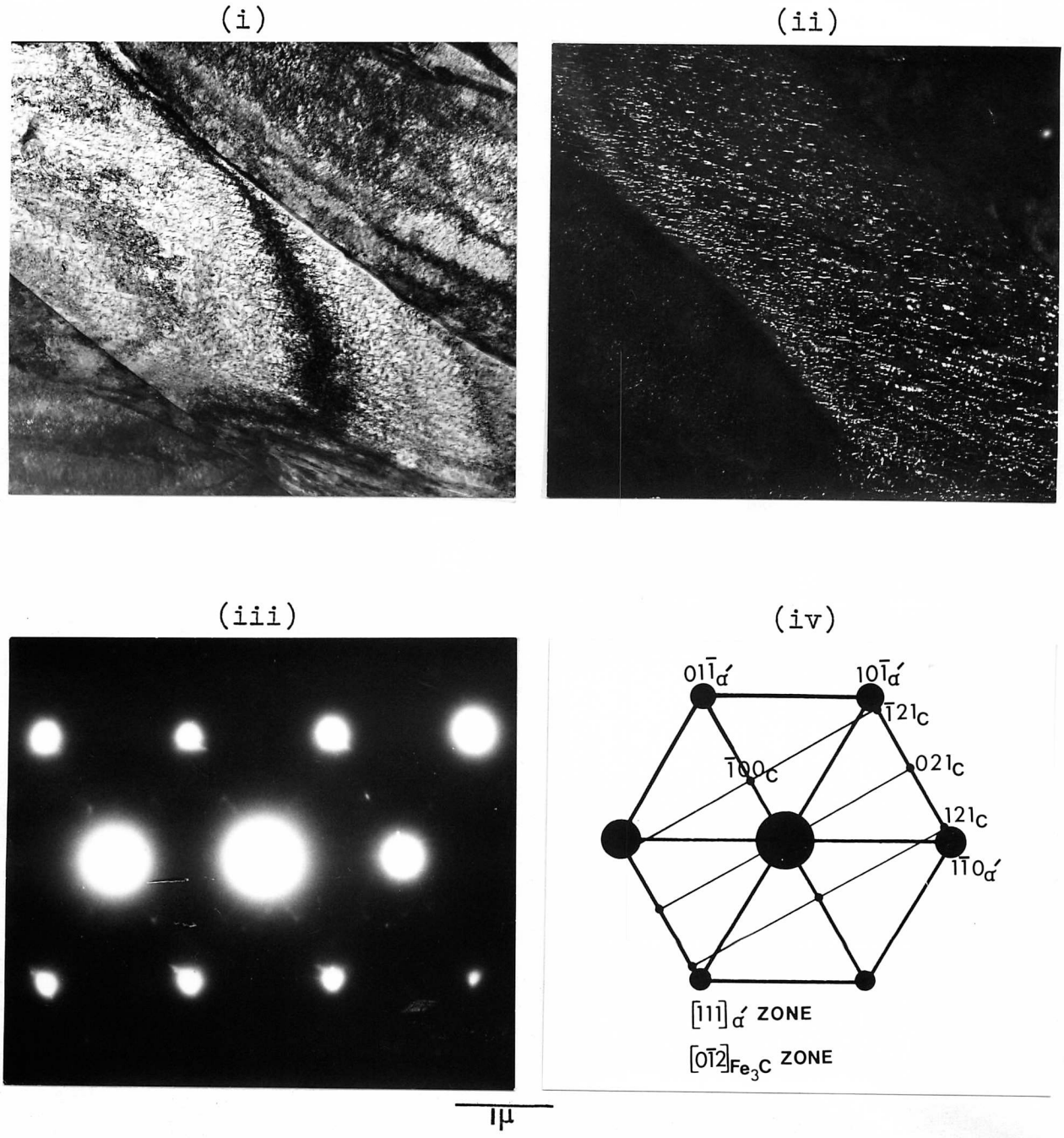

Fig. 2.2b: Thin foil, electron micrographs of the auto-tempered structure.

(i) Bright field.
(ii) Centred dark field using the $(0\bar{2}\bar{1})$ cementite reflection.
(iii) Diffraction pattern.
(iv) Analysis showing the cementite to obey the Bagaryatski relationship with the martensite.

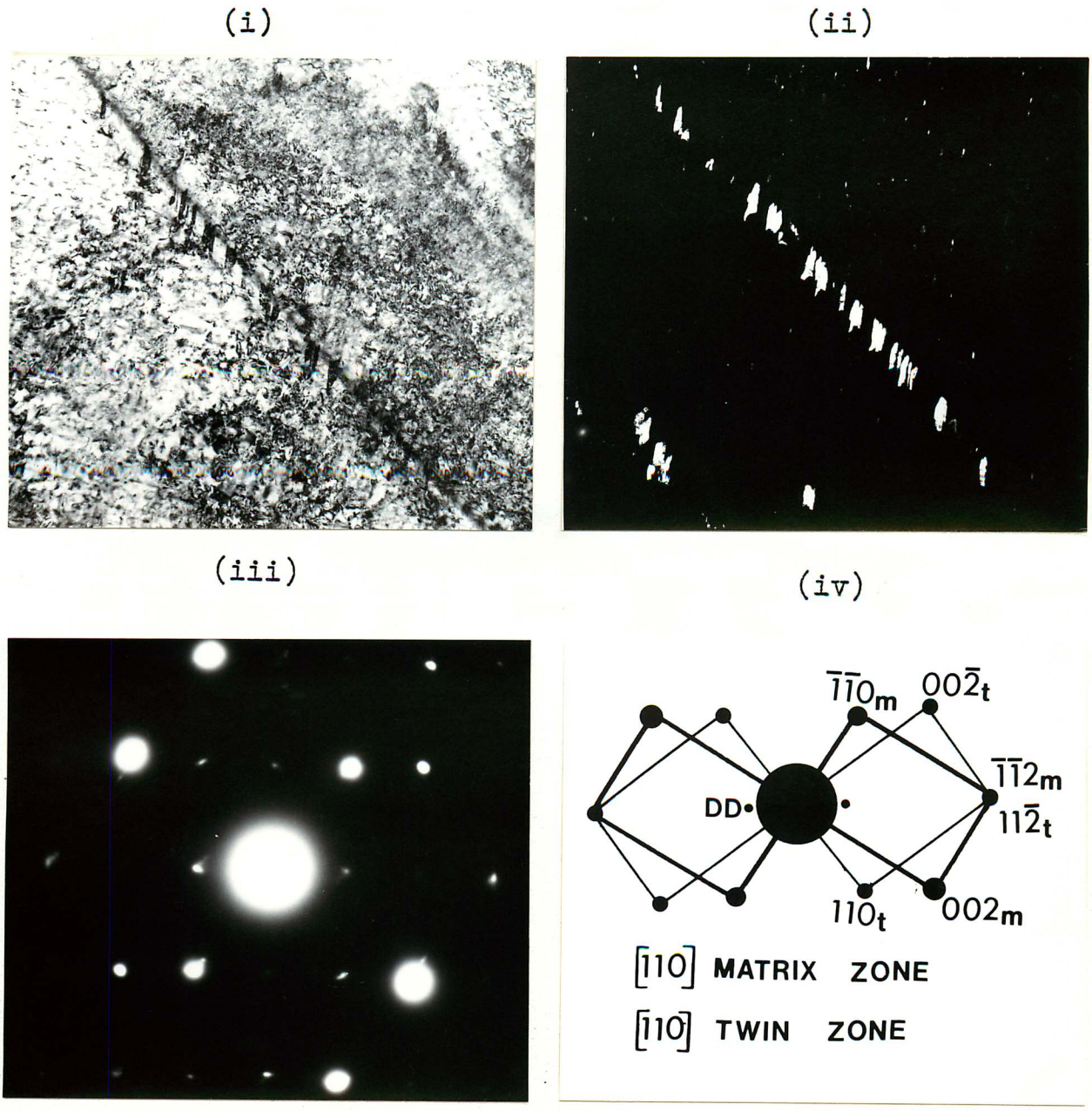

Fig. 2.3: Thin foil electron micrographs of twins along a martensite lath boundary.

(i) Bright field.
(ii) Centred dark field using a (110) twin reflection.
(iii) Diffraction pattern.
(iv) Analysis showing twin relationship.

Chilton et al. (1970), Bozic and Lucic (1977)). Such determinations have employed single surface trace analysis and have yielded information suggesting that the major growth direction of the laths is close to a $\langle 111 \rangle_{\alpha'}$. The validity of this result is open to question because of uncertainty in describing the absolute shape of the martensite unit. If a, b and c are the principal dimensions of the martensite unit then three possible morphologies can be defined:

needle:- $a \gg b = c$ (i.e. circular cross section)

lath:- $a \gg b > c$

plate:- $a \approx b \gg c$

Single surface trace analysis is precise only for the case where the martensite unit is a true needle. This is because only when the unit is needle-like can the locus of possible major growth directions be considered to lie in a plane perpendicular to the plane of the foil. The existence of a habit plane indicates that the unit is not a needle but either a lath or a plate.

If the unit is a true plate, then no major growth direction can be defined, as this could lie anywhere in the habit plane.

If the unit has a lath morphology, as is currently accepted, the locus of possible growth directions does not necessarily lie in a plane perpendicular to the foil surface. It will in fact lie at some angle to the surface of the foil depending on the inclination of the habit plane. Single surface trace analysis is therefore only valid when the habit plane is normal to the foil surface.

These discrepancies are evident in the published work on growth directions, as large angular deviations are common, in some cases covering over half a stereographic triangle (Chilton et al., 1970).

However, assuming that the martensite unit in low carbon steels is not platelike and that a major growth direction can therefore be defined, then single surface trace analysis provides a means of acquiring some idea as to the true nature of the martensite lath.

The habit plane of the laths can be determined accurately and as indicated earlier, this proved to be a $\{110\}_{\alpha'}$ plane. The major growth direction must lie in the habit plane and the locus of all possible directions can be represented as a great circle on a stereogram. This great circle will intersect the great circle representing the particular diffraction pattern being considered, at the trace of the long direction of the laths. If a number of traces are plotted, a clustering around the major growth direction would be expected if the martensite units are in fact lath shaped.

As shown by figure 2.4b this was not found to be the case, as there is no strong grouping of traces around any particular pole.

Two possible explanations can be offered for the fact that no apparent grouping occurred when a number of traces were superposed on the same stereogram:

(a) That no consistent major growth direction can be defined in lath martensites.

(b) The martensite unit in low carbon martensites has

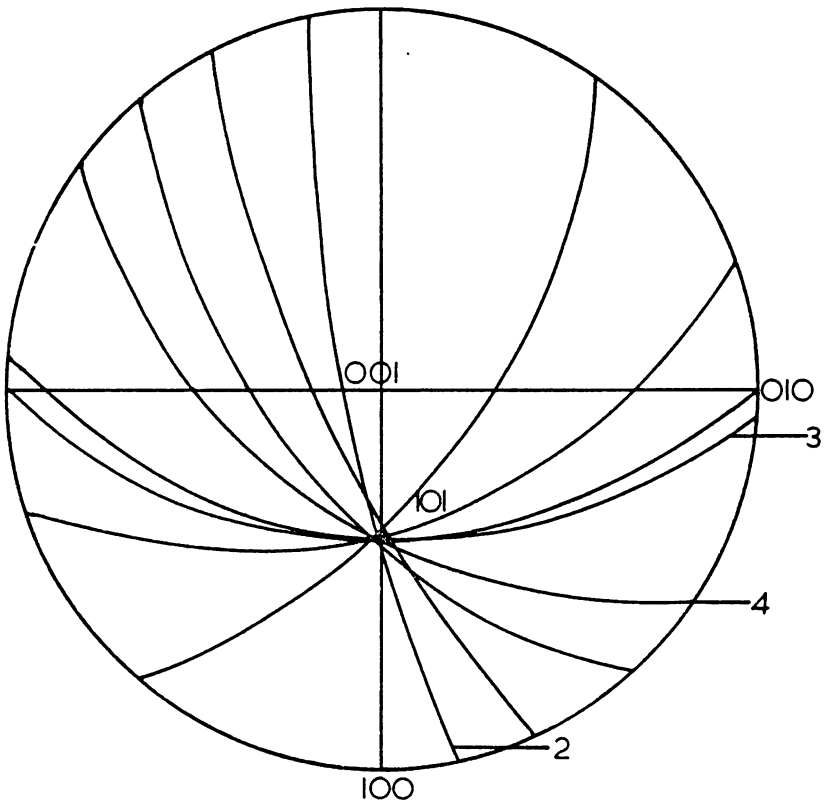

(a)

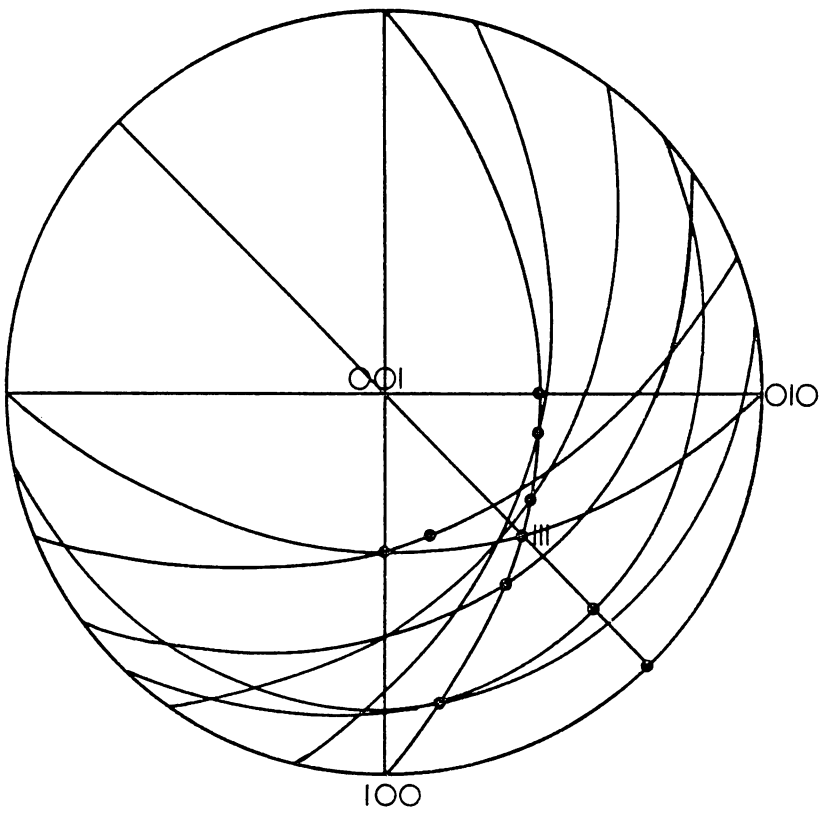

(b)

Fig. 2.4:

(a) Trace analysis of martensite laths consistent with a $\{110\}_{\alpha'}$ habit plane.

(b) Trace analysis of martensite laths showing inconclusive grouping of the traces around any particular growth direction.

a platelike rather than a lath morphology.

2.6.3 Incidence of Retained Austenite

Selected area electron diffraction of individual packets revealed the presence of certain reflections which could not be associated with the martensite crystal structure. Dark field imaging, using these reflections, generally indicated that they were associated with interlath films, characteristic of previously reported retained austenite (Thomas, 1973). However, diffraction evidence was examined in terms of commonly occurring phenomena in quenched steels in order to establish that the interlath films could only be retained austenite. These phenomena are:

(a) Double diffraction.

(b) Carbide.

(c) Twinning.

Where possible, results are presented which show the co-existence of retained austenite with the above phenomena, thereby providing conclusive evidence that the interlath films are of retained austenite.

(i) Double Diffraction:

This phenomenon occurs when a diffracted beam is rediffracted by the crystal. This often results in diffraction spots near the straight-through beam, as the first order reflection, which is doubly diffracted, acts as the zero order reflection to give a further series of spots. Double diffraction often occurs in conjunction with a structural boundary, where a diffracted beam encounters

a crystal of a different orientation.

Figure 2.5 is an example of double diffraction occurring at twin boundaries. The pattern is in fact 2^{o} off a twin orientation but has been analysed as standard for clarity.

(ii) Carbide and Twinning:

The presence of a cementite dispersion, as a result of autotempering of the steel during the quench, has been outlined previously (figure 2.2). The possibility that some cementite may precipitate along the lath boundaries has therefore to be investigated. Figure 2.6 shows a series of micrographs taken at the boundary between a large autotempered lath and a packet. Twinning is evident in the large lath and the diffraction pattern shows characteristic streaking in a $\langle 112 \rangle_{\alpha'}$ direction.

Cementite is shown to be present, not as a film, but in the form of small precipitates produced on autotempering. Centred dark field microscopy indicates the occurrence of cementite precipitation on the twin boundaries and shows that these precipitates are of single orientation. An abundance of retained austenite is also apparent, particularly along the packet boundary. Doubly diffracted spots are also evident close to the straight-through beam in the diffraction pattern.

Figure 2.6 demonstrates the co-existence of twins, carbide and retained austenite, and therefore establishes conclusively the existence of films of retained austentie at lath and packet boundaries.

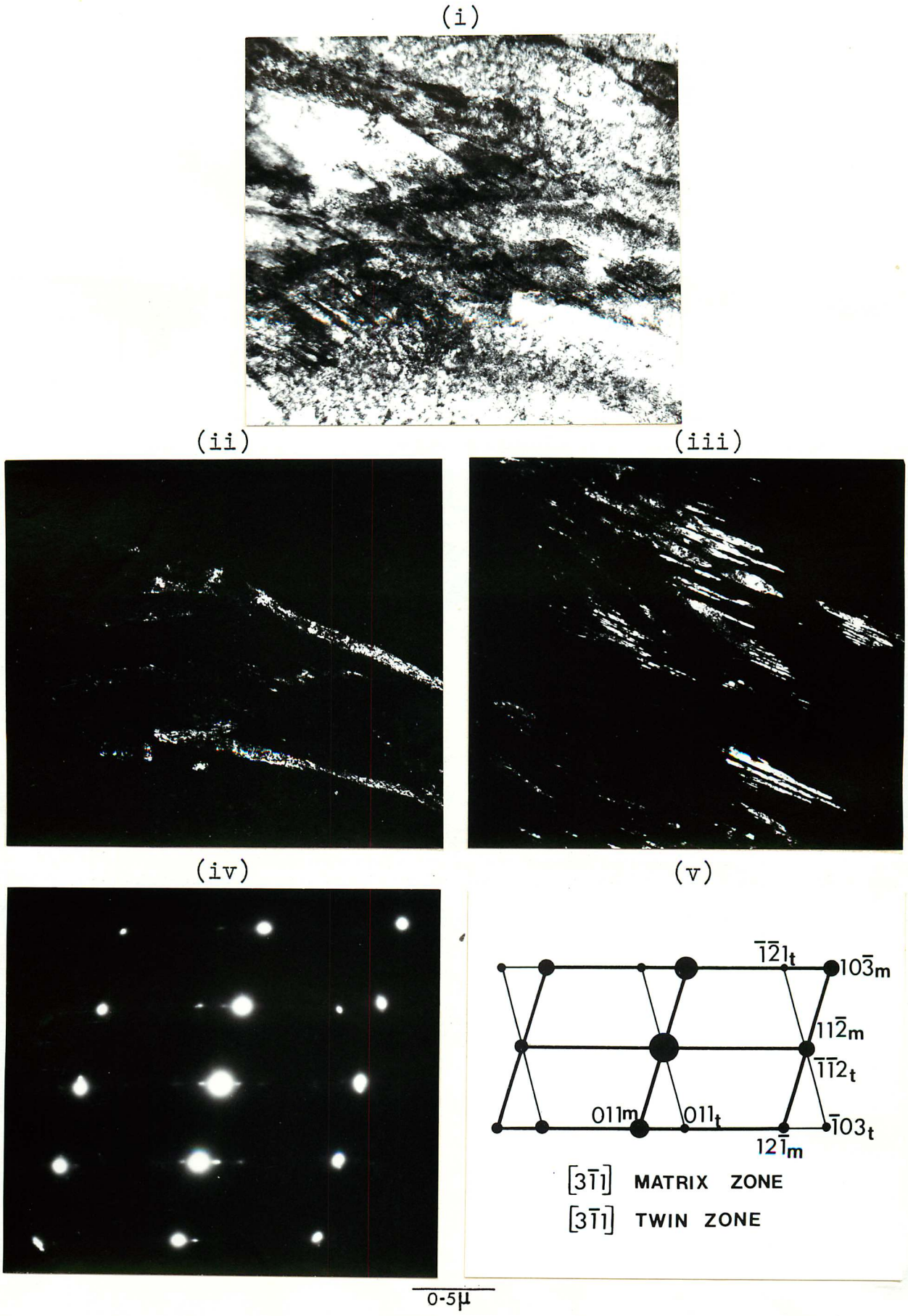

Fig. 2.5: Thin foil electron micrographs of double diffraction and twinning.
(i) Bright field.
(ii) Centred dark field using a double diffracted reflection.
(iii) Centred dark field using the (011) twin reflection.
(iv) Diffraction pattern.
(v) Analysis showing double diffraction and twinning.

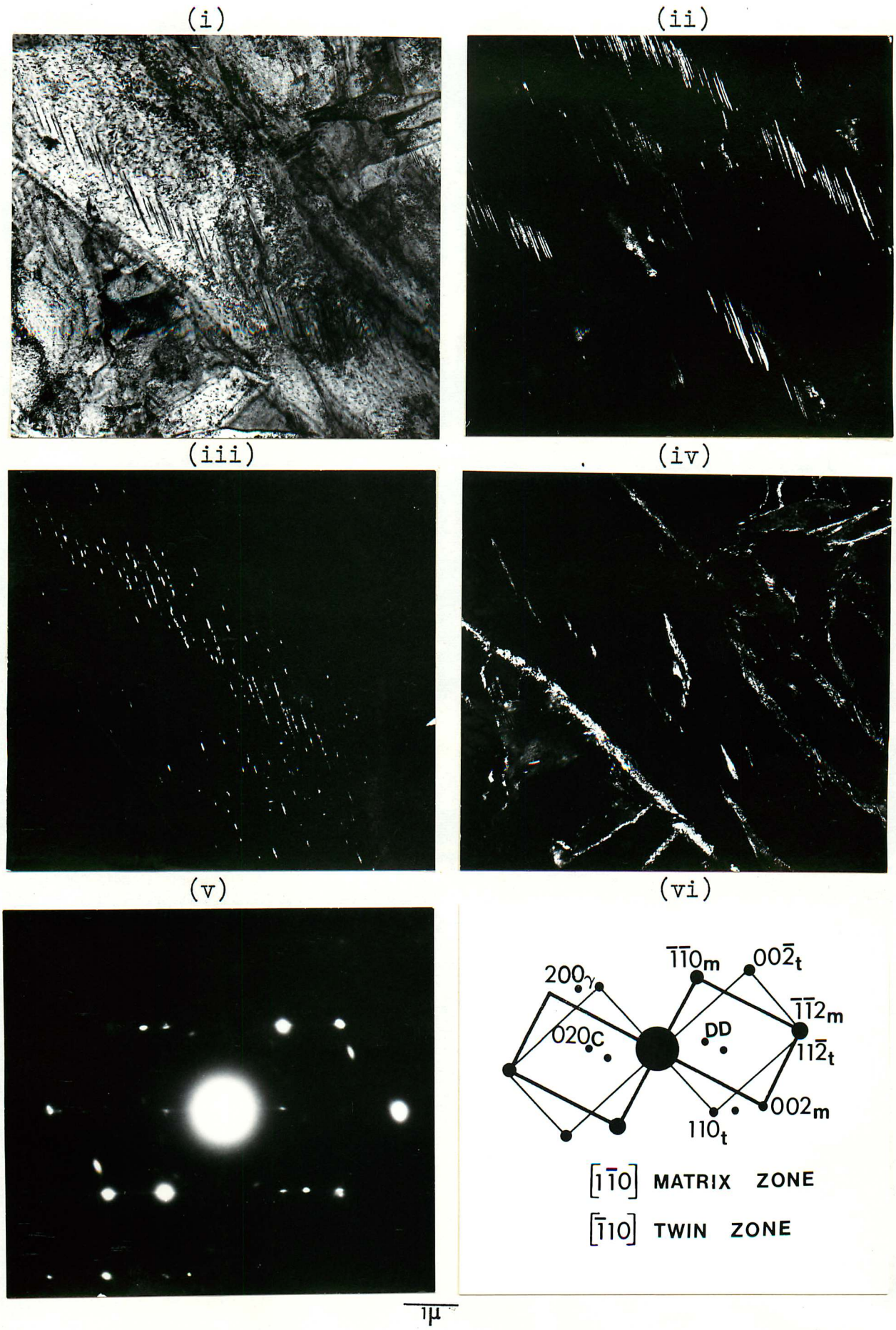

Fig. 2.6: Thin foil electron micrographs of twinning, cementite and retained austenite.
(i) Bright field.
(ii) Centred dark field using the (110) twin reflection.
(iii) Centred dark field using the (020) cementite reflection.
(iv) Centred dark field using the (200) austenite reflection.
(v) Diffraction pattern.
(vi) Analysis showing twinning, cementite and retained austenite.

2.6.4 Morphology, Orientation and Distribution of Retained Austenite

(i) Austenite/Martensite Orientation Relationship:

Before any precise orientation relationship can be defined between the martensite and the retained austenite, two possible complications must be considered. Firstly, what influence does the martensitic transformation have on the orientation of the retained austentite and secondly, can the orientations of the laths within a single martensite packet be described in terms of one relationship?

A simplified analysis of the shear processes occurring during transformation, enables an estimate to be made of the maximum possible distortion of the austenite. Assume first that the austenite adjacent to a martensite lath is displaced during the formation of the lath, that is, the shape change accompanying the formation of the lath is accommodated plastically by the surrounding austenite matrix. The adjacent austenite can thus be considered to undergo a homogeneous shear similar in magnitude to the average shape strain of the martensite. This shape strain is defined as the displacement of a point initially at unit distance from the habit plane and hence the shear displacement can be converted into a rotation. This approach predicts that the maximum possible displacement of the surrounding austenite will be only a few degrees. However, in practice the austenite shear will not be homogeneous and also different regions will be subjected to shears of different sign. The nett result is that a certain amount of broadening of diffraction spots

may be expected but not a displacement in any particular direction.

Dark field imaging (figure 2.7) shows the orientation spread to be very small, as large areas of retained austenite can be illuminated using one reflection, the objective aperture used, having an angular spread of 3^{o}.

As discussed earlier (section 2.4.2), by choosing different variants of the Kurdjumov-Sachs orientation relationship, adjacent laths in a packet can be separated by high-angle, low-angle or twin boundaries. In this steel, low-angle boundaries were found to be the most common though twin boundaries were also observed.

Figure 2.8 shows interlath austenite illuminated using a $\{002\}_{\gamma}$ reflection. The lack of streaking in the ferrite pattern suggests that the degree of misorientation between the laths is small and hence they can be considered to have the same orientation. Crystallographic analysis reveals that the $(002)_{\alpha'}$ and $(002)_{\gamma}$ reflections are separated by approximately 10^{o} and as such are consistent with the Nishiyama-Wassermann orientation relationship*.

A similar situation is outlined in figure 2.9 where the more regular lath morphology can be seen. The single orientation lath structure is clearly revealed in the ferrite dark field, where the entire packet is illuminated

---

*It should be appreciated that there is only approximately 5^{o} difference in orientation between the N-W and K-S orientation relationships. The inherent inaccuracies of electron diffraction make conclusive differentiation between the two relationships difficult, and only under ideal conditions can an orientation be expressed unambiguously as one relationship or the other.

Fig. 2.7:

Composite thin foil electron micrographs of the martensite structure. Centred dark fields using the (200) austenite reflection.

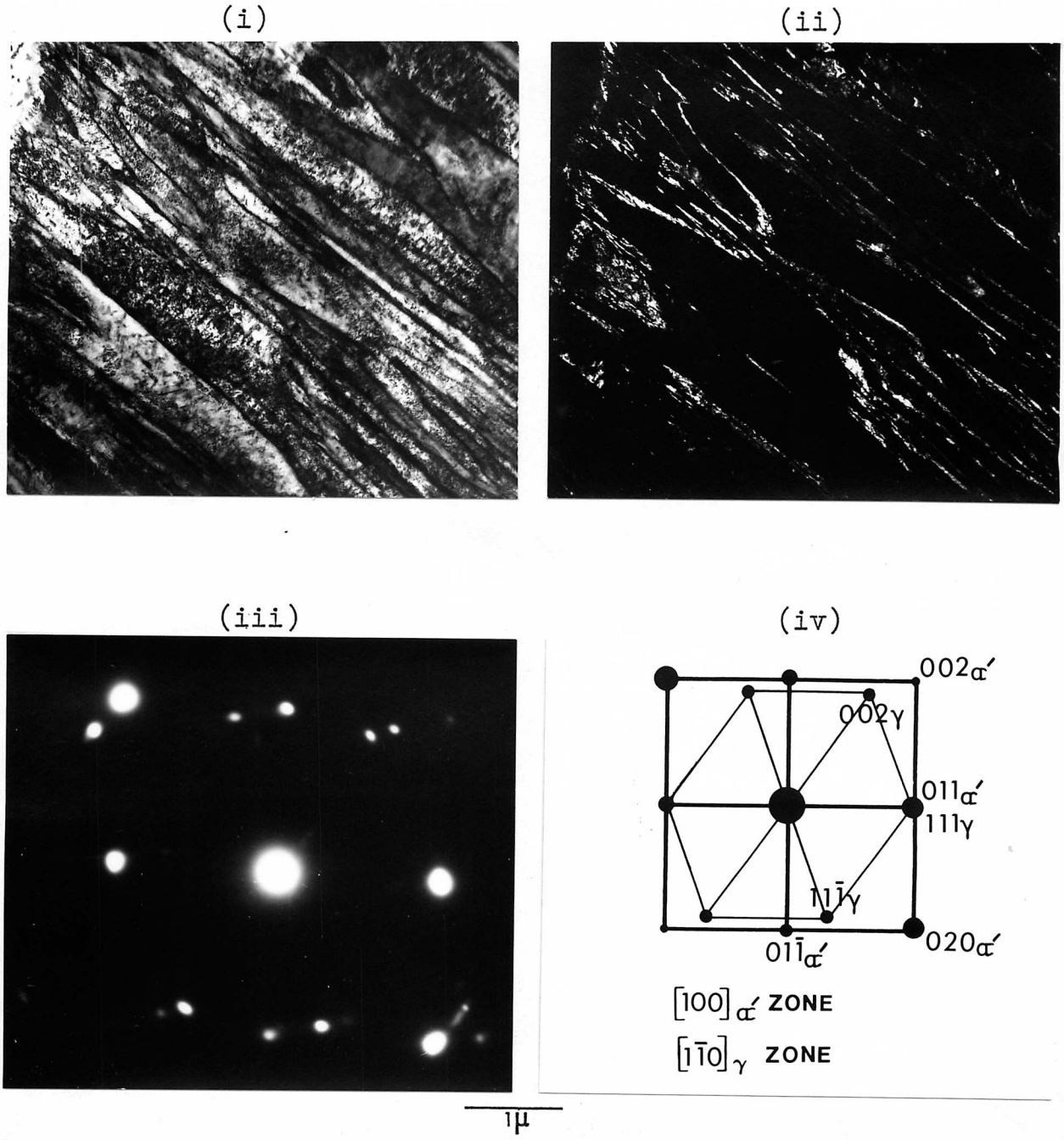

Fig. 2.8: Thin foil electron micrographs of the interwoven martensite structure.
(i) Bright field.
(ii) Centred dark field using the (00$\bar{2}$) austenite reflection.
(iii) Diffraction pattern.
(iv) Analysis consistent with either the K-S or N-W relationships between the martensite and retained austenite.

using one reflection. The bright field and the martensite dark field micrographs also highlight the dislocation substructure within the martensite laths. The interlath austenite in this case appears fragmented and streaking of the austenite reflections can be detected. This streaking is a consequence of the film-like morphology of the interlath austenite.

It is interesting to note that a high-resolution dark field micrograph, using an oxide reflection, only illuminates the oxide film associated with the austenite. This is because the oxide tends to grow epitaxially and consequently displays a different orientation on the ferrite as opposed to the austenite.

Analysis of the diffraction pattern again reveals that the martensite laths obey a N-W relationship with the austenite.

As discussed previously this may explain the presence of retained austenite in these steels, as the N-W relationship does not permit twin related laths. It was explained earlier (section 2.5.2) that twin related laths could provide a favourable condition by which any remaining austenite might transform.

However, further work has shown this explanation to be unsatisfactory. Figure 2.10 shows large quantities of interlath austenite in conjunction with twin related martensite laths. The twin related variants tend to be between groups of laths rather than individual ones; the groups themselves being composed of laths of similar orientation. This suggests that the shears associated

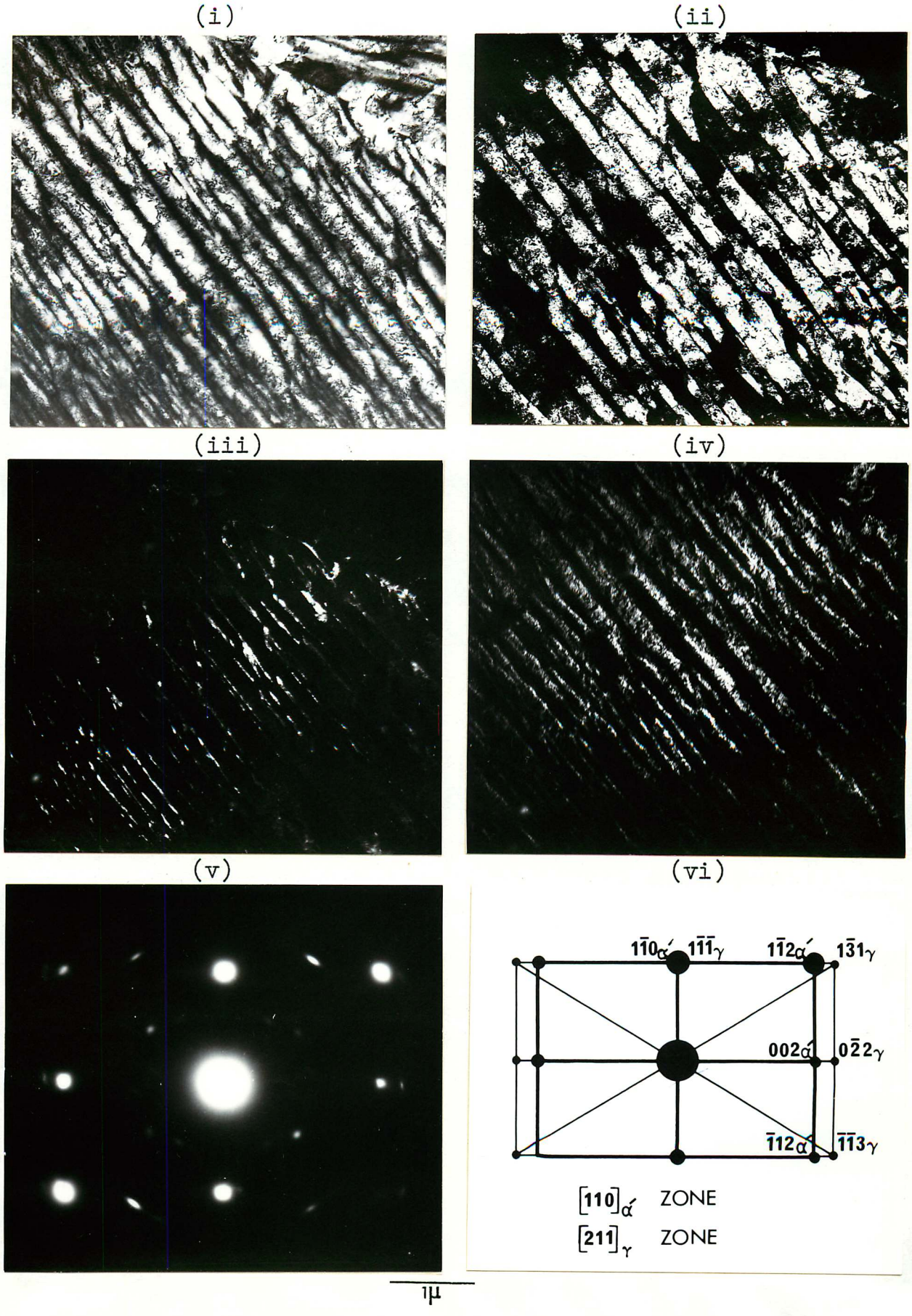

Fig. 2.9: Thin foil electron micrographs of the regular martensite structure.
(i) Bright field.
(ii) Centred dark field using the (002) ferrite reflection.
(iii) Centred dark field using the $(0\bar{2}2)$ austenite reflection.
(iv) Centred dark field using an oxide reflection.
(v) Diffraction pattern.
(vi) Analysis consistent with N-W relationship between martensite and retained austenite.

with the transformation accumulate as a packet is formed, until some magnitude is reached when the twin variant becomes favoured. Figure 2.10 also shows that a reflection which illuminates one twin variant also illuminates internal twins within the other laths.

The distribution of the austenite appears to be uniform across the packet and shows no apparent change in volume fraction whether associated with a twin or a low-angle boundary. On this basis, there is no crystallographic explanation for the presence of retained austenite in these steels. Retained austenite is present as interlath and interpacket films whether the N-W or the K-S relationship is obeyed, and is not excluded by the presence of twin related laths.

(ii) Austenite Film Thicknesses:

The thickness of the interlath austenite was measured using a series of tilting experiments, as represented in the diagram shown in figure 2.11. The derived relationship from the model gives the thickness of the austenite, t, as a function of the projected width, w, of the austenite film and the inclination, θ, of the foil normal to the beam direction.

Measurements of the projected width of the austenite against the angle of tilt were then taken to give values for the thickness of the austenite films. In order to obtain optimum accuracy, individual films were measured for a series of tilts, rather than averaging values of film thicknesses for each tilt.

The results revealed that the austenite thickness

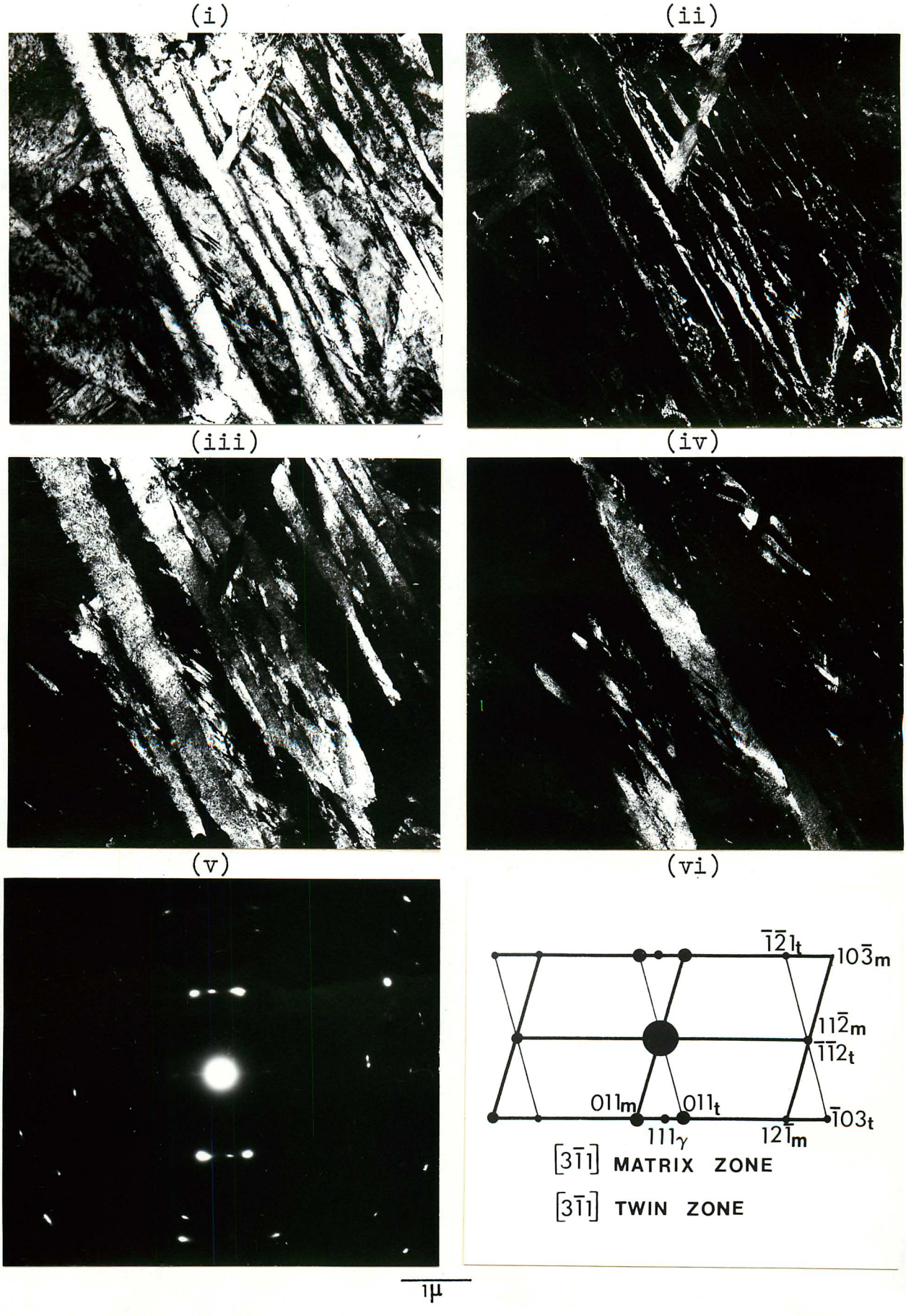

Fig. 2.10: Thin foil electron micrographs of a twinned martensite structure.
(i) Bright field.
(ii) Centred dark field using the (111) austenite reflection.
(iii) Centred dark field using the (011) matrix reflection.
(iv) Centred dark field using the (011) twin reflection.
(v) Diffraction pattern.
(vi) Analysis showing twin relationship and retained austenite.

varied depending on whether the films were located within the "interlocked" lath structure or the more regular one. The laths within the "interlocked" structure were separated by films of 83Å (standard deviation σ = 31.5) thickness while the laths within the more regular packets were separated by films of 320Å (standard deviation σ = 93). This supports the evidence that there is a genuine morphological difference between the two kinds of packet and that the apparent differences are not merely a result of sectioning effects.

(iii) Internal Structure and Distribution of Retained Austenite:

The results outlined so far demonstrate that the austenite is not only present as an interlath film but is also situated at packet boundaries. Figure 2.12 illustrates the boundary between two adjacent packets. The retained austenite along the packet boundary appears not to differ significantly in morphology or orientation from the austenite situated between the laths.

A high-resolution examination of the internal structure of the austenite is hampered not only by the magnetic nature of the specimen, but also because the austenite is sandwiched between two martensitic regions. Good contrast is therefore difficult to achieve particularly when working at high magnifications. Figure 2.12 is a high magnification micrograph of an interlath austenite film and also the martensite packet from which it originates. Some form of dislocated internal structure is evident though analysis of the dislocation types is

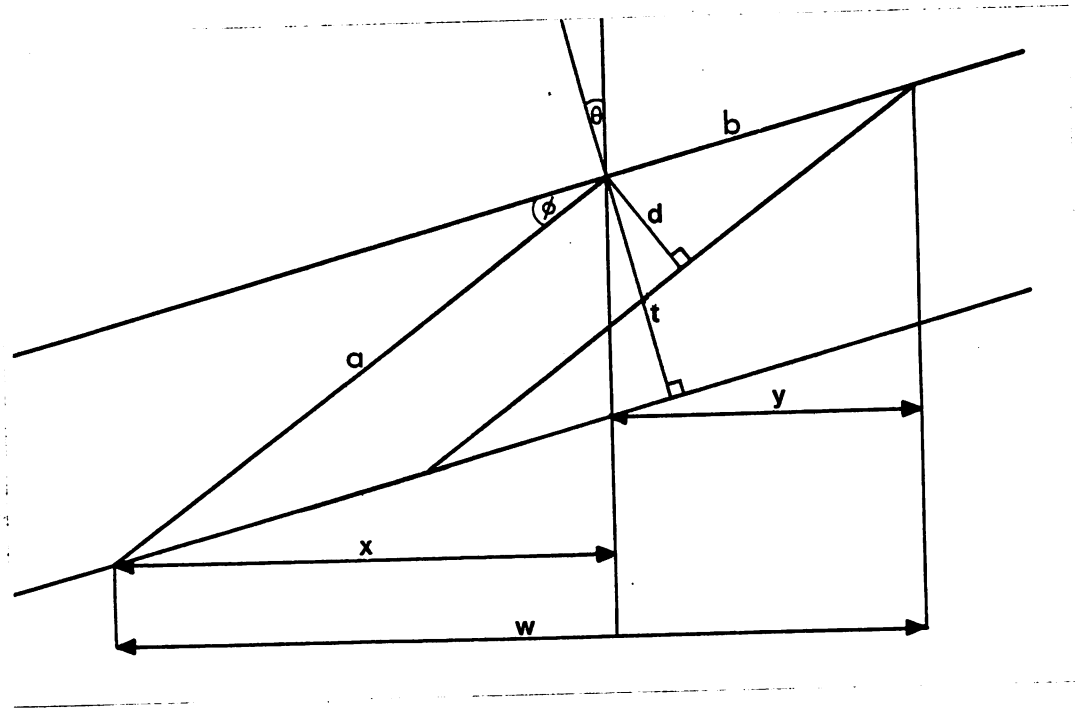

Fig. 2.11:
Derivation of the relationship used to measure retained austenite film thicknesses.

Consider an austenite film, thickness d, inclined at an angle ϕ, within a foil, thickness t. The projected width of the film is w and the tilt of the foil is θ.

$$w = x + y$$

To find x:

$$a = t/\sin\phi$$
$$x = a\cos(\phi+\theta)$$
$$x = t\cos(\phi+\theta)/\sin\phi$$

To find y:

$$b = d/\sin\phi$$
$$y = b\cos\theta$$
$$y = d\cos\theta/\sin\phi$$

$$w = t\cos(\phi+\theta)/\sin\phi + d\cos\theta/\sin\phi$$

$$d = (w - t\cos(\phi+\theta)/\sin\phi)\sin\phi/\cos\theta$$

$$d = w\sin\phi/\cos\theta - t\cos(\phi+\theta)/\cos\theta$$

$$d = (w\sin\phi - t\cos(\phi+\theta))/\cos\theta$$

$$d = (w\sin\phi - t\cos\phi\sin\theta + t\sin\phi\sin\theta)/\cos\theta$$

but t and ϕ are constant

$$d = wk_1/\cos\theta - k_2 + k_3\tan\theta$$

precluded by insufficient resolution.

2.6.5 Thermal and Mechanical Stability of the Retained Austenite

(i) Mechanical Stability:

Specimens for deformation experiments were prepared by quenching 1 mm. thick strip in iced brine to produce a martensitic structure. The strip was then rolled to impart the required deformation. Electron microscopy revealed no trace of austenite after approximately 30% reduction in thickness. As shown in figure 2.13, the lath structure contains bands of a much higher dislocation density than the surrounding material. The banding appears at the sites of the original austenite films which have decomposed to martensite under the influence of the deformation. Thus decomposition has taken place at room temperature, and hence represents a relatively low transformation temperature, resulting in enhanced dislocation generation to accommodate the transformation strains.

(ii) Thermal Stability:

(a) Tempering

The behaviour of quenched steels on tempering has been the subject of many investigations and a number of review articles (Speich and Leslie (1972), Honeycombe (1973)). It has been shown that in an alloy steel containing a strong carbide forming element, the tempering reaction passes through six stages to produce a coarse dispersion of alloy carbide. In general, tempering bet-

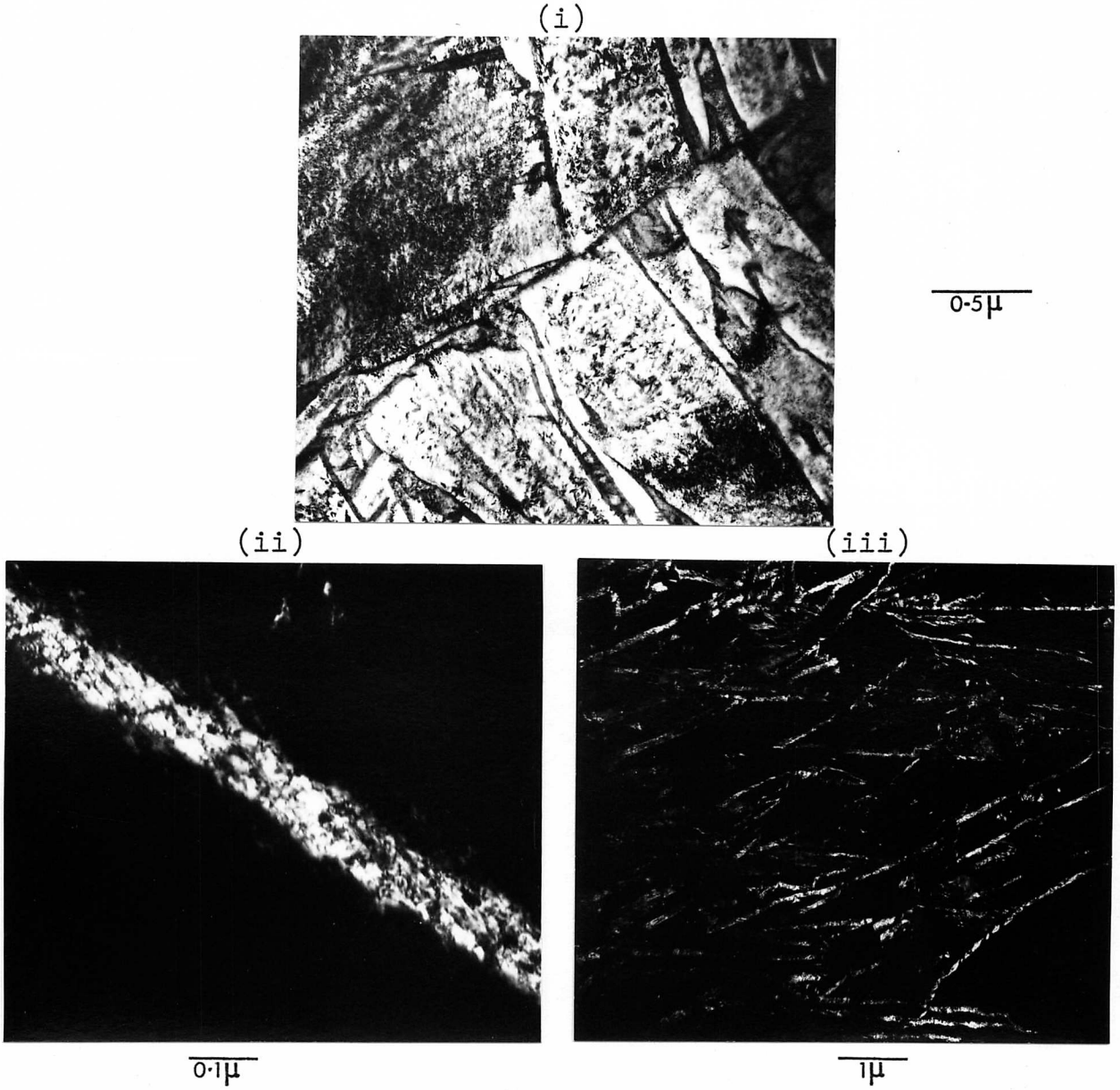

Fig. 2.12: Thin foil electron micrographs of retained austenite.
(i) An interpacket boundary.
(ii) High magnification centred dark field of retained austenite using the (200) austenite reflection.
(iii) Centred dark field of packet in which (ii) is situated.

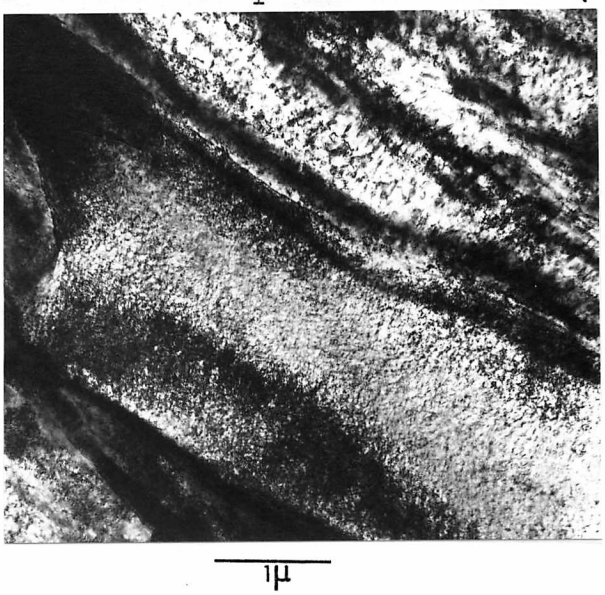

Fig. 2.13: Thin foil electron micrograph of the martensite structure deformed 30% by rolling.

ween 200°C and 400°C for one hour results in transformation of any retained austenite present, but the manner in which this occurs has not been investigated in detail.

Tempering at high temperatures produced further evidence for the existence of twin-related groups of laths in the martensite structure. Figure 2.14 is a high resolution study of the tempering of a quenched specimen for 30 mins. at 700°C. This has resulted in the complete decomposition of the retained austenite. Crystallographic analysis reveals the presence of twinning and dark field imaging shows that this is caused by large, twin-related laths. These laths were completely free from internal sub-boundaries and the dislocation density was much reduced.

This structure can be directly correlated with the untempered martensite (figure 2.10), where groups of laths within a packet were found to be separated by low-angle boundaries, but the groups themselves were found to be twin-related. It is concluded that during tempering, the retained austenite decomposes, and, as the misorientation between adjacent laths in a group is small, the interlath boundaries disappear. The twin variants after tempering are therefore the original groups of laths, where the laths within a group were separated by low-angle boundaries.

(b) Refrigeration

Specimens initially quenched in iced brine were immersed in liquid nitrogen for 30 mins. and examined in the electron microscope. The structure showed no change

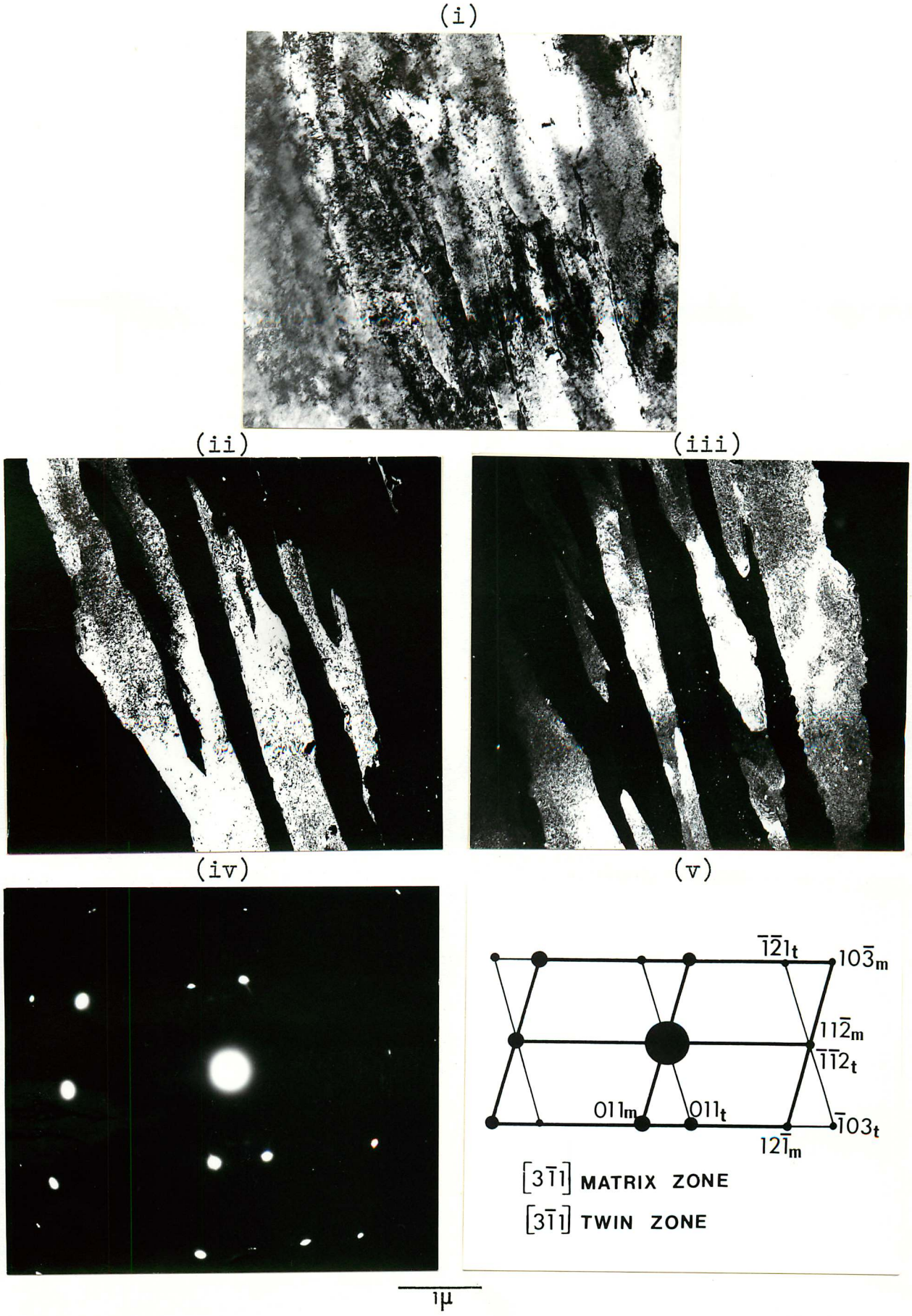

Fig. 2.14: Thin foil electron micrographs of the martensite structure tempered at 700°C for 30 mins.
(i) Bright field.
(ii) Centred dark field using the (011) matrix reflection.
(iii) Centred dark field using the (011) twin reflection.
(iv) Diffraction pattern.
(v) Analysis showing twin relationship.

from the quenched condition and it can be concluded that the films of retained austenite were completely stable under cryogenic conditions.

2.7 Summary and Conclusions

The chapter has investigated the incidence of retained austenite in some low-alloy, vanadium bearing steels. The related literature has been reviewed to introduce the concepts which may govern austenite retention. This has involved surveys of martensite formation and reported observations to date of the existence of retained austenite in low-alloy steels.

The results provide a characterisation of the martensite using optical and electron microscopy and investigate the existence of a habit plane and growth direction for the martensite laths. The laths were shown to occupy a $\{110\}_{\alpha'}$ habit plane. The difficulties in defining a discrete growth direction were discussed.

The presence of interlath and interpacket retained austenite has been proved conclusively and its orientation relationship has been established with respect to the martensite. The work showed that the retained austenite was not distorted in orientation from the original austenite and hence the orientation relationship describes the orientation of the martensite relative to the parent austenite. This has been shown to be either the Nishijama-Wassermann or the Kurdjumov-Sachs relationships and evidence suggests that both may be obeyed in different regions of the same martensite.

The retained austenite films are further characterised in terms of their distribution and morphology, and finally their stability under deformation, tempering and refrigeration were studied. 30% deformation resulted in the decomposition of the austenite films but refrigeration at -196°C for 30 mins. left the structure unaffected. Tempering for 30 mins. at 700°C effected the complete decomposition of the retained austenite to leave large twin-related martensite laths. These were correlated with the untempered structure where groups of laths were found to be twin-related. Tempering removed the inter-lath austenite to leave large laths, as the misorientation between laths in a particular group was small.

CHAPTER THREE

THE AUSTENITE TO FERRITE TRANSFORMATION IN VANADIUM BASED LOW-ALLOY STEELS

3.1 Introduction

The decomposition of austenite to proeutectoid ferrite, by diffusional processes, can display many morphological variations, (Dubé and Aaronson, 1958). The mechanisms by which these different types of ferrite grow depend upon the nature of the austenite/ferrite boundary associated with the particular ferrite crystal. The exact form that this interface displays is directly related to the relative orientations of the austenite and ferrite crystals.

In the absence of detailed crystallographic evidence, growth modes have been postulated based on the observed growth morphologies, and by comparing the growth kinetics with those predicted by classical diffusion theories, (Aaronson, 1962). Where the growth rate was not in agreement with that predicted by classical theories, mechanisms by which a mobile interface might exhibit more rapid kinetics have been suggested, (Kinsman, Eichen and Aaronson, 1975). These postulates can only be proven through direct crystallographic evidence.

The previous chapter has described how quenched low-alloy steels can retain the high-temperature austenite phase, generally as interlath films. The work reported in this chapter utilises these films to identify the crys-

tallography associated with certain morphologies of the austenite to ferrite transformation.

3.2 Scope of Chapter

In low-alloy steels, where a carbide forming element is present, the ferrite reaction may be modified by precipitation of alloy carbides. Two areas of the literature can be considered to be relevant and are reviewed in sections 3.3 and 3.4. Section 3.3 deals with the ferrite reaction in the absence of precipitation. The observed morphologies and growth modes are discussed in terms of the proposed crystallography operating in each case. Section 3.4 then investigates how the ferrite reaction may be modified by the precipitation of alloy carbide. This involves a survey of the so called "interphase" and "fibrous" precipitation reactions.

The results and discussion are presented in section 3.5 and a summary and conclusions are given in section 3.6.

3.3 The Proeutectoid Ferrite Reaction

The nucleation and growth of proeutectoid ferrite by a diffusional process can result in a wide range of ferrite morphologies. The first attempt at a formal classification of these morphologies was made by Dubé and Aaronson (1958) and has been termed the Dubé classification. The system is outlined in fig. 3.1 and describes:

(a) Grain boundary allotriomorphs: These are ferrite crystals which nucleate at austenite grain boundaries and whose major growth direction lies along the boundary.

(b) Widmanstätten sideplates: These are acicular crystals and nucleate either on the austenite grain boundary or on a pre-existing allotriomorph. Those nucleated directly on the boundary are termed "primary sideplates", and those nucleated on allotriomorphs, "secondary sideplates".

(c) Sawteeth: These have a triangular cross-section and again can be nucleated and grow as primary or secondary species.

(d) Idiomorphs: These crystals are roughly equi-axed and are usually found intragranularly although they are sometimes observed at grain boundaries.

(e) Intragranular Widmanstätten plates: These again display a typical plate morphology but are found within the grains.

(f) Massive structures: This is not a fundamental morphology as it results from the impingement of crystals of other types or from grain growth.

The classifications can be considered separately in terms of their morphology, crystallography and growth kinetics; possible growth mechanisms can then be deduced from this information.

(a) Grain Boundary Allotriomorphs

This morphology is observed at all transformation temperatures and is normally the first type to appear on the austenite grain boundaries. The allotriomorphs grow rapidly along the austenite boundaries because of enhanced diffusion rates associated with the high energy boundary. Thickening of the ferrite occurs more slowly and the

mechanisms by which this thickening occurs has been the subject of some controversy. If an allotriomorph is considered to nucleate at an austenite grain boundary where the adjacent austenite grains are irrationally oriented and if the ferrite crystal displays a rational orientation relationship with one of the austenite crystals, two types of interphase boundary can then be described:

(i) The boundary between the allotriomorph and the austenite crystal to which it is not related will be incoherent. Growth will therefore be controlled by volume diffusion of carbon.

(ii) The boundary between the allotriomorph and the austenite grain to which it bears a rational orientation relationship will be of a specific nature, because of the degree of lattice correspondence, as described by the orientation relationship. This specific lattice matching is suggested by the growth front morphology where facetted structures are often observed. These facets have been shown to influence growth kinetics, as the degree of lattice mismatch will vary depending on the orientation of the interphase boundary at any particular point (Aaronson, 1962).

Regions of good lattice correspondence can be described as approaching coherency and hence migration of such a boundary will be controlled by a slow interface reaction. Incoherent regions, or regions of high disorder, will migrate by diffusion of individual atoms across the interphase boundary. Incoherent growth can normally operate rapidly in the temperature range of the ferrite

reaction and hence incoherent boundaries can be expected to propagate more rapidly than coherent facets. Growth kinetics above that expected by standard diffusion theory are achieved in this way; the mechanism being known as the "Ledge Mechanism" and will be dealt with in greater detail when considering the growth of Widmanstätten sideplates.

Any particular allotriomorph ought therefore to be capable of growing into either of the adjacent austenite grains and indeed this has been observed (Aaronson, 1962). These results are, however, in conflict with those of Spretnak and Speiser (1954). They conclude that ferrite nucleates from austenite by a shear mechanism and consequently is unable to grow into adjacent austenite grains. Smith (1953) adopted a quite contrary viewpoint; he hypothesised that crystals could only grow by the movement of incoherent boundaries, and hence not into a grain to which the allotriomorph is related. This is clearly not the case.

The actual orientation relationship obeyed by ferrite allotriomorphs nucleating with respect to a particular austenite grain has been suggested using an indirect method. Close observation of sideplates nucleated on pre-existing allotriomorphs has shown that the sideplate is not normally separated from the allotriomorph by a discrete boundary. It can therefore be considered to be of the same orientation (Heckel and Paxton, 1961). The orientation of the allotriomorph to the austenite grain containing the appendant sideplate must therefore be of the same orientation

as the sideplate itself. Mehl, Barrett and Smith (1933) using a coarse grained, manganese steel show that pro-eutectoid ferrite sideplates obey the Kurdjumov-Sachs (1930) relationship with the grain into which they grow. Therefore the allotriomorph from which the sideplate evolves will probably also be Kurdjumov-Sachs related to the austenite grain.

(b) Widmanstätten Plates

As seen from the Dubé classification system, three types of ferrite precipitate display a Widmanstätten morphology. Essentially, they can be described as plate-like whether they be primary or secondary sideplates or intragranular plates. They all obey the same orientation relationship and hence arguments concerning growth mechanisms are purely general.

As mentioned previously, when considering the orientation of ferrite allotriomorphs, Widmanstätten plates of ferrite in austenite display the Kurdjumov-Sachs orientation relationship. Early studies by Belaiew (1923) and later by Mehl, Barrett and Smith (1933) attempt to define a habit plane for the plates. They observed that the plates exhibit four trace directions and that the angles between these traces are consistent with precipitation on octahedral austenite planes. The long faces of the plates, assuming them to be both planar and parallel, therefore occupy a $\{111\}_\gamma$ habit. Liu, Aaronson, Kinsman and Hall (1972) claim that this analysis is an oversimplification. They indicate that the trace of the edge of a Widmanstatten plate is not necessarily parallel to the

mean direction of the plate and in fact may deviate from this by a few degrees.

The growth mechanism of the plates is closely related to this crystallography, as this determines the nature of the advancing interphase boundary.

Three possible boundary types have been described by Smith (1953), though Aaronson (1962) challenged the proposed mechanisms for their growth, as Smith's model did not permit growth on both sides of a prior austenite boundary. Aaronson claims this to be a common occurrence and offers his own theories of boundary structure and the mechanisms by which they move.

(i) Incoherent:

The migration of a boundary whose structure is of a disordered nature is essentially independent of structural factors. These boundaries can therefore be considered to be isotropic and diffusion occurs rapidly along them. They consequently display appreciable mobility at elevated temperatures, where migration is largely by the independent transfer of individual atoms across the interface.

(ii) Coherent:

Coherent boundaries exist when the adjacent lattices are sufficiently well matched to accommodate each other, without the introduction of a defect structure. That is, any small differences in lattice spacing are accommodated by coherency strains. The migration rate of these boundaries is extremely slow, because the free energy change associated with the transfer of atoms across the boundary is small in the absence of a disordered boundary structure.

(iii) Partially Coherent:

Where the lattice mismatch is small, the misfit can be accommodated by the introduction of an intrinsic dislocation array. The spacing of the dislocations decreases as the degree of mismatch increases, until the dislocation cores overlap and individual dislocations can no longer be identified. The boundary thus breaks down to a disordered type.

The presence of dislocations to form a partially coherent boundary has a powerful influence on the possible growth mechanisms of that boundary. For instance, if dislocations within the boundary are sessile in the direction in which the boundary migrates, then growth will stop. Even in the case where the boundary has a completely glissile dislocation structure, growth will be impeded because of the need to impart a composition change at the interface. Such a composition change would occur by the individual transfer of atoms and hence may be incompatible with the movement of glissile dislocations.

It has been suggested that the means by which these factors limiting growth are overcome, in the case of coherent and partially coherent boundaries, is by growth through a ledge mechanism (Aaronson, 1962).

In general terms, the long faces of the ledge are considered to be of either a coherent or a partially coherent nature and the short faces to be incoherent or disordered. The migration of the boundary occurs by the repeated propagation of the incoherent facets lateral to the direction of growth (fig. 3.2).

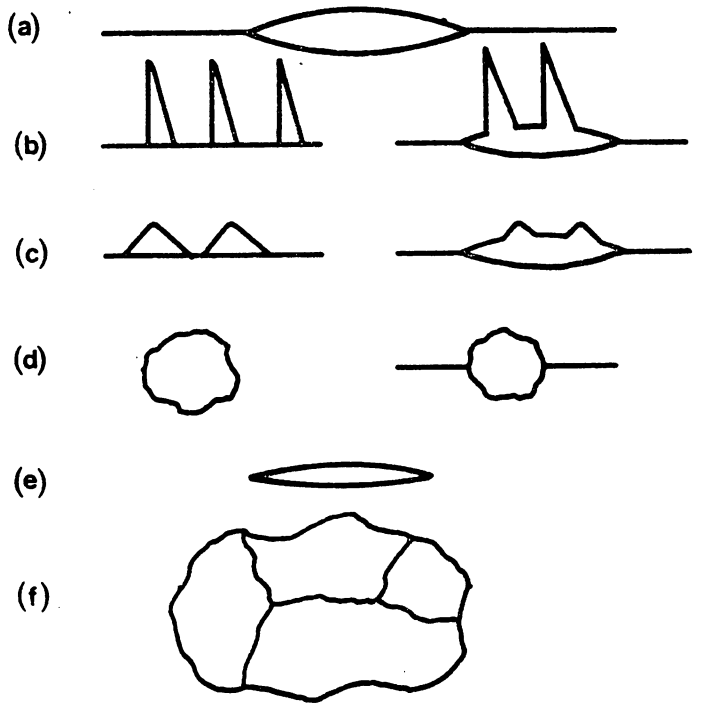

Fig. 3.1: The Dubé morphological classification system
(a) Allotriomorph
(b) Widmanstätten Sideplates
(c) Sawteeth
(d) Idiomorphs
(e) Intragranular Widmanstätten Plates
(f) Massive Structures

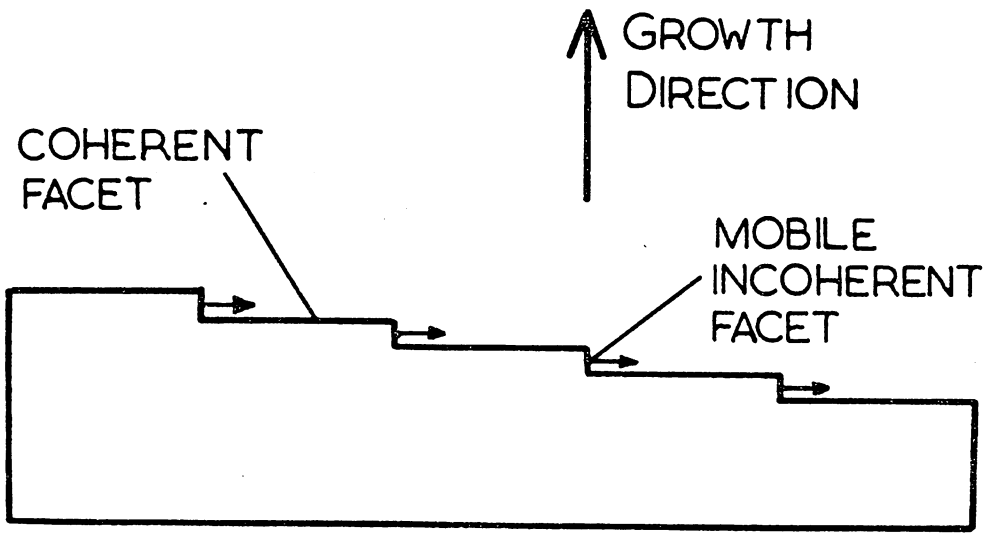

Fig. 3.2: The "Ledge Mechanism" for the growth of proeutectoid ferrite. (After Aaronson, 1962).

Because of the less direct diffusion path, Aaronson et al. (1970) predicts that such a boundary would be less mobile than a disordered boundary at the same temperature.

The orientation dependance of the growth front of an interface where the ledge mechanism is operating, has a strong influence on the morphology of the product. Hence the platelike nature of Widmanstätten precipitation.

The mechanism by which ledges are nucleated or by which a planar boundary degenerates to produce a stepped interface has not yet been established. This is an important consideration as the rate of formation of ledges will have an influence on the migration kinetics of the boundary. The other factors affecting this migration rate will be the height of the disordered ledges and their lateral migration rate. Further work is necessary to establish which, if any, is the rate controlling process.

It should be noted that the ledges responsible for growth are, according to Aaronson (1962), of atomic dimensions. However, if the progress of these ledges is impeded, then they may form what Aaronson has termed "superledges" and which have been viewed using optical microscopy (Aaronson, 1962).

The ledge mechanism of growth has been shown to be generally applicable to alloy systems other than steels, (Laird and Aaronson (1967, 1968, 1969), Aaronson and Laird (1968)). However, considering specifically the decomposition of austenite to ferrite, the nature of the ledges can be more precisely described. Previous work, often using model systems, has intimated that ferrite forms with

a Kurdjumov-Sachs orientation relationship with the austenite (Ryder, Pitsch and Mehl, 1967). These results were later confirmed by King and Bell (1975) working on a 0.47%C steel and using Kossel X-ray microdiffraction. They also confirmed the inference made by Aaronson (1962) that the K-S relationship is displayed by all proeutectoid ferrite crystals, with at least one of the adjacent austenite grains, regardless of morphology.

This identifies the long faces of the ledges to be close to $\{110\}_\alpha$, $\{111\}_\gamma$. However, in considering their mobility Aaronson's definitions of coherency and partial coherency prove inadequate as they provide an oversimplified explanation which does not extend to the three dimensional situation.

Bollman (1976) has shown that the mismatch can be described in terms of three sets of orthogonal dislocation structures in fcc/bcc interfaces. The dislocation spacing for any particular set will vary depending upon the degree of misfit requiring accommodation. Thus, coherency will be approached as the dislocation spacing tends to infinity, while an incoherent boundary will result when the dislocation seperation becomes so small that the cores overlap and individual dislocations cannot be recognised. A boundary may therefore be coherent with respect to one set of planes but incoherent or partially coherent with respect to others.

For an austenite/ferrite boundary, displaying the K-S or N-W orientation relationships, complete coherency is not possible because of the differences in crystal

structure and lattice spacing between the two phases.

The $(110)_\alpha / (111)_\gamma$ facet can be described as coherent in the dimension where the planes are parallel and the dislocation spacing is clearly infinite. However, the other two sets of boundary dislocations are spaced so closely together that the dislocation cores overlap and the individual dislocations lose physical significance. The boundary might be said to be disordered with respect to these dislocations.

The so called incoherent facet, (Aaronson, 1962) when described in terms of the three dislocation structures, in fact possesses one set of dislocations which have a finite meaningful spacing because of the similarity of lattice spacing between the $\{110\}_\alpha$ and $\{111\}_\gamma$ planes. The other two dislocation sets again are sufficiently closely spaced as to lose any physical significance.

Recent work by Southwick, Howell and Honeycombe (1977) on an α/γ duplex steel, has investigated the influence of boundary orientation on the nature of the interfacial structure, where the two phases are related by a K-S orientation. Fig. 3.3 is a dark field image of an austenite grain growing within a ferrite matrix (N.B. The fact that this is ferrite transforming to austenite and not vice versa has no influence on the boundary structure). The boundary is seen to be free of dislocations along the coherent facet, where the $(111)_\gamma$ and $(110)_\alpha$ planes abut. As the boundary deviates, a dislocation structure is introduced, the spacing decreasing as the degree of misfit increases. However, it can be seen from the use of this reflection

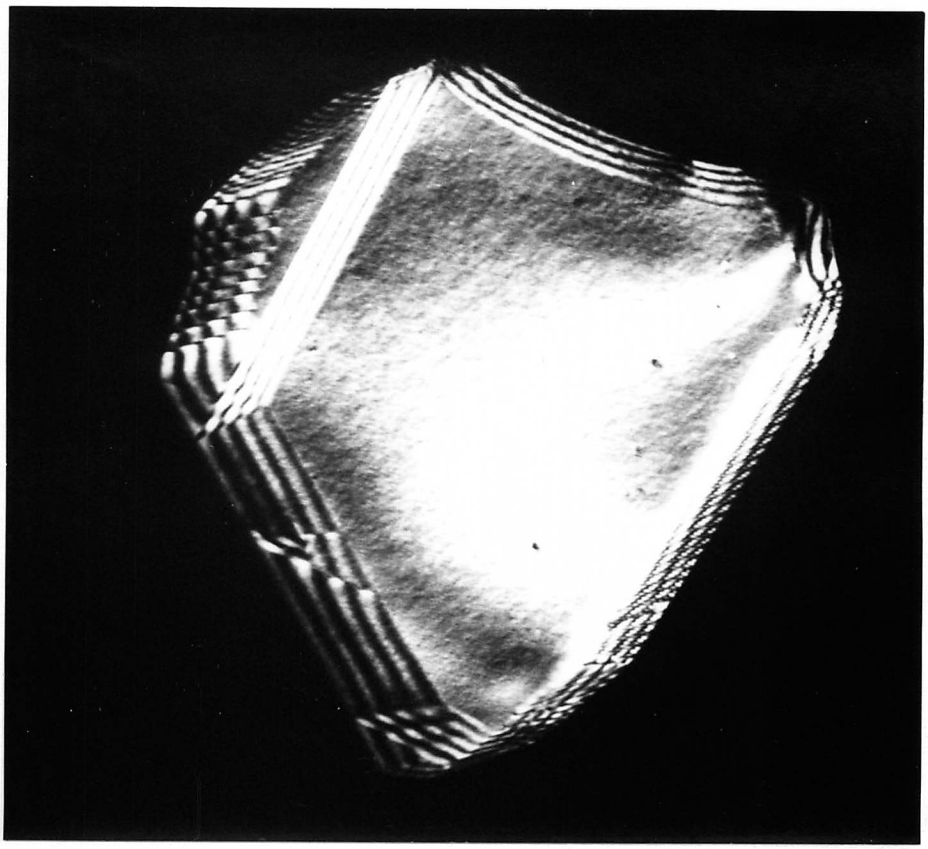

Fig. 3.3: Centred dark field thin foil electron micrograph of a 26Cr-6.5Ni-0.03C duplex steel, using the (200) austenite reflection.

(Courtesy of P.D. Southwick, P.R. Howell and R.W.K. Honeycombe)

that the boundary never achieves complete incoherency with respect to all the intrinsic dislocation structures.

In practice, the $(110)_\alpha/(111)_\gamma$ facet is immobile as there is no mechanism by which it can readily move. The shorter facet of the ledge is of a sufficiently disordered nature to enable it to propagate by the volume diffusion of solute.

The boundary as a whole thus moves outward by the lateral movement of ledge facets along the interface as shown in fig. 3.2.

3.4 Interphase Precipitation

The proeutectoid ferrite reaction in steels has been shown to be influenced by the presence of a strong carbide forming element. Precipitation of alloy carbide in a number of systems has been found to occur in association with the austenite to ferrite transformation (Honeycombe, 1976).

The structure of the transformation product is a characteristic one, consisting of rows of fine aligned precipitates, and has led to much speculation as to the mechanism by which the reaction occurs.

The first observations of aligned precipitation were made by Morrison (1963) and Leslie (1963) during an investigation of the use of niobium as an austenite grain refining element. Increments of strength above that predicted by the Hall (1951)-Petch (1953) relationship were shown to be caused by

Since these early investigations, the phenomenon of aligned precipitation has been observed in a number of ferrous systems. Normally this requires the presence of a strong carbide forming element, and to date aligned precipitation of this kind has been observed in steels bearing niobium carbide (Morrison, 1963); vanadium carbide (Greday, 1964); chromium carbide (Mannerkoski, 1964); molybdenum carbide (Davenport, Berry and Honeycombe, 1968); titanium carbide (Freeman, 1971); tungsten carbide (Davenport and Honeycombe, 1971) and tantalum and zirconium carbides (Paetke, Beaven and Edmonds, 1975).

However, aligned dispersions are not restricted solely to alloy carbides, aligned copper precipitation having been reported by McIvor (1969) in mild steels.

The phenomenon of interphase precipitation seeems possible, therefore, in any system where there is a considerable difference in solute solubility between the high temperature and low temperature phases, particularly where one of the precipitating solute species has a low diffusivity in the low temperature phase.

3.5 Fibrous Precipitation

Baker and Nutting (1959) working on the tempering of Cr-Mo-V-W steels, encountered fibrous alloy carbides adjacent to austenite grain boundaries and occurring in parallel arrays normal to the boundary. Many workers have since reported similar microstructural observations, e.g. fibrous alloy carbide has been observed in steels bearing molybdenum (Edmonds and Honeycombe, 1973); vanadium

(Batte and Honeycombe, 1973); and chromium (Campbell and Honeycombe, 1974).

Berry and Honeycombe (1970) have suggested that this morphology may be an alloy carbide equivalent of the pearlite reaction where the fineness of the structure is a function of the diffusivity of the carbide former rather than that of carbon.

Both the fibrous and interphase reactions are known to occur under similar conditions of temperature and composition; in fact they are often encountered in the same area of the same specimen. The reasons why two very different transformation products should form under identical conditions has not been established. Work by Batte and Honeycombe (1973) has suggested that fibre formation is more prevalent at higher temperatures, where the transformation occurs at a lower rate. These findings were substantiated by the work of Wilyman (1976), who went on to show that fibre formation was also encouraged by the addition of certain alloying elements, notably manganese and nickel. These were also found to reduce considerably the overall rates of transformation, moving the TTT curves to lower temperatures and longer times.

3.6 Mechanisms of Interphase and Fibrous Precipitation

Early work by Morrison (1963) was the first to propose that the alignment of precipitates in rows is associated with the ferrite transformation front. He proposed that precipitation could occur on dislocations introduced parallel to the interface as a result of the auste-

nite/ferrite transformation. These views were later reaffirmed by Tanino, Suzuki and Aoki (1968), working on vanadium and niobium low-alloy steels.

However, this opinion is not widely accepted; the majority of workers favour theories that precipitation is more closely associated with the interface itself. Heikkinen (1973a) pointed out that dislocation trails of the length usually associated with the rows of precipitate are rarely seen. Instead he has proposed a mechanism by which precipitation occurs on the austenite/ferrite interface pinning it (1973b). The interface then progresses by a bowing mechanism between the precipitates (fig. 3.4b).

Gray and Yeo (1968) discarded the possibility that precipitation occurred in the austenite because the rows of precipitate never crossed ferrite grain boundaries. They proposed that precipitation occurred at the austenite/ferrite boundary but in association with the austenite rather than the ferrite. This general view was supported by Davenport, Berry and Honeycombe (1968) though they produced evidence to suggest that the precipitate grew in association with the ferrite rather than the austenite. This is inferred by the fact that the alloy carbide in a vanadium bearing steel was shown to obey an orientation relationship with the ferrite. This was interpreted as the Baker-Nutting (1959) relationship, commonly found in quenched tempered vanadium steels.

They also noticed that in any one area only one habit of the possible three was displayed. Further work by Davenport and Honeycombe (1971) proposed that the particular habit offering the shortest diffusion path for the alloying element is selected. Unwin and Nicholson (1969), investigating grain boundary precipitation, discovered that single habits were frequently displayed over the entire boundary between two adjacent grains. They attributed this to the precipitates occupying the habit which involves the least surface strain energy.

Davenport and Honeycombe (1971) went on to suggest a mechanism for the deposition of aligned precipitate involving the partitioning of carbon. This is shown in fig. 3.4a where the advancing interface migrates to cause a build-up of carbon ahead of the reaction front. At a critical concentration, precipitation of the alloy carbide occurs, depleting the carbon concentration in the adjacent austenite. This results in an increase in the driving force for the reaction. The interface can thus migrate until the process is repeated.

A mechanism, propounded by Campbell and Honeycombe (1974), involves the translation of incoherent ledges, lateral to the advancing interface in much the same manner as Aaronson (1962) has described for proeutectoid ferrite. However, the height of the ledges corresponds more closely to what Aaronson termed "superledges". Campbell and Honeycombe produced convincing electron micrographs of the process in a chromium steel, where the precipitation is particularly coarse. No evidence has yet been presented

to show that this mechanism operates in other systems, where the precipitation is of a much finer nature. The process is shown schematically in fig. 3.4c.

The theories of fibrous growth, in contrast to that of interphase precipitation, are by no means well developed. Edmonds (1973) considered that at high temperatures, where diffusion rates are high but nucleation rates for precipitation are low, it may be possible for a slow moving interface to allow the continued growth of alloy carbide to produce a fibrous morphology. Similar ideas were proposed by Edmonds and Honeycombe (1973) working on an iron-molybdenum steel. They pointed out that a ferrite allotriomorph is often related to one or other of the austenite grains at the boundary on which it nucleates and that growth of the coherent side is normally slow. They suggested that the sluggishness of the coherent boundary may permit the continual growth of alloy carbide to produce fibres. However, there is no direct evidence in support of this theory owing to the lack of crystallographic evidence to describe the austenite/ferrite orientation relationship.

3.7 Results and Discussion

3.7.1 Alloys and Heat Treatments

The alloys used in this chapter were identical to those used in the previous chapter for the study of retained austenite, i.e.:

A1 Fe-IV-0.2C

A2 Fe-IV-0.2C+1.5Mn

A3 Fe-IV-0.2C+1.5Ni

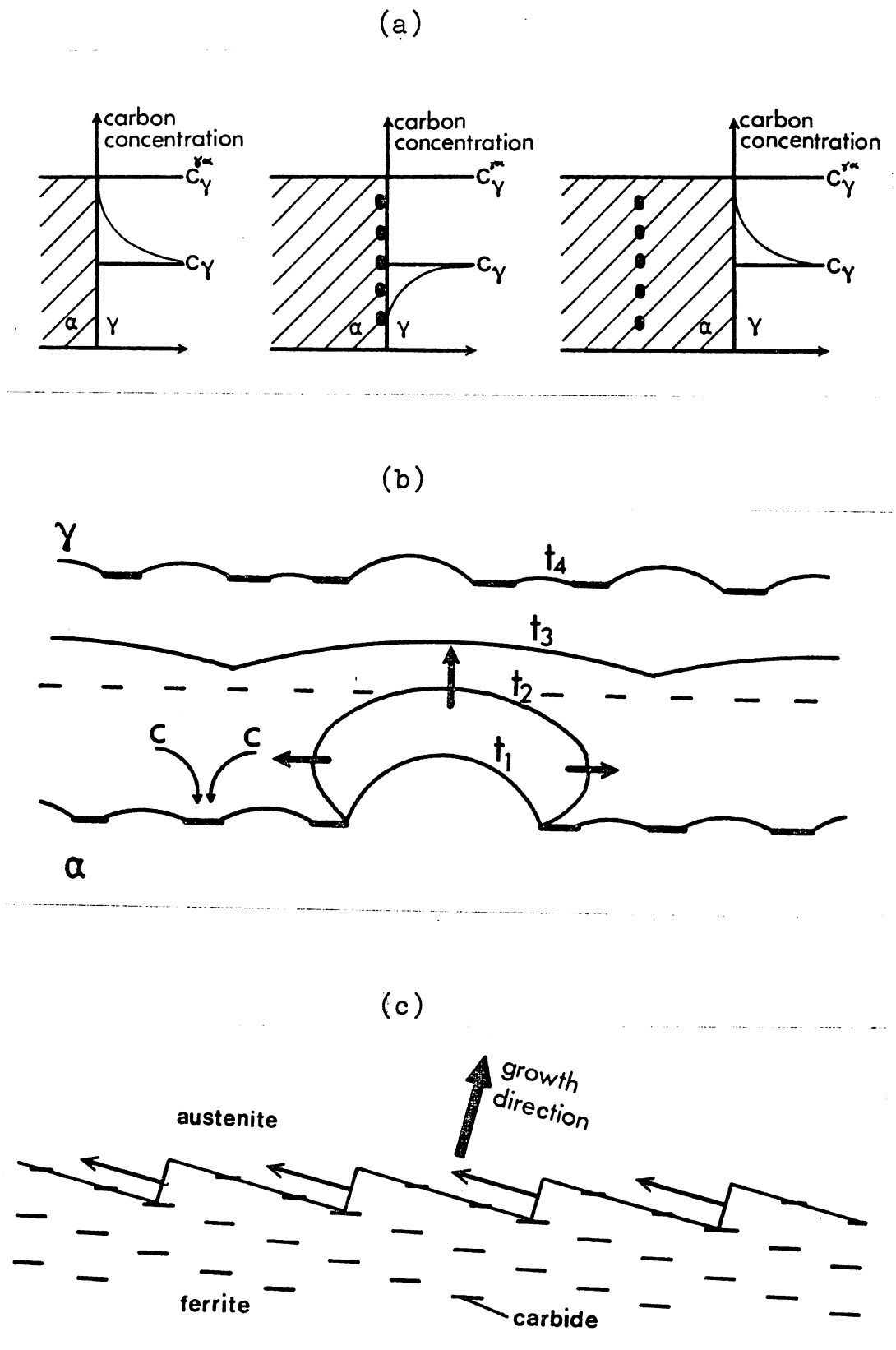

Fig. 3.4: Mechanisms for the formation of aligned carbide dispersions.

(a) After Davenport and Honeycombe, 1971.
(b) After Heikkinen, 1973b.
(c) After Campbell and Honeycombe, 1974.

The work of the previous chapter revealed no major difference between the alloys so far as the phenomenon of retained austenite is concerned. However, in this chapter the influence of quaternary additions of nickel and manganese on the characteristics of the ferrite reaction have been investigated.

The experiments were largely based on partial transformation studies and consequently, accurate data on the transformation kinetics was required. The existing data of Batte (1970) and Wilyman (1976) on similar alloys proved incompatible because of their use of a two stage solution treatment to reduce the austenite grain size. TTT curves for the three alloys were determined using 3mm. diameter rod specimens cut into 15mm. lengths. The specimens were sealed in silica tubes to prevent oxidation and decarburisation and were austenitised at 1200°C for 30 mins. Transformations were carried out in a molten tin bath followed by quenching into iced brine. This practice both facilitated the retention of austenite in the partially transformed specimens and also the preservation of the interphase boundary structure by minimising boundary migration during the quench.

The TTT curves for the three alloys are shown in fig. 3.5. The quaternary additions of nickel and manganese can be seen to depress the curves to lower temperatures and longer times.

3.7.2 Optical Investigations

The high solution treatment temperature resulted in a large austenite grain size of approximately 300μm.

(i)

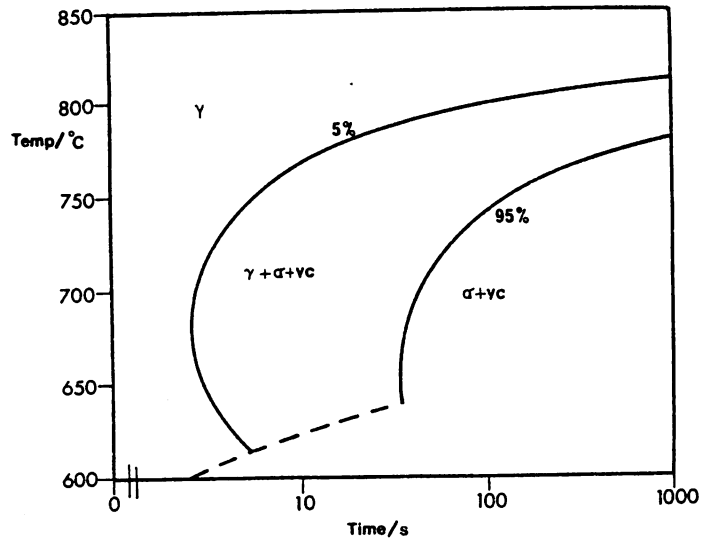

(ii)

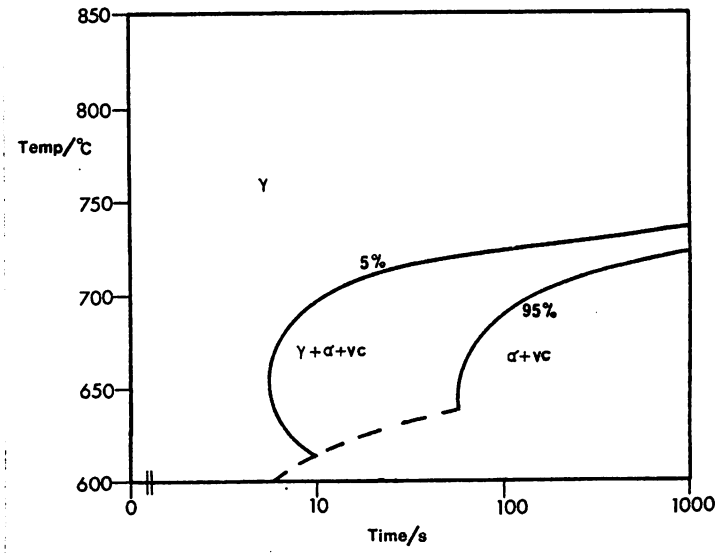

(iii)

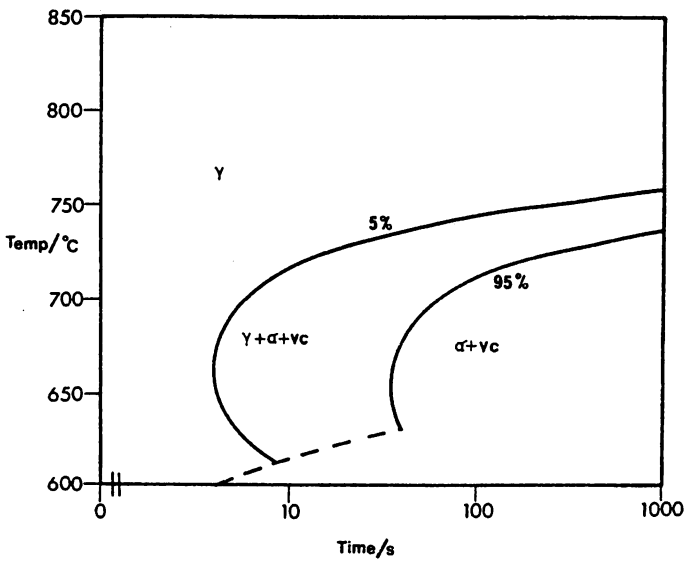

Fig. 3.5: Isothermal transformation curves after solution treatment at 1200°C for 30 mins.

(i) Fe-IV-0.2C
(ii) Fe-IV-0.2C-1.5Mn
(iii) Fe-IV-0.2C-1.5Ni

Although this hindered electron microscopic investigation of specimens with only a small amount of transformation, because of the low incidence of grain boundaries, it assisted in the interpretation of optical microstructures. This is because impingement of ferrite grains was not encountered until longer reaction times.

Fig. 3.6 shows a series of micrographs in the very early stages of transformation, the specimens having been transformed at temperatures ranging from 675°C to 795°C. The ferrite has nucleated exclusively at the austenite grain boundaries. In general, but more particularly at the lower transformation temperatures, the ferrite nuclei grow into one grain only and on many occasions, separate nuclei can be seen to abut from each side of a prior austenite grain boundary. Qualitatively the number of ferrite nuclei present on the boundaries can be seen to increase with decreasing temperature.

The morphology of the nuclei themselves suggests allotriomorphic growth with a strong preference for development into one or other of the adjacent austenite grains. The transformation front displays a marked facetted appearance throughout the transformation range, although this is more evident at the lower transformation temperatures (fig. 3.6). The micrographs also show that impingement of ferrite nuclei is often accompanied by the introduction of either a sub-grain or a grain boundary.

3.7.3 Preliminary Electron Microscopy Investigations

Bright and dark field electron microscopy of fully

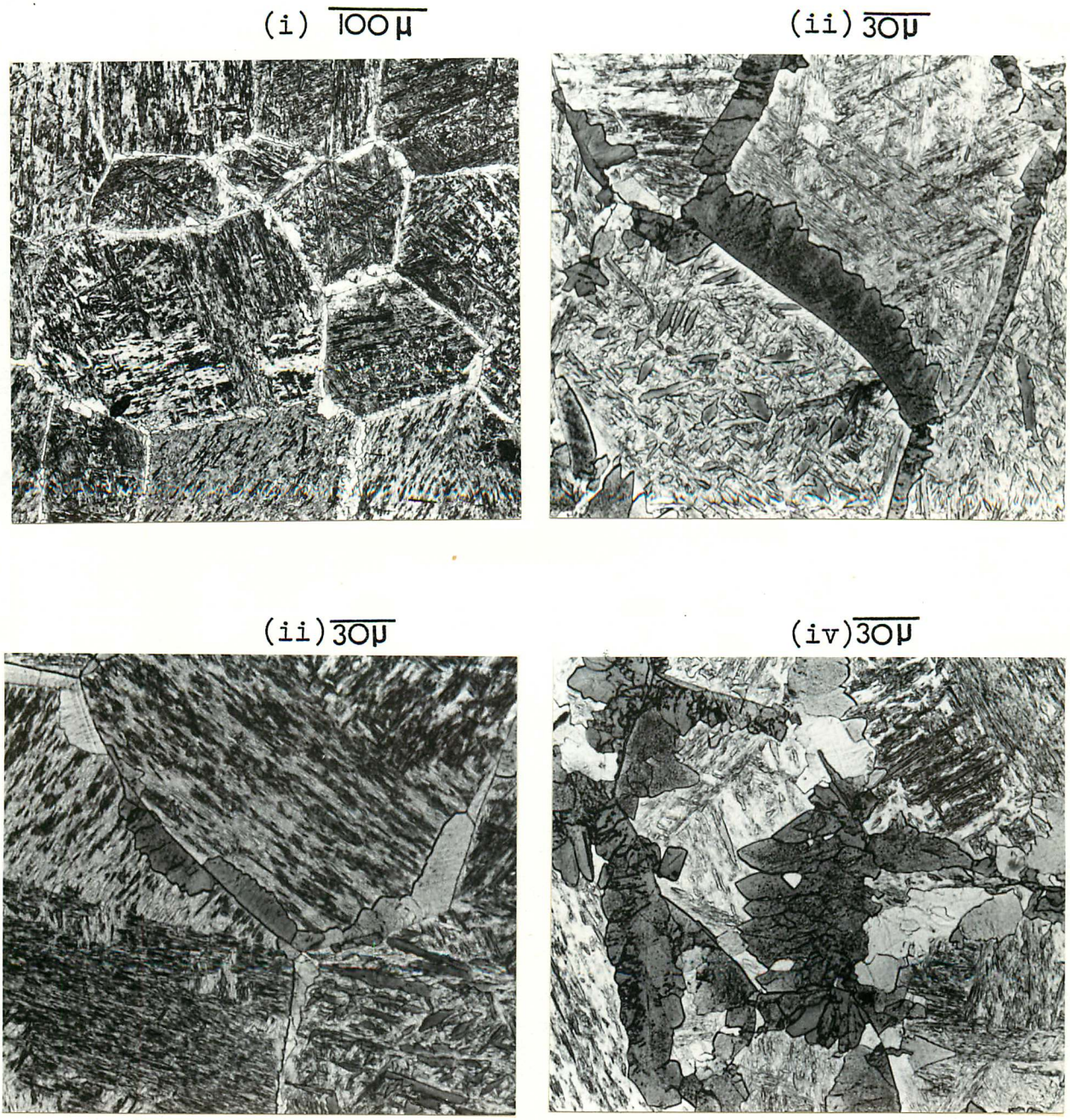

Fig. 3.6: Optical micrographs of partially transformed and quenched structures.
(i) Fe-IV-0.2C transformed 2 mins. at 795°C.
(ii) Fe-IV-0.2C transformed 10 secs. at 675°C.
(iii) Fe-IV-0.2C-1.5Mn transformed 30 secs. at 700°C.
(iv) Fe-IV-0.2C-1.5Ni transformed 30 secs. at 725°C.

transformed specimens revealed the classical structures of interphase and fibrous precipitation. In agreement with other workers (Dunlop (1974), Wilyman (1976)) the incidence of fibrous precipitation increased with increasing transformation temperature. A much more marked influence on the relative amounts of interphase and fibres was experienced by the additions of manganese and nickel. Alloys A2 and A3 exhibited appreciable fibrous growth even at the lower transformation temperatures. This is a result of the diffusivities of both vanadium and carbon being reduced by the presence of substitutional solute additions.

Fig. 3.7 shows a series of micrographs of interphase and fibrous precipitation in the three alloys. Diffraction evidence confirmed that the precipitate in all three alloys, whether of an interphase or fibrous nature, was of vanadium carbide and displayed the Baker-Nutting (B-N) (1959) orientation relationship with the ferrite (fig. 3.7).*

The B-N relationship is in fact an alternative expression of the Bain (1930) relationship. The Bain relationship expresses the orientation of the bcc ferrite lattice with respect to the fcc austenite, while the B-N relation-

---

* Considerable care must be taken in the interpretation of diffraction patterns in these steels as the precipitates have a platelet morphology and can result in excessive streaking of diffraction spots (fig. 3.8). These streaks may well extend to adjacent reciprocal lattice layers so that diffraction intensity is recorded anomalously, producing erroneous results. It is advisable therefore, to index zones where the streaking is in the plane of the pattern.

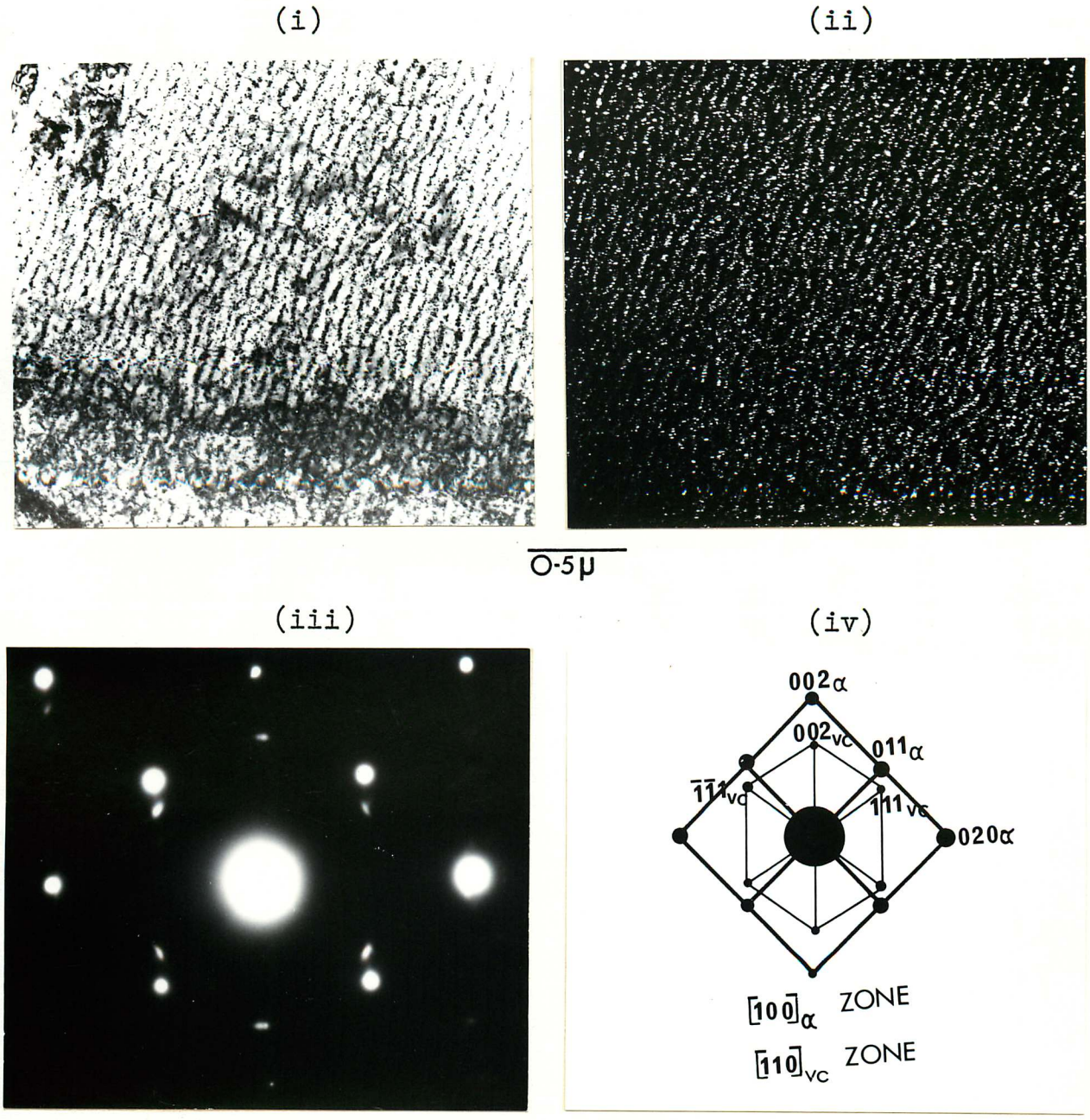

Fig. 3.7a: Thin foil electron micrographs of ferrite, directly transformed at 795°C in Fe-IV-0.2C.
(i) Bright field.
(ii) Centred dark field using the $(11\bar{1})$ vanadium carbide reflection.
(iii) Diffraction pattern.
(iv) Analysis showing the B-N relationship.

(i)

(ii)

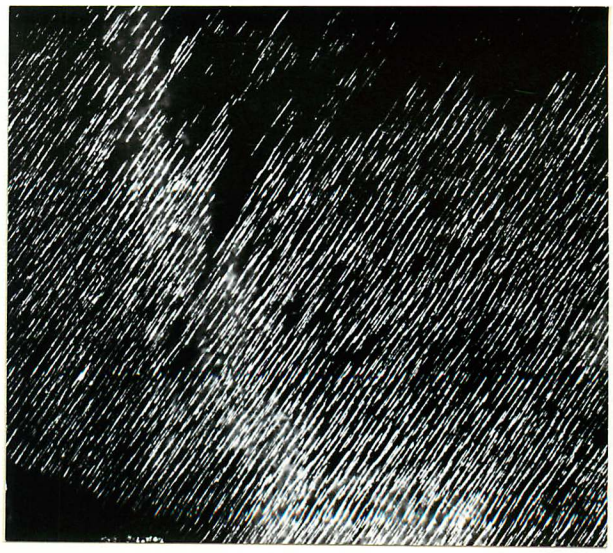

0·5 μ

(iii)

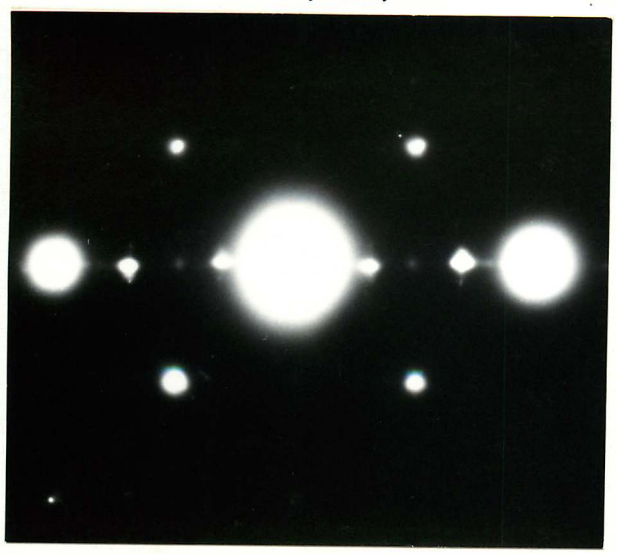

(iv)

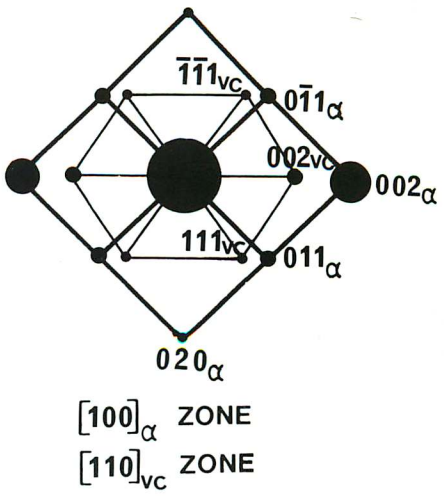

Fig. 3.7b: Thin foil electron micrographs of ferrite, directly transformed at 725°C in Fe-IV-0.2C-1.5Ni.
(i) Bright field.
(ii) Centred dark field using the (oo2) vanadium carbide reflection.
(iii) Diffraction pattern.
(iv) Analysis showing the B-N relationship.

ship describes the orientation of an fcc precipitate with respect to a bcc matrix. Fig. 3.9 shows that the two relationships are equivalent.

The parallelism of the aligned precipitate rows, as shown by electron microscopy, poses the question as to whether the precipitate sheets conform to a rigid habit plane. To investigate this, single surface trace analysis was carried out on a number of fully transformed specimens, over the complete range of transformation temperatures. Fig. 3.10 reveals that the traces cluster strongly around a $\{110\}_{\alpha}$ plane. This identifies a habit plane of low index and suggests that the reaction front may proceed according to a precise crystallography. A $\{110\}_{\alpha}$ habit in particular infers that the ferrite crystal might bear a K-S or an N-W relationship with the austenite into which it is growing. This is because if the transformation obeys either of these relationships, then parallelism is displayed between the $(110)_{\alpha}$ and $(111)_{\gamma}$ planes. These are also the conditions described by Aaronson (1962) for growth of a coherent interface by a ledge mechanism.

Evidence was therefore sought to relate the parallel precipitate rows to the transformation front. Partial transformation studies were employed whereby specimens are quenched into iced brine after a small percentage of the austenite had transformed to ferrite.

Fig. 3.11 is a carbon extraction replica showing examination of the early stages of transformation in the ternary and the nickel quaternary alloys. The simple ternary alloy displayed angular protruberances along the

(i)

0·5μ

(ii)

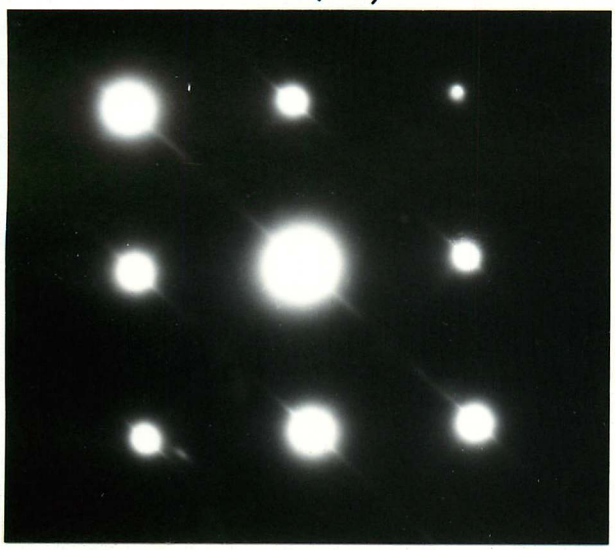

(iii)

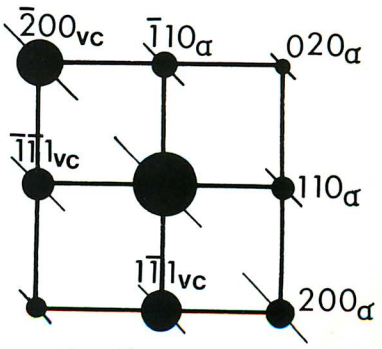

Fig. 3.8: Thin foil electron micrographs of Fe-IV-0.2C directly transformed at 700°C for 2 mins.
(i) Bright field.
(ii) Diffraction pattern showing streaking in the (100) direction.
(iii) Analysis showing the B-N relationship.

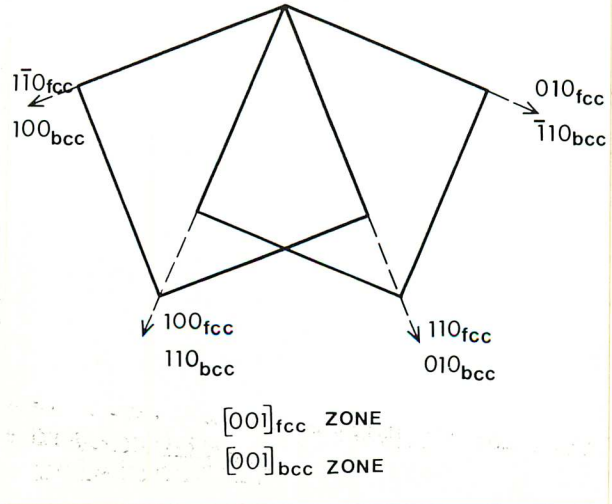

Baker-Nutting Relationship

$(001)_{vc}$ // $(001)_{\alpha}$
$(\bar{1}10)_{vc}$ // $(010)_{\alpha}$
$(110)_{vc}$ // $(100)_{\alpha}$

Bain Orientation

$(100)_{bcc}$ // $(100)_{fcc}$
$(01\bar{1})_{bcc}$ // $(010)_{fcc}$
$(011)_{bcc}$ // $(001)_{fcc}$

Fig. 3.9: Derivation of the Baker-Nutting and Bain orientation relationships.

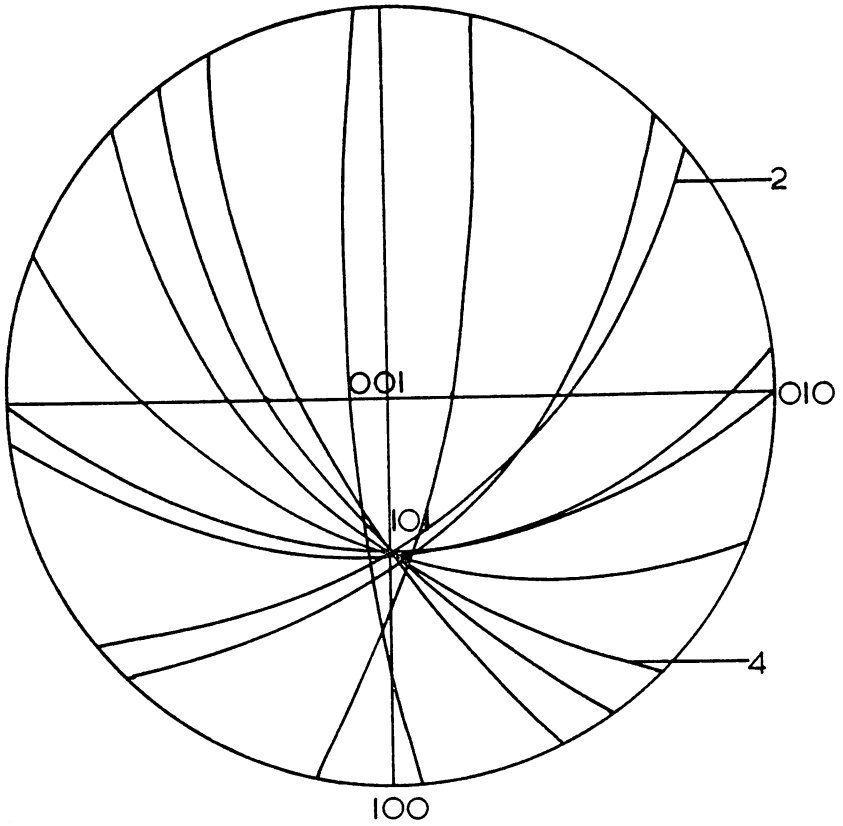

Fig. 3.10: Trace analysis of the sheets of interphase precipitation consistent with a $\{110\}_\alpha$ habit plane.

austenite boundaries where the individual ferrite crystals nucleate (fig. 3.11a). However, precipitation was too fine to be extracted by the replica technique. Quaternary additions of nickel produced a large percentage of fibre formation, as shown in fig. 3.11b. Careful examination also reveals a small amount of transformation on the opposite side of the prior austenite grain boundary.

Thin foil examination of the same series of specimens produced further indirect evidence that the long faces of the ferrite nuclei are parallel to $\{111\}_\gamma$ planes. Fig. 3.12 illustrates a series of ferrite nuclei along an austenite grain boundary adjacent to a single martensite packet. As confirmed in the last chapter, martensite laths in low carbon steels occupy a $\{111\}_\gamma$ habit. This particular foil specimen was not sufficiently thin to obtain conclusive diffraction information, but the fact that the martensite laths lie parallel to the long faces of the ferrite crystals, is consistent with these faces being parallel to $\{111\}_\gamma$ planes and also to $\{110\}_\alpha$ planes should a K-S or N-W relationship be obeyed.

Figs. 3.13a and 3.13b are of a single ferrite allotriomorph, which has nucleated at an austenite grain boundary in the vanadium/manganese steel. These micrographs display strong morphological evidence for the inferences previously outlined, although diffraction evidence proved insufficient for a conclusive analysis.

Fig. 3.13a depicts the two morphologies of alloy carbide precipitate associated with the same ferrite nucleus. The fibrous side of the prior austenite boundary

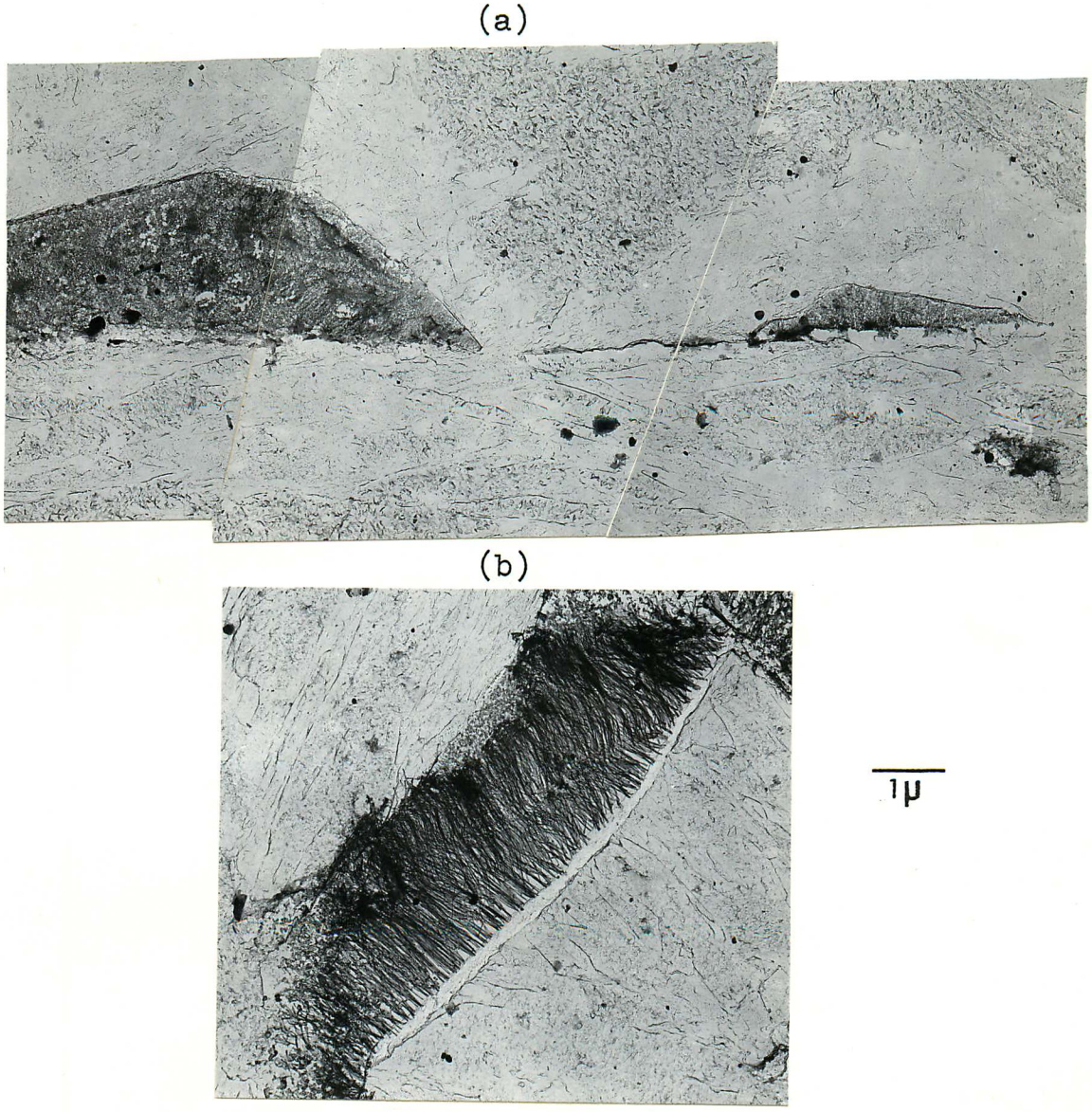

Fig. 3.11: Extraction replica electron micrographs of partially transformed and quenched ferritic structures.
(a) Composite electron micrograph of Fe-IV-0.2C directly transformed for 5 secs. at 700°C.
(b) Fe-IV-0.2C-1.5Ni directly transformed at 750°C for 30 secs.

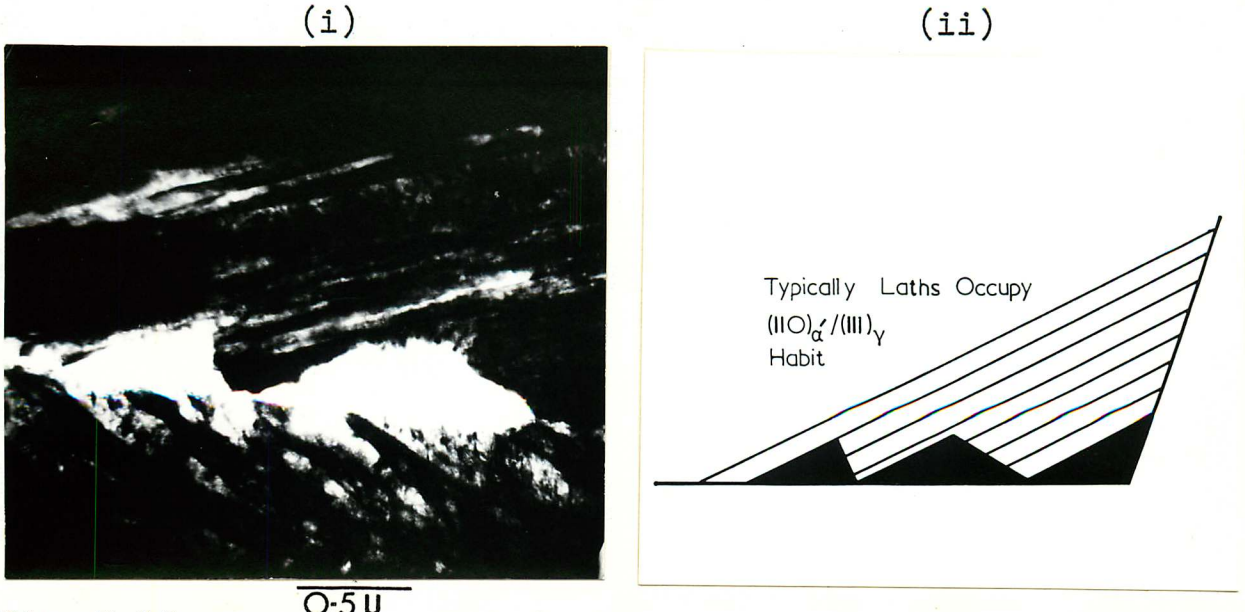

Fig. 3.12:
(i) Centred dark field thin foil electron micrograph using the (110) ferrite reflection. Fe-IV-0.2C directly transformed at 700°C for 5 secs. and quenched.
(ii) Schematic diagram of (i).

exhibits a smooth interface with the austenite, the growth direction of the fibres being perpendicular to the interface. The other side of the prior austenite boundary contains interphase precipitation, the sheets lying parallel to the growth front of the ferrite. The sheets of interphase precipitation were found to be consistent with a $\{110\}_{\alpha}$ habit plane and hence, the growth front is identified as parallel to $\{110\}_{\alpha}$.

Fig. 3.13b is of the same ferrite crystal and again shows fibrous growth normal to the advancing interface on one side of the prior austenite boundary, and aligned precipitation on the other side. However, a further interesting feature is evident on the fibrous side of the ferrite crystal. The ferrite/austenite interface is decorated along its length by a series of angular protruberances. These could be illuminated in dark field by a reflection consistent with the ferrite crystal structure and hence could be interpreted as either proeutectoid ferrite, bainite or martensite. On morphological grounds the structures do not possess bainitic or martensitic character, yet this is a familiar form of proeutectoid ferrite observed in previous sections of this chapter. It seems likely that on quenching, sympathetic nucleation of ferrite occurred on the incoherent side of the austenite/ferrite boundary.

This phenomenon of sympathetic nucleation has been described by Aaronson and Wells (1956) and involves the formation of a ferrite nucleus on an austenite/ferrite boundary rather than an austenite/austenite boundary. It

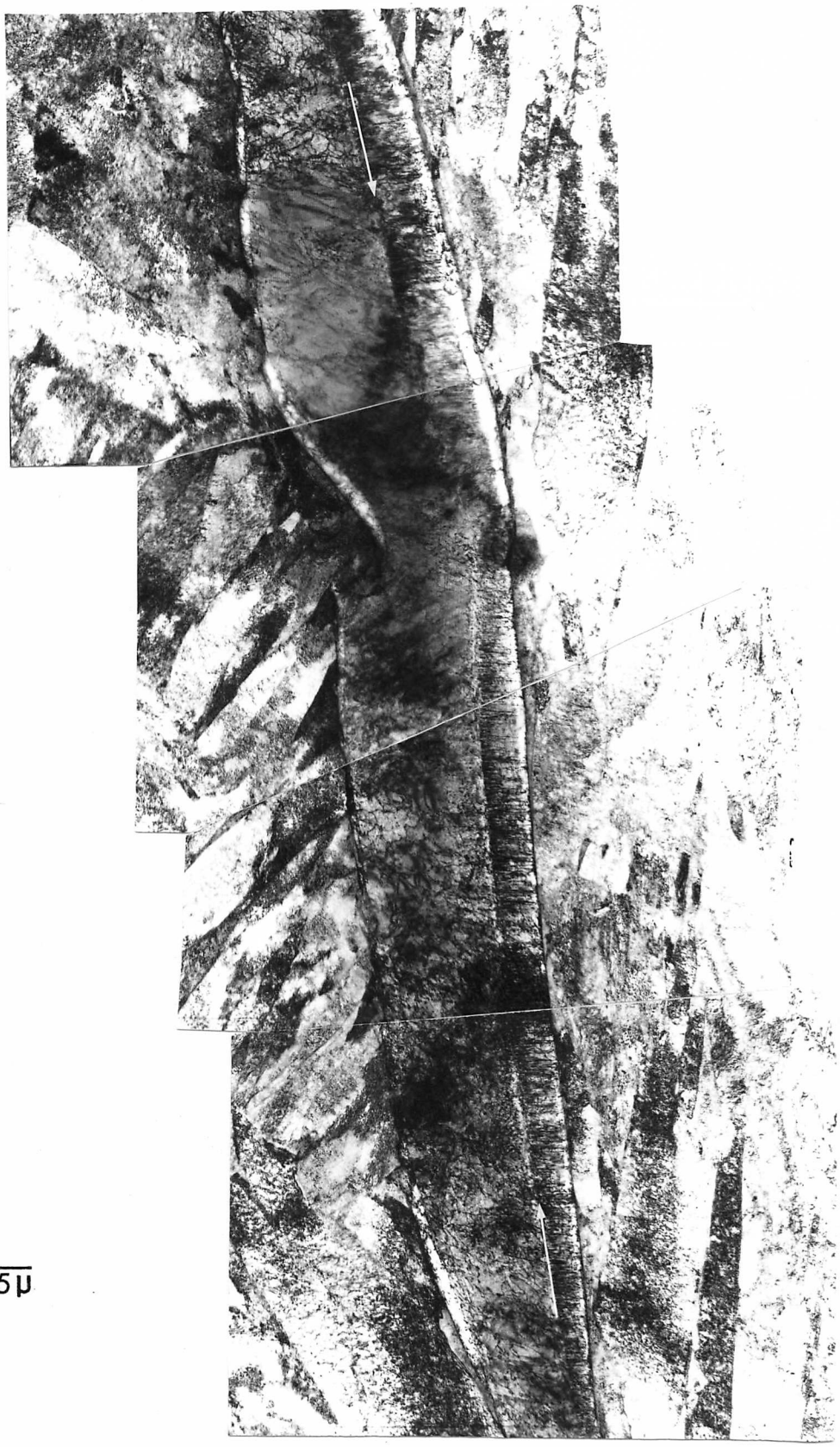

Fig. 3.13a: Composite thin foil electron micrograph of Fe-IV-0.2C-1.5Mn directly transformed at 725°C for 30 secs. and quenched.

Fig. 3.13b: Composite thin foil electron micrograph of Fe-IV-0.2C-1.5Mn directly transformed at 725°C for 30 secs. and quenched.

is thought to occur when the austenite/ferrite interface is immobilised, either by a decrease in temperature or by pinning.

The features shown in fig. 3.13b are consistent with this, as the protruberances only occur on the incoherent side of the ferrite crystal. They would thus be produced during quenching as the reduction in temperature increases the driving force sufficiently for nucleation to occur.

Unfortunately, incomplete diffraction evidence precluded attempts to relate these nuclei to the incoherent side of the prior austenite boundary.

3.7.4 Establishment of Crystallography using Retained Austenite

A series of micrographs illustrating partial transformation in the simple ternary alloy are shown in fig. 3.14. The specimen was transformed for 15 secs. at 775°C to give approximately 5% transformation. The bright field micrograph indicates that a ferrite nucleus has formed on an austenite boundary and has grown into the adjacent austenite grains. Observation of the prior austenite boundary reveals precipitation of vanadium carbide. Such precipitation is common and probably occurs before the austenite boundary is consumed by the ferrite nucleus. Dark field imaging showed that the ferrite was of single orientation and also that interphase precipitation of vanadium carbide had occurred on the side of the prior austenite boundary containing the major growth front. The aligned vanadium carbide precipitate was consistent with the B-N orienta-

tion relationship.

Diffraction intensity was insufficient to provide dark field evidence for the presence of carbide on the opposite side of the prior austenite boundary though the bright field micrograph indicates that some fibrous precipitation has occurred.

Thin films of retained austenite between the martensite laths are shown to be illuminated strongly in the dark field and are consistent with a K-S orientation relationship with the martensite. To establish the crystallography governing the transformation, the diffraction evidence from the ferrite was compared to that in both of the prior austenite grains.

No rational orientation relationship could be found to relate the ferrite crystal with the retained austenite in the grain adjacent to the ferrite containing the fibrous precipitation. This identifies the austenite/ferrite interface as incoherent. Consequently, growth is expected to be controlled by the diffusion of solute and involves the random transfer of atoms across the incoherent boundary.

Comparison of the ferrite orientation with that of the retained austenite adjacent to the interphase precipitation, revealed parallelism between the $(110)_\alpha$ and the $(111)_\gamma$ planes. Furthermore, the zones of the diffraction patterns indicate that the $[100]_\alpha$ and $[110]_\gamma$ directions are also parallel. This identifies the austenite grain adjacent to the interphase precipitation as being K-S related to the ferrite. The interface can therefore be

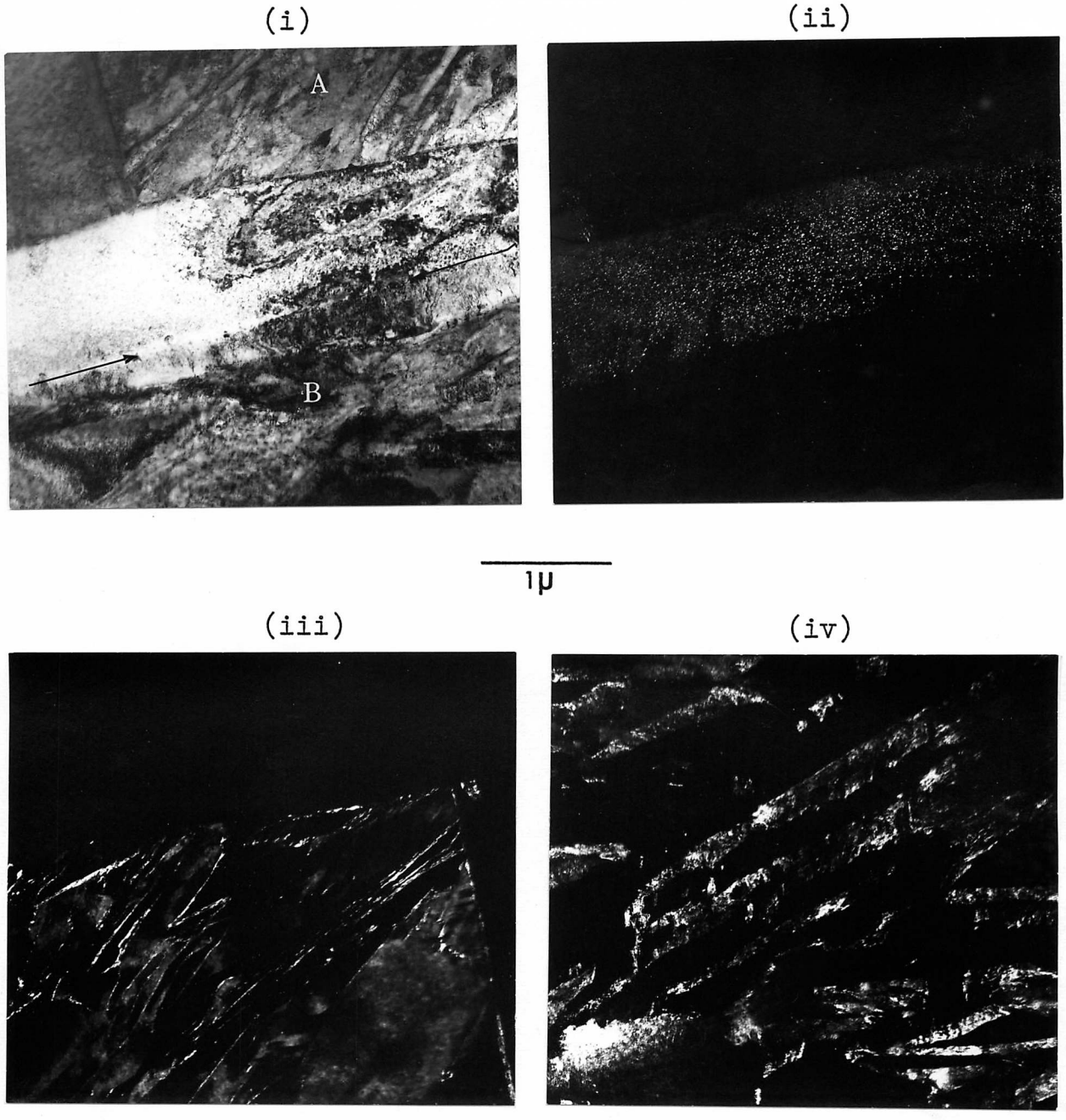

Fig. 3.14: Thin foil electron micrographs of fe-IV-0.2C directly transformed at 775°C for 15 secs. and quenched.
(i) Bright field.
(ii) Centred dark field using the (111) vanadium carbide reflection.
(iii) Centred dark field from area A using the (020) austenite reflection.
(iv) Centred dark field from area B using the (200) austenite reflection.

(v)

(vi)

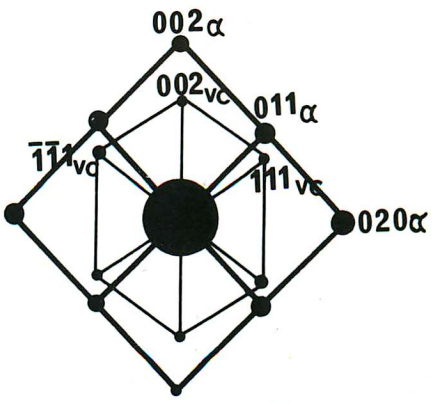

$[100]_{\alpha}$ ZONE

$[110]_{VC}$ ZONE

(vii)

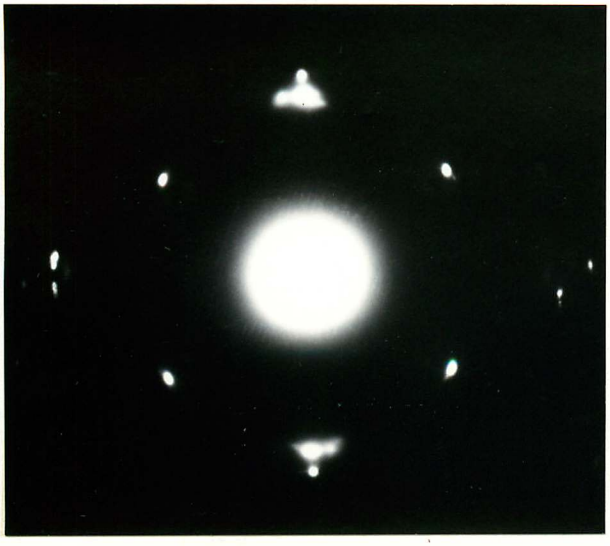

(viii)

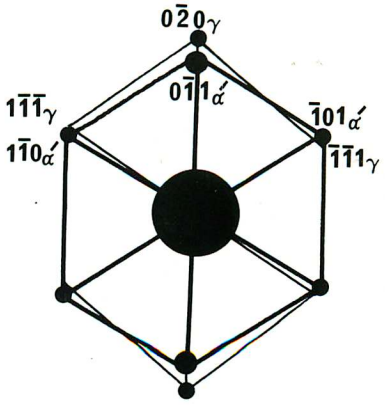

$[11\bar{1}]_{\alpha}$ ZONE

$[10\bar{1}]_{\gamma}$ ZONE

Fig. 3.14 continued: Crystallographic analysis showing the austenite and ferrite to be K-S related.
(v) Diffraction pattern of the ferrite.
(vi) Analysis showing the ferrite and vanadium carbide to be B-N related.
(vii) Diffraction pattern of area A.
(viii) Analysis showing the austenite and martensite to be K-S related.

considered to be coherent in nature.

A second series of micrographs, shown in fig. 3.15, is of the nickel, vanadium steel, which has been transformed for 30 secs. at 725°C resulting in approximately 10% transformation to ferrite. The combined effects of nickel and the high transformation temperature has resulted in a significant amount of fibre formation. Fig. 3.15 shows two separate ferrite nuclei, as confirmed by dark field imaging, forming upon the same austenite grain boundary, which have impinged laterally during growth.

The crystallographic situation is essentially similar to the previous example. The ferrite containing interphase precipitation obeys a K-S relationship with respect to the austenite grain into which it is growing. The interphase sheets themselves occupy a $\{110\}_\alpha$ habit and can be seen to be parallel to the transformation front. The interphase boundary can therefore be identified as the coherent $(110)_\alpha/(111)_\gamma$ interface.

On the other hand, the austenite/ferrite boundary adjacent to the fibrous precipitation bears no rational relationship to the austenite into which it is growing. The interphase boundary is therefore incoherent. Dark field imaging using a VC reflection shows that the fibrous growth is normal to the transformation front. The fibrous colony was in fact shown to bear a K-S relationship with the austenite grain on the opposite side of the prior austenite boundary to the major growth direction.

Fig. 3.16 is a third example of the ferrite reaction, transformation having occurred for 5 secs. at 675°C. The

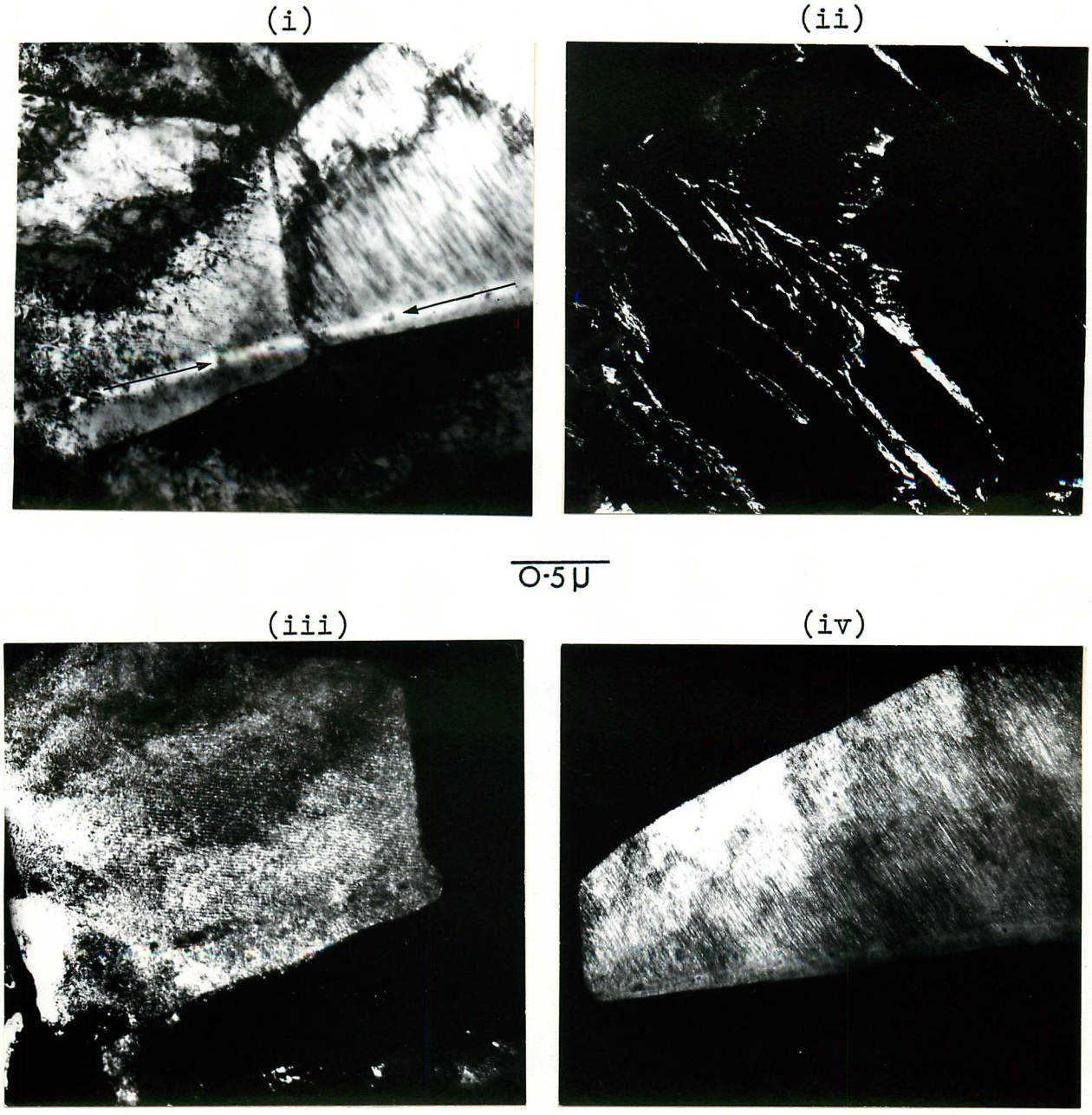

Fig. 3.15: Thin foil electron micrographs of Fe-IV-0.2C-1.5Ni directly transformed at 725°C for 30 secs. and quenched.
(i) Bright field.
(ii) Centred dark field using the (200) austenite reflection.
(iii) Centred dark field using the (111) vanadium carbide reflection.
(iv) Centred dark field using the (111) vanadium carbide reflection.

ferrite is of a very angular nature and growth appears to have occurred on only one side of the austenite boundary. Dark field imaging shows that aligned precipitation of vanadium carbide has occurred parallel to the growth front but that there is no evidence of fibrous precipitation. Diffraction analysis again showed the ferrite to be K-S related to the grain into which it is growing but unrelated to the one on the opposite side of the prior austenite boundary.

Direct morphological information on the nature of the transformation interfaces proved impossible with these alloys, as quenching was not sufficiently rapid to retain the boundary structure intact. However, it was found that by using an Fe-1V-0.2C+4%Cr alloy this problem could be overcome. Fig. 3.17 is of the ferrite/martensite boundary in a partially transformed specimen. The aligned precipitation is again of vanadium carbide bearing a B-N relationship with the ferrite. The stepped nature of the interface can be clearly seen.

This evidence provides conclusive proof for the existence of a ledge mechanism in vanadium bearing low-alloy steels. The ledge height can be seen to conform to the spacing of the precipitate sheets and as such differs in size from the type of ledge which Aaronson (1962) has described, for the growth of proeutectoid ferrite. The ledges are in fact directly analogous to those observed in chromium steels (Campbell and Honeycombe, 1974) and molybdenum steels (Edmonds and Honeycombe, 1973). They are, however, crystallographically consistent with the

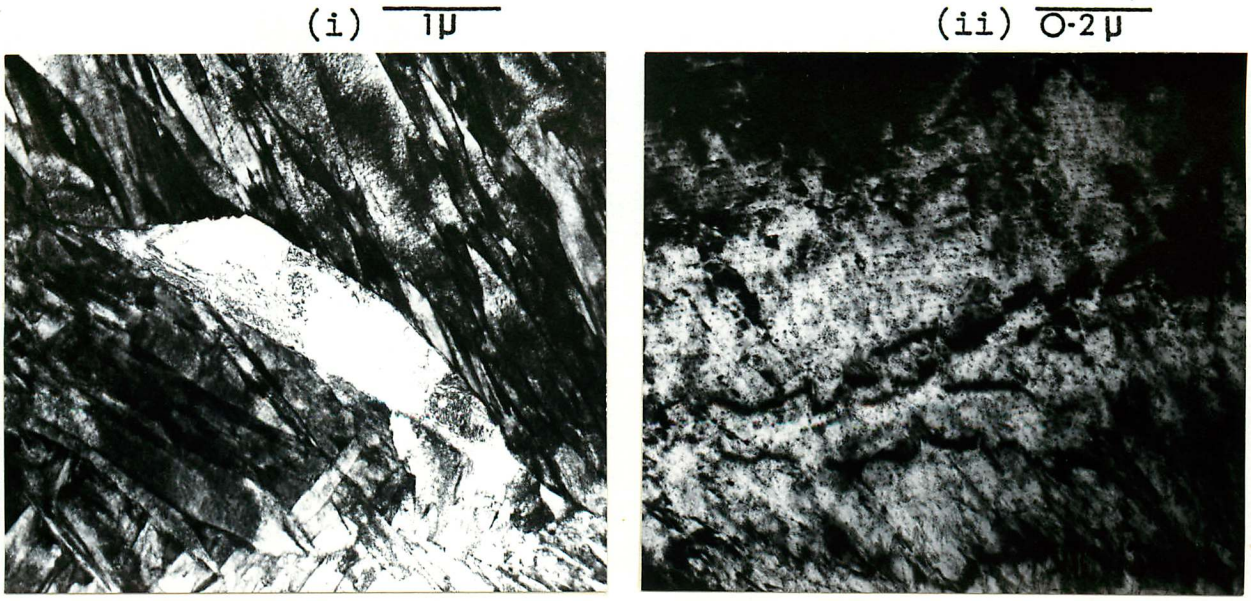

Fig. 3.16: Thin foil electron micrographs of Fe-IV-0.2C directly transformed at 675°C for 5 secs. and quenched.
(i) Bright field.
(ii) Centred dark field using the (110) ferrite reflection.

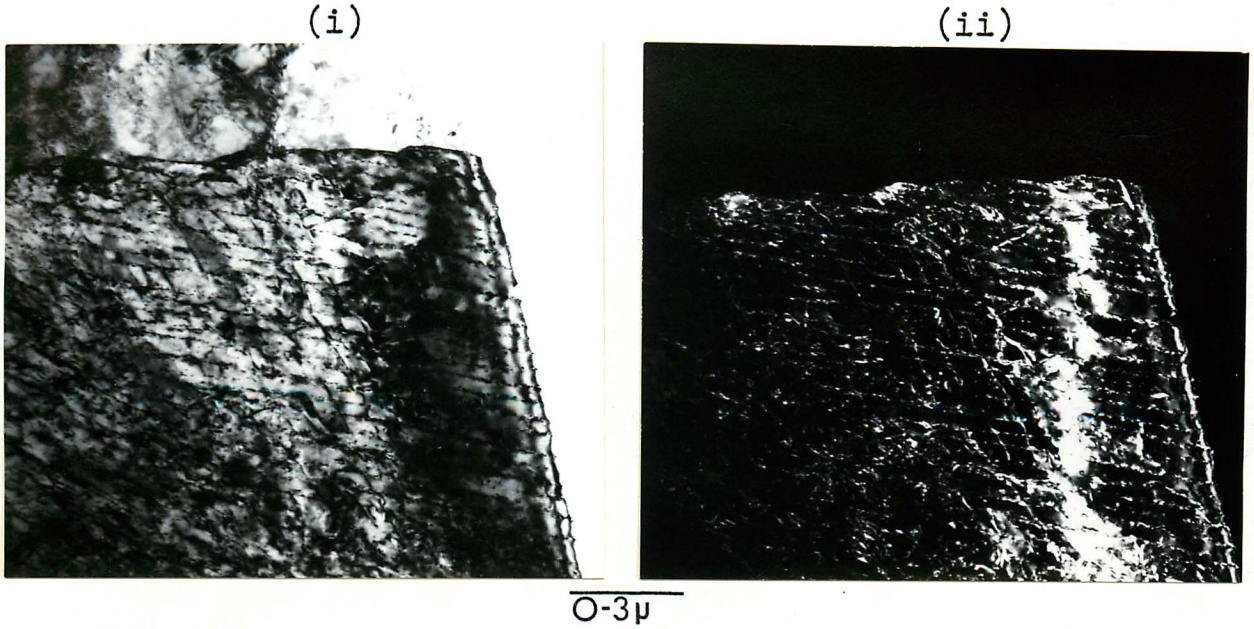

Fig. 3.17: Thin foil electron micrographs of Fe-IV-0.2C-4Cr directly transformed at 700°C for 90 secs.
(i) Bright field.
(ii) Centred dark field using the (200) vanadium carbide reflection.

smaller ledges described by Aaronson, where the growth occurs by the lateral propagation of the incoherent ledge facets.

3.7.5 Habit Plane Selection

It is an interesting characteristic of the interphase precipitation reaction that the vanadium carbide occupies only one of the possible $\{100\}_\alpha$ habit planes, in contrast to quenched and tempered steels, where all three are observed. An explanation of this unique habit selection requires analysis of the three phase crystallography relating ferrite, austenite and carbide at the coherent austenite/ferrite transformation interface.

It has been established that:

(i) The ferrite obeys a K-S orientation relationship with the austenite;

(ii) The vanadium carbide interphase precipitate obeys a B-N orientation relationship with the ferrite.

Fig. 3.18 is a series of stereograms which relate the three possible B-N precipitate orientations to the austenite, assuming that the austenite is K-S related to the ferrite. It is found that selection of only one of the possible B-N habit planes brings the vanadium carbide to within approximately five degrees of a cube/cube relationship with the austenite. The other two possible variants are many degrees away. The precipitate thus occupies that variant of the B-N orientation relationship with the ferrite which enables it to adopt a cube/cube relationship with the austenite. The precipitate must therefore be

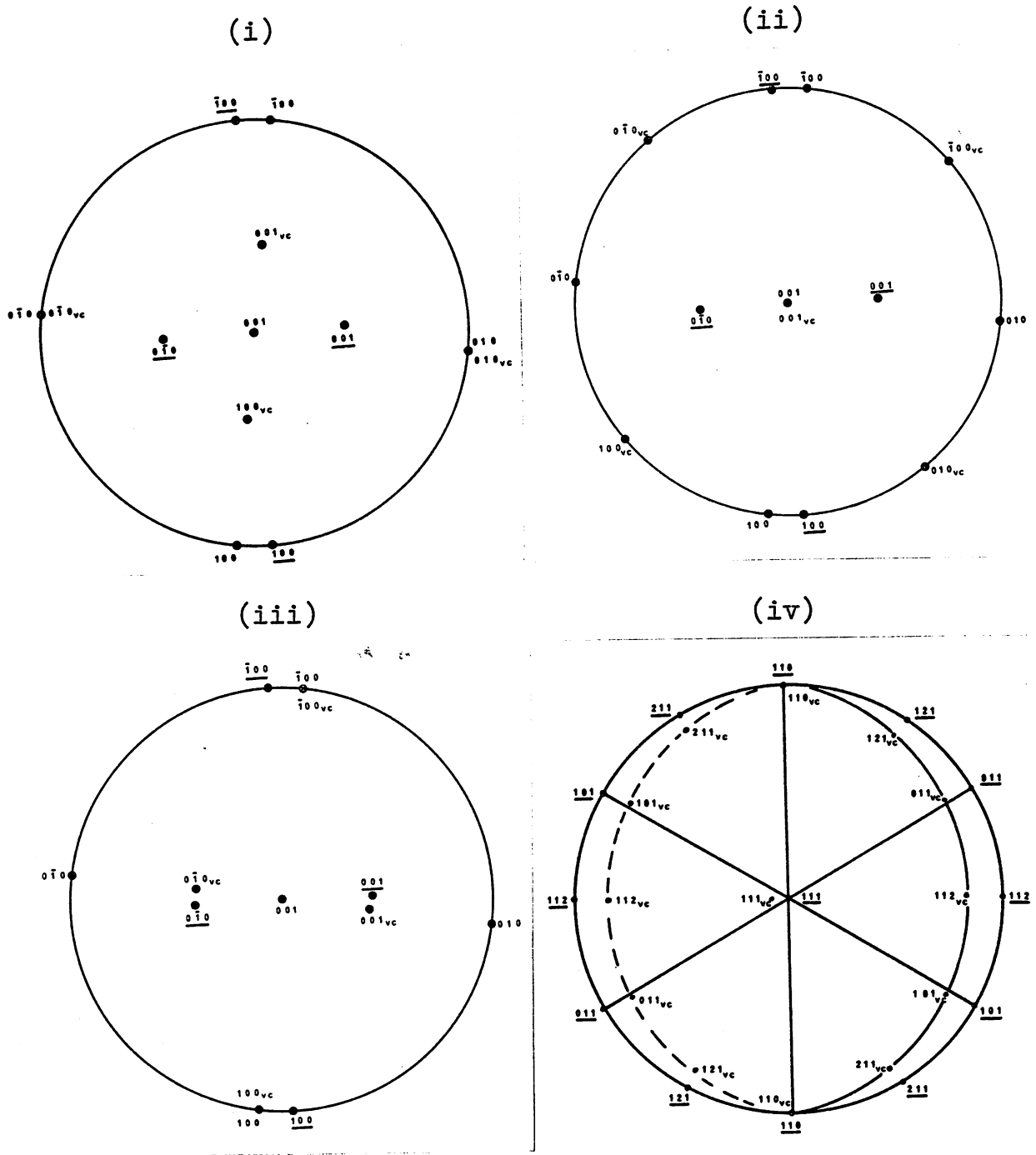

Fig. 3.18: Stereograms of the three possible B-N orientations of vanadium carbide with respect to ferrite.
(iii) Indicates vanadium carbide to be 5° from a cube/cube relationship with the austenite.
(iv) A (111) centred stereogram of the relative orientations of the vanadium carbide and austenite.

nucleated directly on the interphase boundary.

This information is consistent with the previously mentioned statement that the B-N relationship is equivalent to the Bain relationship as the K-S and Bain differ by only five degrees.

3.8 Conclusions

The literature survey discussed the proeutectoid ferrite reaction in terms of the observed morphologies, their growth kinetics and the crystallography governing the reaction. The mechanisms by which the various ferrite morphologies might grow are then discussed. The way in which the ferrite reaction is influenced by precipitation is considered, particular attention being paid to the interphase and fibrous precipitation reactions.

Results of optical and electron microscopy reveal that the transformation front is of a facetted nature. Trace analysis showed that interphase precipitate sheets occupy a $\{110\}_\alpha$ habit plane and further electron microscopy showed that these sheets form parallel to the reaction front.

Replica examination showed that the ferrite nucleates as angular protruberances on the prior austenite boundaries and that any fibrous growth occurs normal to the interphase boundary.

The crystallography governing the interphase reaction was established using partial transformation studies. The ferrite nuclei were shown to be related to the austenite on one side of a prior austenite boundary by the Kurdjumov-

Sachs orientation relationship, but to be unrelated to the austenite on the other side. The austenite orientation was established using interlath retained austenite films.

Fibrous growth was shown to occur into the austenite to which the ferrite crystal was unrelated and interphase growth into the austenite to which the ferrite bore a rational orientation relationship. This identified fibrous growth as being controlled by an incoherent boundary and interphase growth by a coherent boundary. High temperatures and alloy additions were found to encourage fibrous precipitation, the interphase reaction being more prevalent at lower temperatures. Morphological evidence, in conjunction with the previously established crystallography of the reaction, showed that interphase precipitation occurs by a ledge mechanism. No evidence was found to support the mechanisms proposed by Heikkinen (1973b) and Davenport and Honeycombe (1971).

The unique habit plane selected by the interphase precipitate was explained in terms of the carbide dispersion obeying an orientation relationship with both the ferrite and the austenite. It was found that only one variant of the Baker-Nutting orientation relationship would permit the alloy carbide to be cube/cube related to the austenite, assuming the ferrite and austenite to be Kurdjumov-Sachs related. It was therefore concluded that nucleation of the interphase precipitate occurred directly on the interphase boundary. This is contrary to the work of Davenport, Berry and Honeycombe (1968) who suggested that the alloy carbide was nucleated on the ferrite side of the austenite/ferrite interface.

CHAPTER IV

THE REAUSTENITISATION OF FERRITIC, BAINITIC AND MARTENSITIC STRUCTURES IN Fe-IV-0.2C

4.1 Introduction

The formation of austenite, contrary to its decomposition, has been shown to be sensitive to the microstructure from which it forms, as this determines the sites from which the austenite will be nucleated, and also the structure through which it grows, (Roberts and Mehl, 1943). As has been stressed earlier, it is important to characterise the starting microstructure before the phenomena influencing reaustenitisation can be described. The ferrite and martensite structures were investigated in the previous two chapters. In this chapter, the bainite reaction is reviewed briefly and its structure is characterised as observed in the vanadium steel used for this study.

The literature on reaustenitisation from various microstructures is then reviewed followed by presentation of the results of this particular investigation. The results are then discussed and the conclusions of the work outlined.

4.2 The Bainite Reaction

Bainite was first recognised as a discrete transformation product of the decomposition of austenite more than forty-five years ago (Davenport and Bain, 1930). Despite extensive research since this date there has been much controversy over what exactly defines bainite and

the mechanism by which it forms. Some of the major controversies were recently debated by Hehemann, Kinsman and Aaronson (1972). Hehemann suggested that there is little of a fundamental nature about the bainite reaction on which there is general agreement, and that this was a reflection of the complexity of the processes involved. He defines the problem as involving the competitive reaction kinetics between four processes:

(a) the allotropic transformation of austenite to ferrite;

(b) the partitioning of carbon between these phases;

(c) precipitation of cementite (or other carbides);

(d) accommodation and relaxation of the transformation strain.

The interdependance of these phenomena aggravate investigation problems and has resulted in bainite being defined in terms of three independent features of the reaction:

(i) The work of Davenport and Bain (1930) and subsequently Hultgren (1947), identified bainite in terms of its microstructure. It is described as a dispersion of non-lamellar carbides in association with acicular proeutectoid ferrite. This definition has been extended to differentiate between the high and the low temperature forms of bainite. The high temperature form has a feathery appearance with precipitation of cementite along the bainite lath boundaries, while the low temperature form, lower bainite, is finer and more platelike with a dispersion of cementite within the laths themselves. Hultgren (1947) showed that both

forms were initiated by the nucleation of the ferrite phase. Shackleton and Kelly (1965) confirmed the nature of the carbide dispersions in the two forms of bainite and showed that the temperature range over which each form occurred, varied with carbon content. Pickering (1967) investigated this phenomenon further and showed that there was an increase in transition temperature from lower to upper bainite up to about 0.5% carbon but further increases lowered the transition temperature to about 350°C (fig. 4.1). He attributes the initial increase to the slower diffusivity of carbon at higher concentrations, preventing it from diffusing away ahead of the growing bainitic ferrite. As the carbon content is increased further, primary cementite achieves a concentration enabling it to precipitate directly from the austenite. This reduces the surrounding carbon content and enables bainitic ferrite to form.

(ii) Bainite can be described in terms of the kinetic aspects of the reaction. The bainite transformation has its own C-curve, although, as the upper limit of this curve is reached, the percentage of transformation to bainite possible decreases (Lyman and Traiano, 1945). This phenomenon has been explained by Kinsman and Aaronson (1967) in terms of a "solute drag" effect in alloy steels, where the presence of a carbide forming element reduces the activity of carbon in the austenite.

(iii) The bainite reaction can be descirbed in terms of surface relief effects (Ko and Cottrell, 1952). These effects have been related to the martensite transforma-

tion and it has been shown that the crystallography of lower bainite can be described adequately by the phenomenological theory of martensite formation (Srinivason and Wayman, 1968) and that upper bainite displays crystallographic similarities with low-carbon martensites, (Shimizu and Nishiyama, 1963).

Because there is no generally accepted definition of what comprises a bainitic structure, many transformation products in various systems have been described as having bainitic character. Flewitt and Towner (1967) described platelike bainitic structures in α - brass and self-accommodating arrangements of bainite plates were observed by Amity, Rosen and Bor (1967) in a range of uranium-chromium alloys.

A non-acicular bainite has also been identified in a low-carbon nickel steel (Chilton and Speich, 1970) and has been termed "granular bainite".

4.3 The Formation of Austenite

4.3.1 Introduction

The formation of austenite from ferrite/carbide aggregates was first studied in depth by Roberts and Mehl (1943). They concluded that austenite forms by a process of nucleation and growth and that both of these processes are structure sensitive. The resulting austenite consists of strain-free, equi-axed grains of austenite (Paxton, 1967), though Roberts and Mehl (1943) pointed out that carbon concentration gradients may exist within the austenite for appreciable times after austenitisation is

complete. Paxton has concluded that three main factors are important in considering the reaustenitisation reaction, particularly as applied to commercial control of the austenite structure. (He also considers the phenomenon of grain growth once the austenitisation reaction is complete):

(i) The mechanism and rate of nucleation of the austenite:

Roberts and Mehl (1943), studying a series of pearlitic strucutres of various spacing, established that the nucleation rate increasing as the pearlite interlamellar spacing decreased. This increase was found to be roughly proportional to the increase in ferrite/carbide interfacial area.

Work by Speich, Szirmac and Fisher (1966), using laser heating to permit very short holding times, concluded that the efficiency of grain boundary carbides as nuclei was particularly high. A specimen held at 885°C for only 0.008 secs. revealed that all the grain boundary carbides had formed a rim of austenite around them.

(ii) The influence of the composition and coherency of the carbide on the nucleation rate:

Although the theory of nucleation of a third phase from a mixture of two others is not well developed, Paxton (1967) extends the existing theory of two phase reactions. He suggests that any compositional changes in the carbide particles will result in a change in the free energy of the nucleation process. This will also be influenced by strain energy considerations and hence

depend on the coherency of the precipitate.

(iii) The growth rate of the austenite:

Measurements made by Roberts and Mehl (1943) on the growth rates of austenite in pearlites of various interlamellar spacing, showed that a decrease in pearlite spacing was reflected by an increase in the austenite growth rate. Recent work by Nemoto (1977) on a eutectoid, plain carbon steel concludes that the austenite growth rate is controlled by the rate of carbon diffusion. This is consistent with the work of Roberts and Mehl in that a decrease in the pearlite interlamellar spacing will result in a decrease in diffusion distance and hence an increase in growth rate.

The consumption of both spherodised and pearlitic structures by an austenite nodule have been considered theoretically by Hillert, Nilsson and Törndahl (1971). In the case of spherodised steels they described five possible growth modes (fig. 4.2).

Type I considers the growth of austenite from individual cementite particles in a ferrite matrix. In the absence of alloying elements the growth rate can be considered as a one-dimensional growth problem. The growth rate was found to be controlled by diffusion of carbon through the austenite shell. The presence of small amounts of alloy addition were found to decrease the rate of growth through their effect on the diffusivity of carbon. This however, was found still to be the rate controlling process.

Type II describes the advancement of an austenite

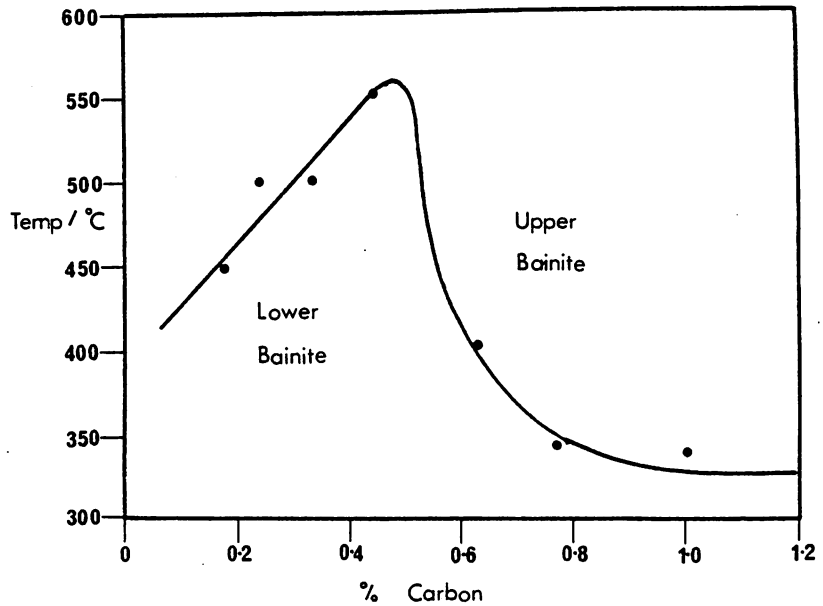

Fig. 4.1: The variation in transition temperature from upper to lower bainite with carbon content. (After Pickering, 1967)

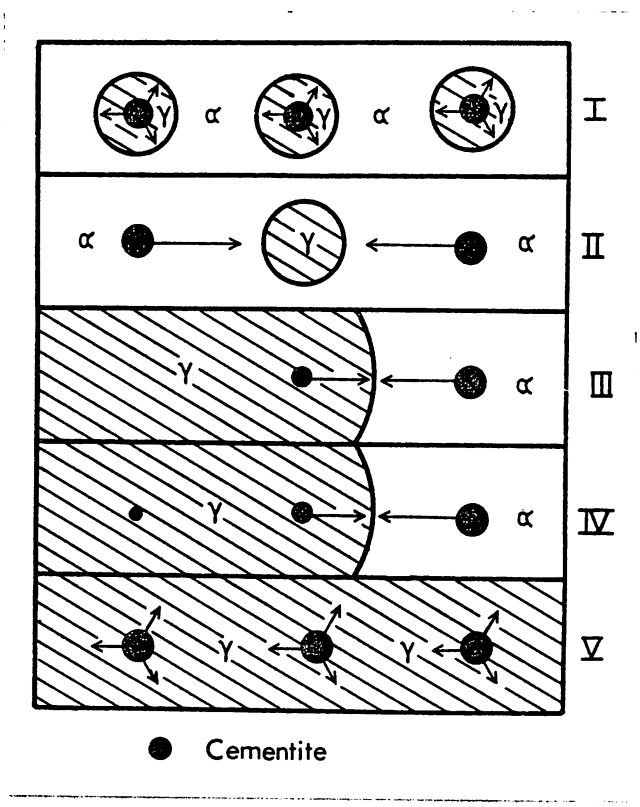

Fig. 4.2: Theoretical growth modes of austenite from spherodised ferrite/carbide aggregates. (After Hillert et al., 1971)

nodule controlled by the dissolution of cementite particles within the ferrite. Hillert et al. claim that alloy additions will have a much more powerful influence on the kinetics of austenite formation than for type I but indicate that no direct experimental evidence is available.

Type III and IV are similar and describe the dissolution of cementite particles before and after the arrival of an advancing austenite interface. This mode may well apply at later stages of the transformation where the austenite/ferrite interface can be approximated to a planar one. The treatment by Hillert et al. assumes a constant growth rate at this stage. A similar approach is adopted for the consumption of a pearlite nodule.

Type V assumes that the austenite transformation has occurred rapidly and has resulted initially in the cementite distribution being largely unaffected. The treatment then considers the dissolution of the cementite particles within the austenite.

These treatments described idealised situations of austenite formation, apparently with reasonable correlation between experiment and result, but do not consider the physical influence of the carbide distributions on the advancing austenite/ferrite boundary.

Recent work by Nemoto (1977) has shown that the pearlitic cementite lamellae in a eutectoid steel serve as a barrier to austenite growth, the austenite/ferrite boundary bowing out between the cementite lamellae. This

pinning effect is also inferred in the work of Roberts and Mehl (1943). They report that austenite has a lower growth rate in aluminium-killed steels than in non-killed steels. The influence of second phase particles on grain-growth is well documented (Gladman, 1973) and it seems likely that such particles also impede the austenite growth front in the aluminium-killed steels.

The interdependance of the nucleation and growth phenomena described will play an important part in determining the final nature of the austenitic structure. A high nucleation rate combined with a low rate of growth will result in a fine austenite grain size. Such grain size control is an important commercial consideration in many heat treatment processes and will be considered more closely in the next chapter. However, before control of the austenite grain size can be optimised, the parameters governing the reaustenitisation process must firstly be defined.

4.3.2 Reaustenitisation from Ferritic Structures

The morphologies of ferrite nuclei forming from a parent austenite structure were first categorised by Aaronson (1962) and is termed the "Dubé Classification", (Dubé and Aaronson, 1958). More recent studies by Fong and Glover (1975), on an Fe-1.93Mn alloy, has investigated austenite precipitate morphologies formed during the reverse reaction and has compared these to the work of Aaronson. The ferrite structure was nitrided at 645°C to form austenite precipitates along the ferrite boundaries

and on cooling, the austenite precipitates were largely retained. This enabled the use of electron diffraction to investigate the crystallography of reaustenitisation. A number of precipitate morphologies were observed, in each case the austenite bearing a relationship within 15^{o} of Kurdjumov-Sachs with at least one ferrite grain at the boundary of precipitation. The observed morphologies included allotriomorphs, idiomorphs and primary sideplates. The allotriomorphic and idiomorphic growth was found to occur exclusively at high angle boundaries and the nuclei to bear a K-S relationship with the ferrite grain into which the least austenite growth occurred. Primary sideplates were found to be K-S related with the ferrite into which they were growing. The growth morphologies can therefore be considered analagous crystallographically to the equivalent growth morphologies observed in pro-eutectoid ferrite.

4.3.3 Reaustenitisation from Acicular Structures

Roberts and Mehl (1943) considered the reaustenitisation process from a martensitic starting microstructure. They concluded that there is a greater abundance of austenite nuclei than in fine pearlitic or spherodised structures but provided little morphological evidence to describe the reaction.

Many subsequent works have described two types of austenite morphology, called globular and acicular austenite (Kula and Cohen (1954), Matsudu and Okanura (1974), Kinoshita and Ueda (1974), Homma (1974)).

The nature of the reverse transformation to form acicular austenite has been the subject of some controversy. Using a high temperature, X-ray technique, D'Yachenko and Federov (1964) established that there was parellelsim between $(111)_\gamma$ and $(110)_{\alpha'}$ planes during reaustenitisation of martensitic structures. Further work by Matsudu and Okamura (1974a, 1974b), on a 9% Ni steel, showed that the acicular austenite and the martensite were in fact K-S related. However, in any one martensite packet, the acicular austenite grains produced, tended to display the same K-S variant. Matsudu and Okamura attributed this to the austenite forming by a martensite reverse transformation, that is, by a process of shear. However, Homma (1974), in agreement with D'Yachenko and Federov (1964), considered the single orientation to be a texture effect. More recent work by Watanabe and Kunitaki (1976) discounts these theories and explain the single orientation in terms of three phase crystallography at the nucleation sites. That is, the orientation relationships governing the cementite/ferrite, the ferrite/austenite and the austenite/cementite are the Bagaryatski (1950), the Kurdjumov-Sachs (1930) and the Pitsch(1963) relationships respectively. In order that all three relationships be satisfied, only one K-S variant is possible, resulting in the similarity of orientation of acicular austenite grains within one packet.

The formation of globular austenite has been shown to be the result of impingement of acicular austenite

nuclei (Homma (1974), Matsudu and Okamura (1974b)). However, once established, the growth of an austenite globule is associated with the dissolution of cementite and obeys a parabolic relationship (Matsudu and Okamura, 1974b). This is indicative of carbon diffusion control.

It is worthy of note that the martensite reverse transformation is common in high alloy steels and in fact is used as a strengthening mechanism for some austenitic stainless steels (Smith and West, 1973). This is accomplished because defects associated with the martensite reaction are retained upon reversion to austenite.

4.4 Results

4.4.1 Introduction

The reaustenitisation behaviour of Fe-IV-0.2C (steel A1, Appendix I) is considered from ferritic, martensitic and bainitic starting microstructures. This has necessitated a small section to characterise the important aspects of the bainite structure in this investigation.

The results are presented so as to facilitate comparison between the austenitising characteristics of the three microstructures and have been divided into two sections dealing with morphological aspects of growth and the kinetics of transformation.

4.4.2 Bainite Structure in Fe-IV-0.2C

Following solution treatment for 30 min. at 1200°C, 3mm. diameter specimens of length 15mm. were isothermally transformed in a tin bath and quenched to establish the

transformation curve for the bainite reaction. Dilatometric studies proved unsuccessful because of the rapidity of the higher temperature ferrite reaction. The transformation curve was determined by optical metallography though this was supplemented by hardness measurements to avoid errors due to confusion of the bainite and martensite structures. The transformation curve and a typical hardness plot are shown in fig. 4.3.

The bainite and ferrite transformation curves overlap at approximately 650°C and not until about 600°C is the transformation product entirely bainitic. Optical examination of the high temperature bainite showed that it displayed a packet morphology in which individual laths could be resolved because of the dark etching lath boundaries (fig. 4.4). The lower temperature structures were essentially similar under the optical microscope but both the lath and packet size appeared smaller.

Electron microscopy examination confirmed that the high temperature reaction product was a typical upper bainite structure. It consisted of parallel ferrite laths with a high dislocation density, and with cementite precipitation along the lath boundaries (fig. 4.5). The cementite was in the form of a film at high transformation temperatures but became discrete precipitates as the transformation temperature decreased. The cementite was shown to obey the Bagaryatski (1950) orientation relationship with the ferrite throughout the transformation range (fig. 4.5).

(i)

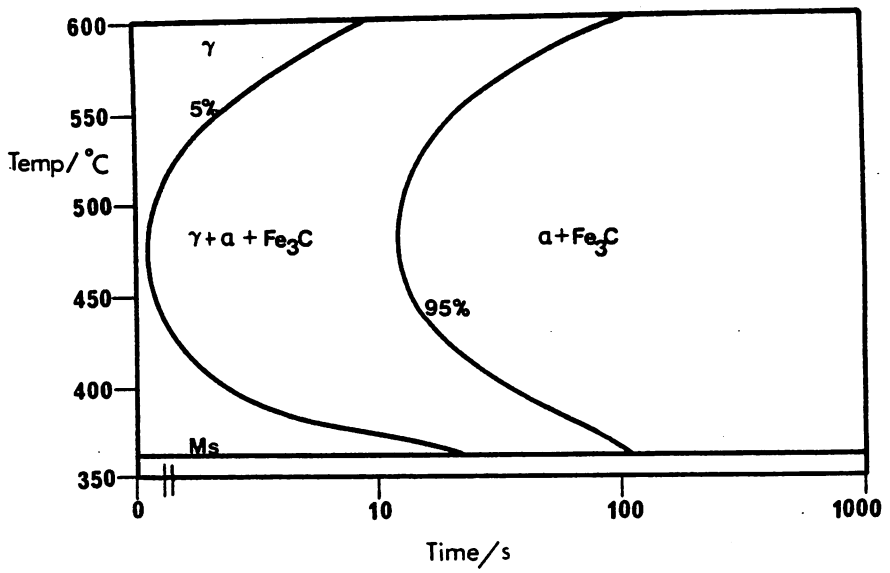

(ii)

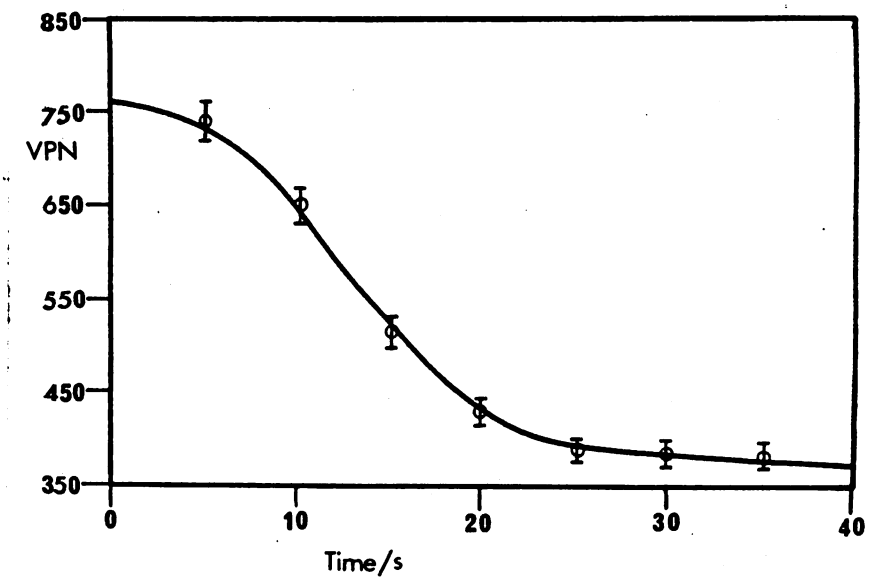

Fig. 4.3:

(i) The bainite isothermal transformation curve in Fe-IV-0.2C solution treated at 1200°C for 30 mins.
(ii) Hardness variation of quenched specimens as a result of transformation to bainite.

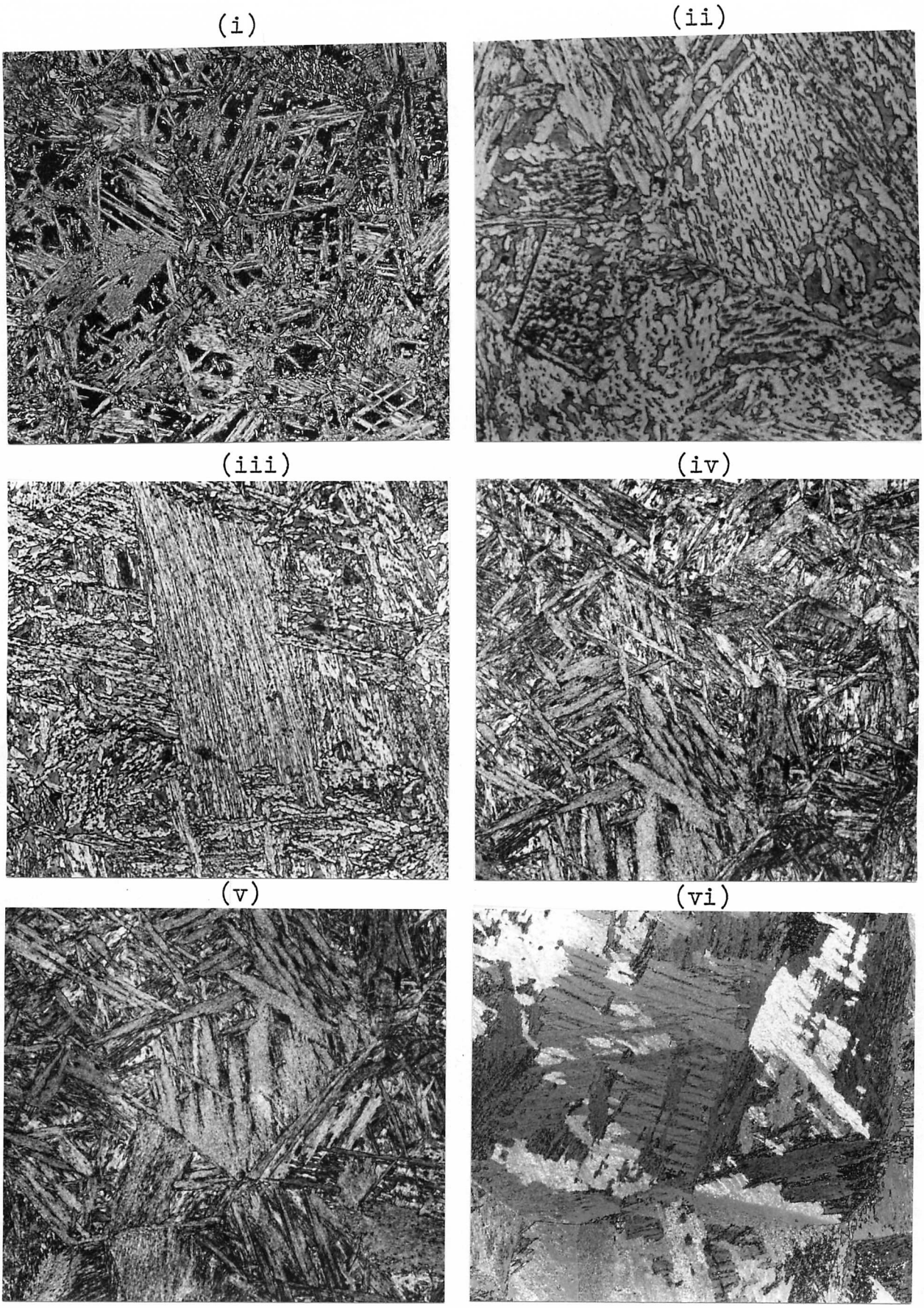

Fig. 4.4: Optical micrographs of the bainite structure.
(i) 3 mins. 600°C. —— 100μ
(ii) 1 min. 550°C.
(iii) 1 min. 500°C. —— 25μ
(iv) 2 mins. 450°C.
(v) 2 mins. 400°C. —— 35μ
(vi) 2 mins. 375°C. —— 100μ
(Phase contrast micrograph)

At transformation temperatures in the range 350°C - 425°C cementite precipitation occurred within the laths themselves at an angle of approximately 60° to the major growth direction of the laths (fig. 4.5b). This is consistent with the classical description of lower bainite and was seen to be of a much finer nature than the upper bainite, the lath width having decreased from approximately 0.4-0.15μm over the transformation range.

The bainite used the for reaustenitisation experiments was an upper bainite transformed at 450°C for 2 mins. Cementite precipitation was at the lath boundaries in the form of discrete carbides and the lath width was approximately 0.2μm.

4.4.3 Morphological and Crystallographic Aspects of Reaustenitisation

Isothermal reaustenitisation experiments were performed using the salt pot technique described in Appendix 1.2. The specimens were made from 3mm. rod cut into 15mm. lengths, from which optical and electron microscopy specimens were prepared. The specimens used had structures consisting of:

(a) ferrite formed by isothermal transformation for 2 mins. at 700°C;

(b) martensite formed by an iced brine quench from 1200°C;

(c) bainite formed by isothermal transformation for 2 mins. at 450°C.

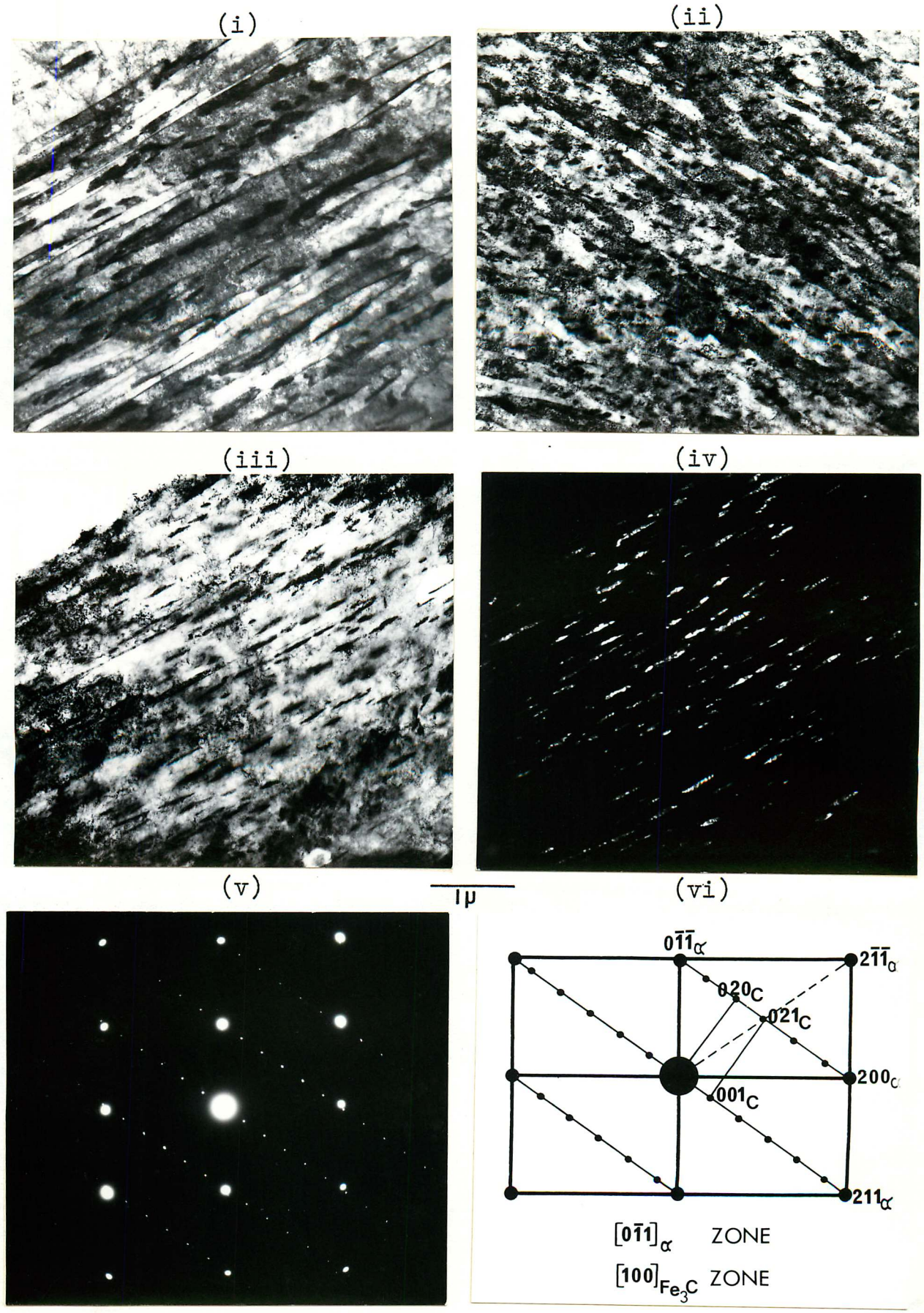

Fig. 4.5: Thin foil electron micrographs of the bainite structure.
(i) Bright field. 1 min. 550°C.
(ii) Bright field. 2 mins. 375°C.
(iii) Bright field. 2 mins. 450°C.
(iv) Centred dark field of area shown in (iii) using the (001) cementite reflection.
(v) Diffraction pattern of area shown in (iii)
(vi) Analysis showing Bagoryatski orientation relationship.

(i) Optical Investigation:

The initial stages of the reaustenitisation reaction were found to be very structure sensitive in that the distribution of austenite nuclei* varied greatly between the ferrite, martensite and bainite starting microstructures. Fig. 4.6 shows the three microstructures after reheating to 840°C for 15 secs. This represents a small degree of superheating, the Ac_1 temperature being established at approximately 820°C. Nucleation in the bainitic and martensitic structures is seen to be concentrated at the prior austenite grain boundaries and despite the small percentage of transformation, site saturation has occurred. Some nucleation is also evident within the prior austenite grains. Nuclei formed at the prior austenite grain boundaries are largely idiomorphic in character while two types are in evidence within the grains. The smaller nuclei are acicular in shape and are situated along lath boundaries, while the larger ones have a similar morphology to those on the grain boundaries.

Nucleation of austenite in the ferrite starting microstructure does not delineate the prior austenite boundaries as in the case of the martensitic and bainitic structures. This is because in most areas, the prior austenite boundary has ceased to exist owing to the growth of the ferrite into both of the adjacent austenite grains. The

---

* Reference will normally be given to the reformed austenite directly, despite the fact that quenching of partially transformed structures results in the transformation of any austenite to martensite. The different etching characteristics enabled the austenite to be distinguished from the starting microstructures.

nuclei therefore appear more randomly distributed as they conform to the ferrite grain boundaries, which are of a more irregular nature. The nuclei display allotriomorphic rather than idiomorphic character.

Isothermal reaustenitisation at 950°C for 5 secs. results in a modification of the nucleation behaviour. The increased superheating provides a greater driving force for nucleation so that rather more intragranular nucleation is observed in the martensite and bainite structures while nucleation on sub-grain boundaries becomes evident in the ferrite structure. Generally nucleation is more profuse (fig. 4.7).

Acicular austenite nuclei within the prior austenite grains of the martensitic and bainitic structures, soon coalesce to form globular austenite grains although some acicularity is retained where the globular grain coincides with a lath boundary. The later stages of the transformation are shown in fig. 4.8 where the structures are consumed by the thickening of the nodules formed in the early part of the transformation.

A number of specimens were heated in the infra-red, focussed radiation furnace (Appendix 1.3) to investigate the influence of heating rate on the reaustenitisation reaction. As the heating rate was lowered, the distribution of austenite nuclei became concentrated around the high energy nucleation sites, that is the prior austenite grain boundaries in the martensite and bainite structures and the ferrite grain boundaries in the fer-

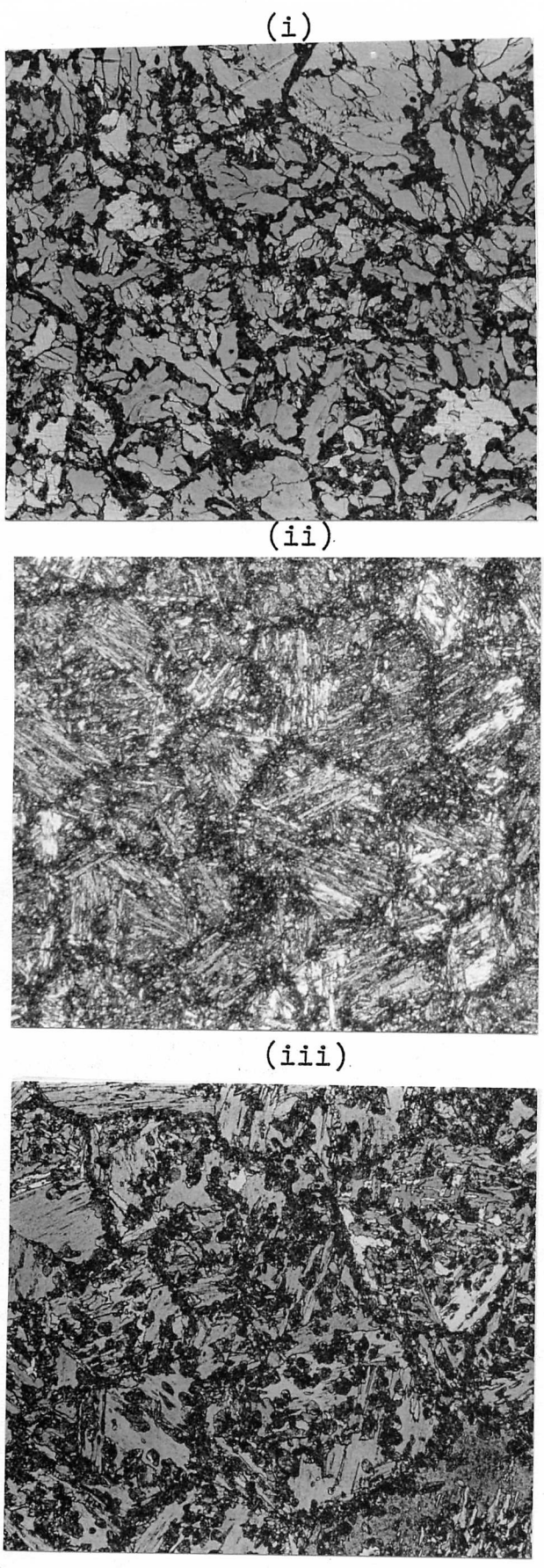

Fig. 4.6: Optical micrographs of structures transformed at 840°C for 15 secs. and iced brine quenched.
(i) Ferrite. ——— 100 μ
(ii) Bainite. ——— 100 μ
(iii) Martensite. ——— 100 μ

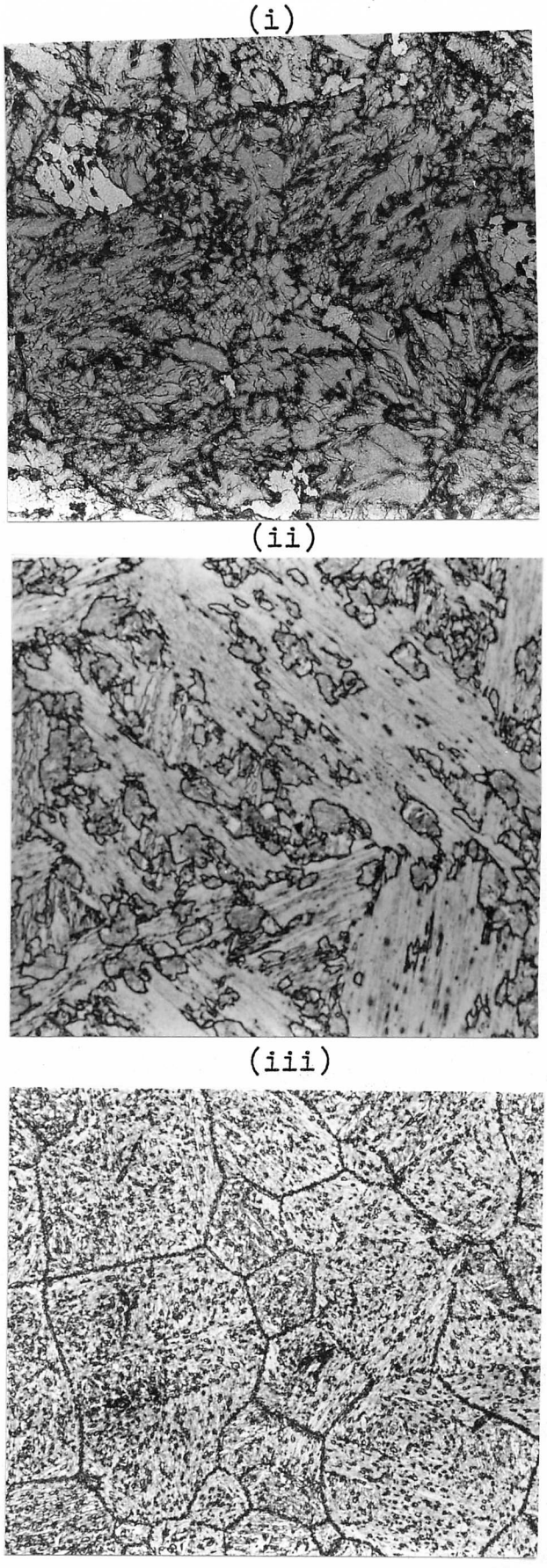

Fig. 4.7: Optical micrographs of structures transformed at 950°C for 5 secs. and iced brine quenched.
(i) Ferrite. ——— 100 μ
(ii) Bainite. ——— 50 μ
(iii) Martensite. ——— 100 μ

ritic structure. At very low heating rates, growth of the austenite tended to be allotriomorphic, even in the martensite and bainite structures, and could be a result of high boundary diffusion rates, whilst nucleation rates and growth rates through the matrix will be low, owing to the small driving force at low degrees of superheat (fig. 4.9).

(ii) Electron Microscopy Investigation:

Replica examination confirmed the morphological information provided by optical metallography but produced further evidence for the very early stages of nucleation. Fig. 4.10 is of an allotriomorph formed on a ferrite grain boundary and shows that growth has occurred predominantly into one grain only. The extraction replica also indicates a region around the growing austenite nodules, where the carbide dispersion is of a coarser nature. This was considered to be the result of either:

(a) coarsening of the interphase precipitation ahead of the advancing austenite;

(b) coarsening in the austenite after the interface had advanced, the zone of coarser precipitate being revealed as the austenite/ferrite interface retreated on quenching;

(c) dissolution of the interphase precipitation at the austenite/ferrite interface followed by reprecipitation in the austenite;

(d) an artefact of the replica technique.

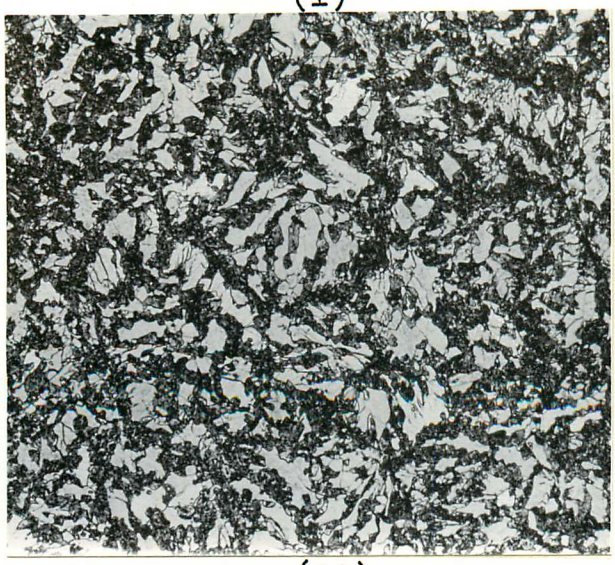

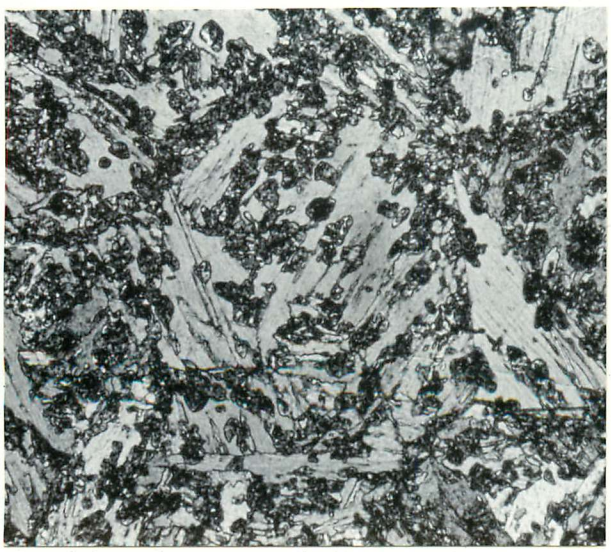

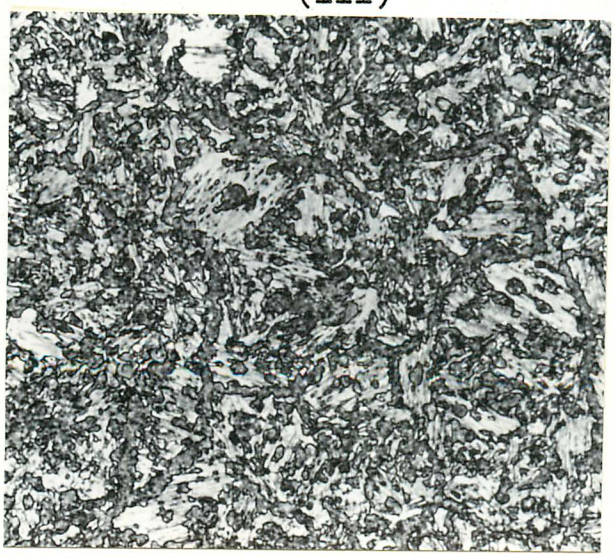

Fig. 4.8: Optical micrographs of structures heated to 900°C for 20 secs. and iced brine quenched.
(i) Ferrite. ——— 200μ
(ii) Bainite. ——— 100μ
(iii) Martensite. ——— 150 μ

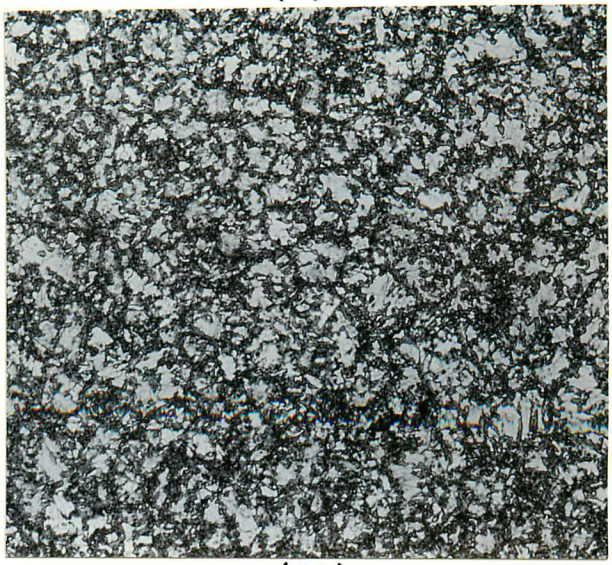

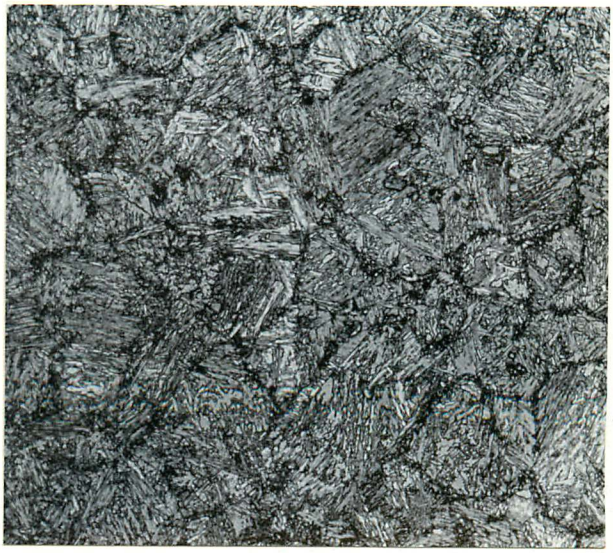

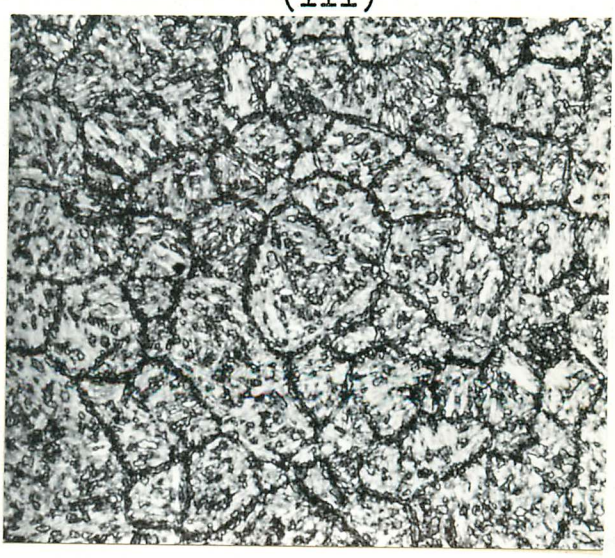

Fig. 4.9: Optical micrographs of structures heated at 0.05°Cs^{-1} to 850°C and iced brine quenched.
(i) Ferrite. ——— 200μ
(ii) Bainite. ——— 150 μ
(iii) Martensite. ——— 150 μ

Thin foil examination enabled the phenomenon to be studied more closely and immediately revealed that this was a real effect. As shown in fig. 4.11 a ferrite grain has been partially consumed by the growing austenite and this austenite is surrounded by a zone of coarser precipitates. Dark field imaging showed that this rim of precipitates was of ferrite having the same orientation as the parent ferrite. It was therefore concluded that the austenite nodule partially retransforms during quenching to reveal the rim of coarser precipitates.

It was also noted that the coarsened precipitates in the rim could sometimes be illuminated using the same reflection as the virgin interphase precipitates, while on other occasions an alternative reflection was needed. This could be explained in terms of coarsening occuring on other B-N variants to the interphase precipitation, as observed by Dunlop and Honeycombe (1975) working on a similar steel, or that dissolution occurred followed by reprecipitation in the austenite. This was resolved by a more detailed analysis of the martensite formed by the quenching of partially transformed specimens.

Fig. 4.12 shows an austenite nodule growing into the surrounding ferrite matrix. Dark field imaging has illuminated retained austenite, predominantly around the perimeter of the nodule and diffraction analysis established that this austenite is K-S related to the surrounding ferrite. This suggests that the austenite was nucleated on a sub-boundary in the ferrite, as the surrounding matrix is of single orientation. The coarsened particles

2μ

Fig. 4.10: Extraction replica electron micrograph of the ferrite structure transformed at 850°C for 15 secs. and iced brine quenched.

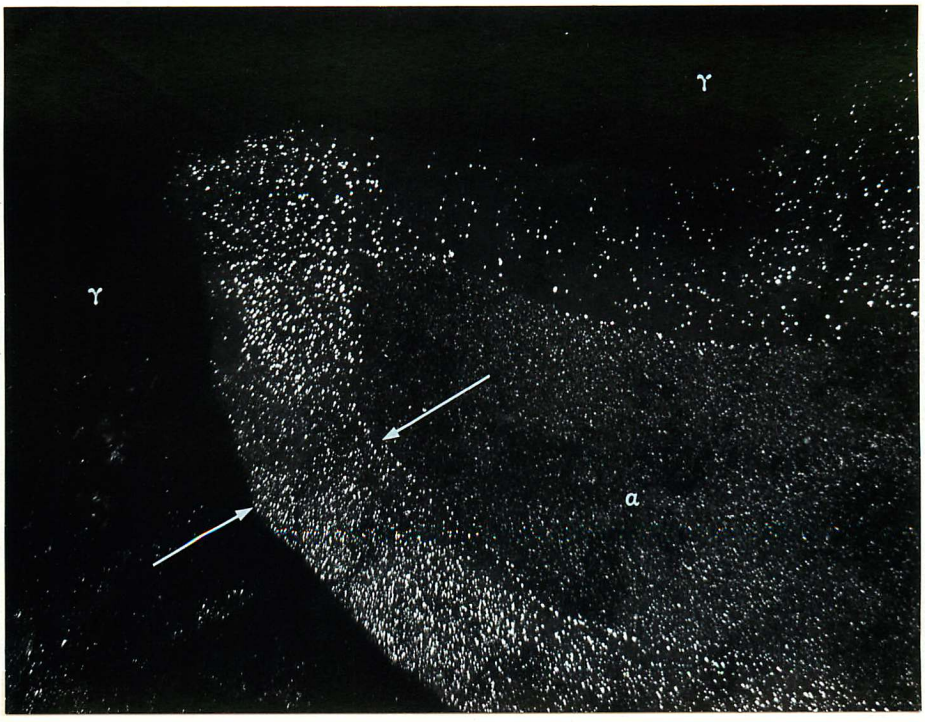

1μ

Fig. 4.11: Thin foil electron micrograph of the ferrite structure, transformed at 900°C for 15 secs. and iced brine quenched. Centred dark field using a (111) vanadium carbide reflection.

are illuminated in dark field and are shown to be cube/cube related to the retained austenite. However, this is not confirmation of a mechanism of dissolution at the austenite/ferrite interface following by reprecipitation in the austenite. The last chapter established that the interphase precipitates not only have a B-N relationship with the ferrite but are also cube/cube with the austenite. Thus, if the growing austenite is K-S related to the ferrite, then the precipitates need not alter orientation in order to lie in a cube/cube relationship with the austenite. However, in this case, the coarsened precipitates are seen to be illuminated by an independant reflection and hence, must have been reprecipitated in the austenite.

It is interesting to note in fig. 4.13 that dissolution of coarser precipitates on a ferrite sub-boundary remains incomplete as the precipitates are still evident in the austenite nodule. Preferential growth of the nodule along the ferrite sub-boundaries can also be seen.

The crystallography of a grain boundary nucleated nodule is established in fig. 4.14 and is found to be K-S related to the ferrite grain into which growth has not occurred. The austenite orientation was identified using the retained austenite formed during the quench. It is again more strongly illuminated around the perimeter of the growing austenite nodule, which suggests that the retention of austenite may be influenced by solute concentration gradients.

(i)

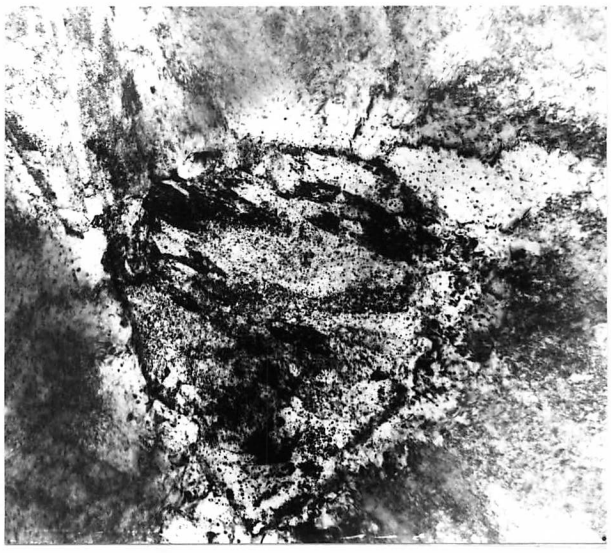

1μ

(ii)

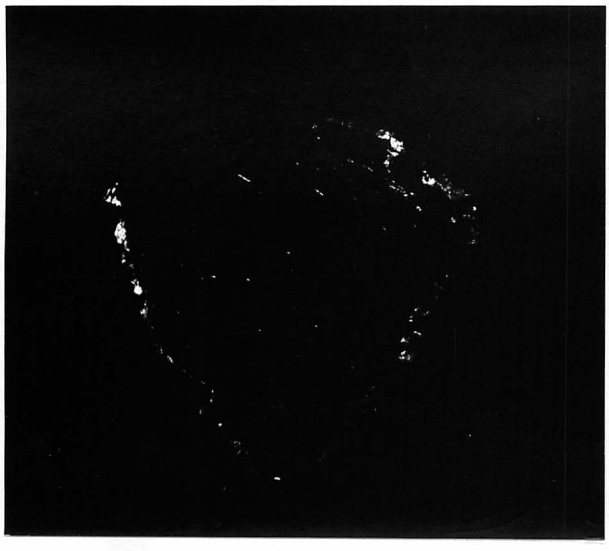

(iii)

Fig. 4.12: Thin foil electron micrographs of the ferrite structure, transformed at 840°C for 15 secs. and iced brine quenched.
(i) Bright field.
(ii) Centred dark field using a (020) austenite reflection.
(iii) Centred dark field using a (020) vanadium carbide reflection.

(iv)

(v)

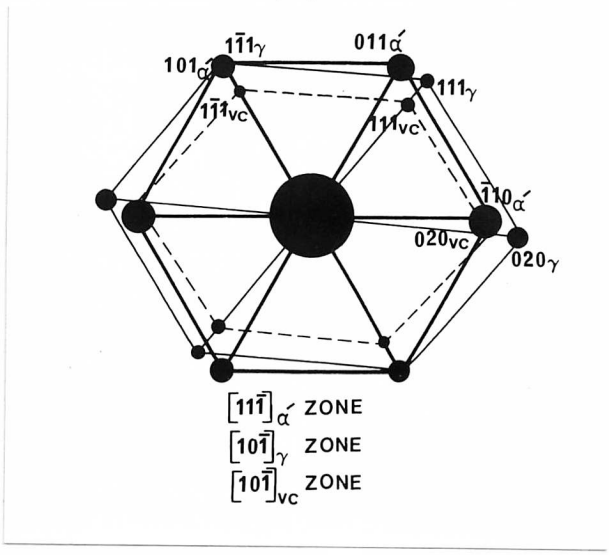

(vi)

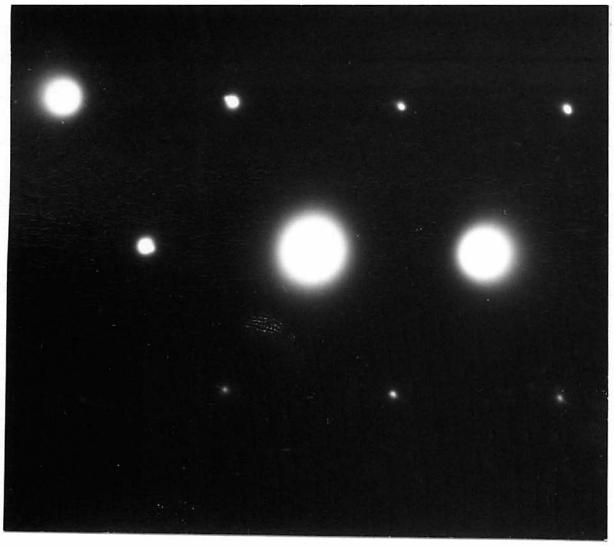

(vii)

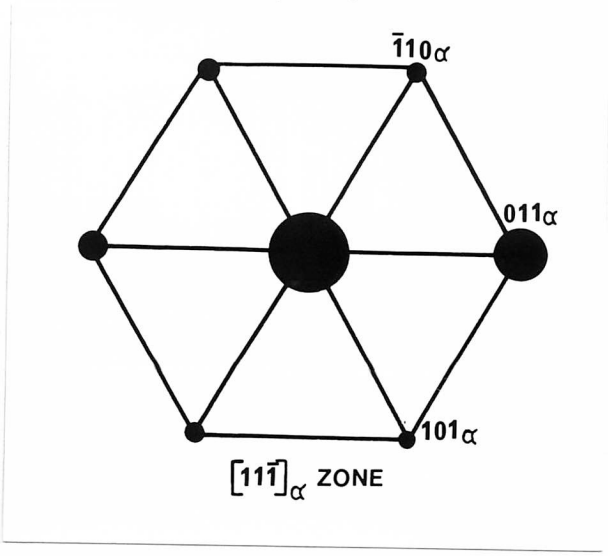

Fig. 4.12: (continued)
(iv) Diffraction pattern of the area shown in (i).
(v) Analysis of (iv).
(vi) Diffraction pattern of surrounding matrix.
(vii) Analysis of (vi)

Fig. 4.13: Thin foil, bright field, electron micrograph of the ferrite structure, transformed at 875°C for 15 secs. and iced brine quenched.

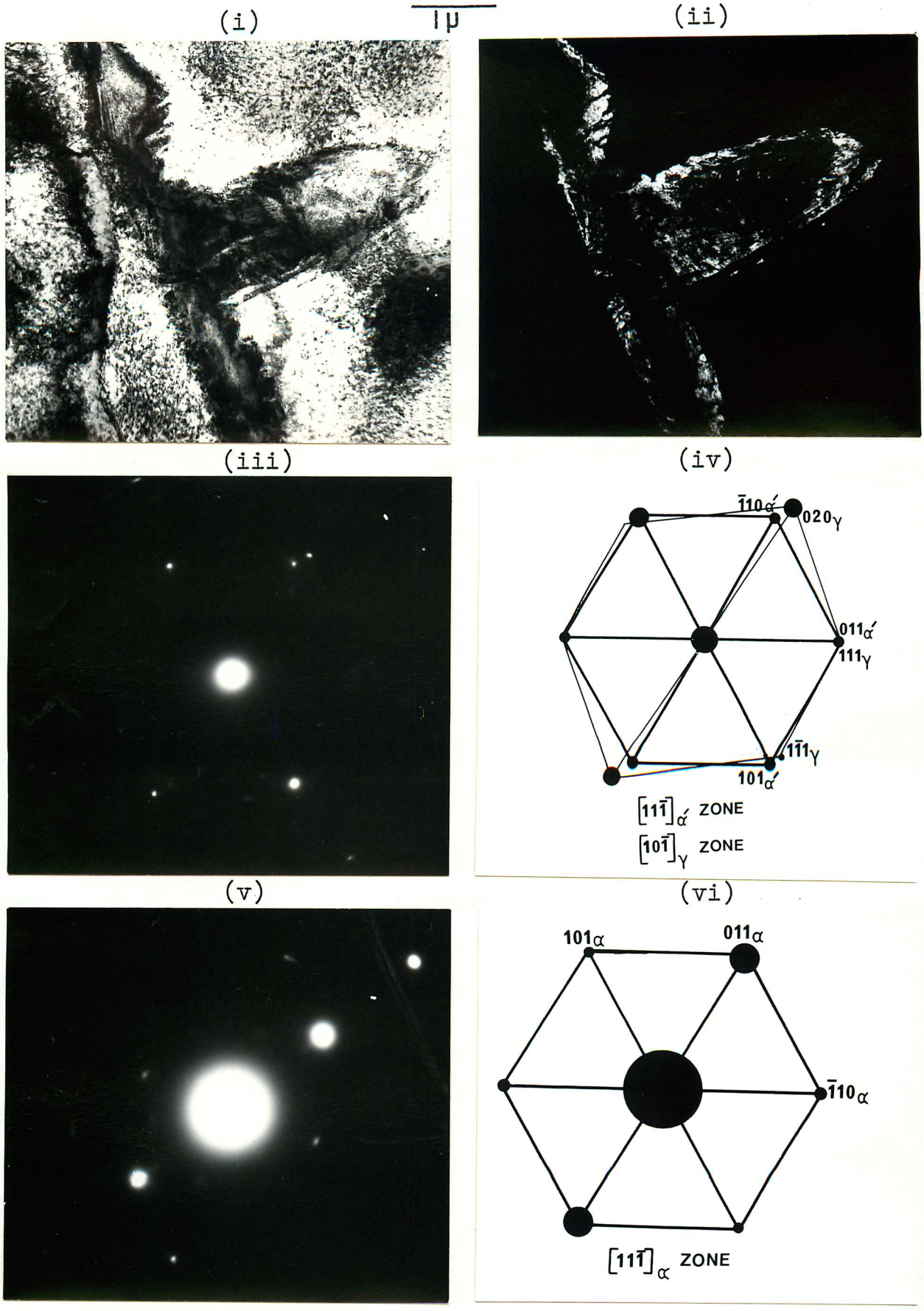

Fig. 4.14: Thin foil electron micrographs of the ferrite structure heated at 840°C for 15 secs. and iced brine quenched.
(i) Bright field.
(ii) Centred dark field using a (020) austenite reflection.
(iii) Diffraction pattern of the area shown in (i)
(iv) Analysis of (iii).
(v) Diffraction pattern of the matrix on the opposite side of the prior austenite boundary.
(vi) Analysis of (v).

Growth of austenite into the martensite and bainite structures was found to occur by a similar nucleation and growth process. However, even at the most rapid heating rates, the starting microstructures became modified as a result of the heating process. This is shown in fig. 4.15a and 4.15b. These are micrographs in the bainite and martensite specimens respectively, from regions which have not been consumed by the growing austenite. The specimens have been held at 840°C for 15 secs. only, yet both structures contain a fine dispersion of vanadium carbide. All three B-N habits are present indicating a tempering reaction. No evidence of cementite was found in the bainite structure indicating that complete and rapid dissolution of the interlath cementite must have occurred.

4.4.4 Kinetics of Reaustenitisation

(i) Isothermal Reaustenitisation:

Prolonged holding (1,000 hrs.) at elevated temperatures followed by quenching, established the Ae_1 and Ae_3 temperatures to be approximately 820°C and 905°C respectively. Specimens austenitised in this region adopted transformation curves of the type shown in fig. 4.16a, being typically sigmoidal and indicative of a nucleation and growth mechanism. The total percentage of transformation increased with increasing temperature up to the Ar_3 temperature.

The influence of temperature on the reaustenitisation process is shown in fig. 4.16b. It can be seen that the nucleation times in the bainite and martensite structures

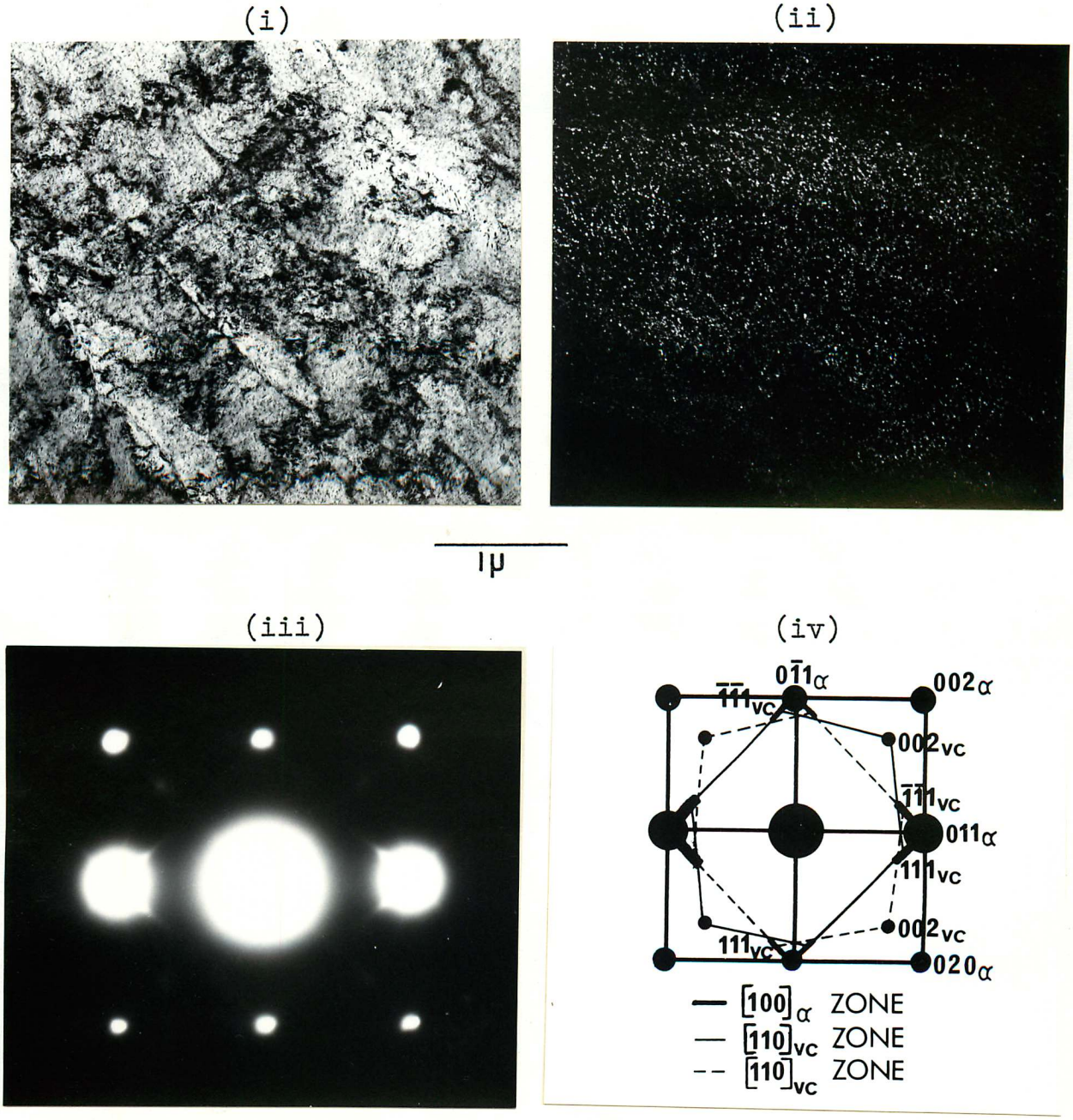

Fig. 4.15: Thin foil electron micrographs of the bainite structure held at 840°C for 15 secs. and iced brine quenched.
(i) Bright field.
(ii) Centred dark field using the (111) vanadium carbide reflection.
(iii) Diffraction pattern.
(iv) Analysis of (iii).

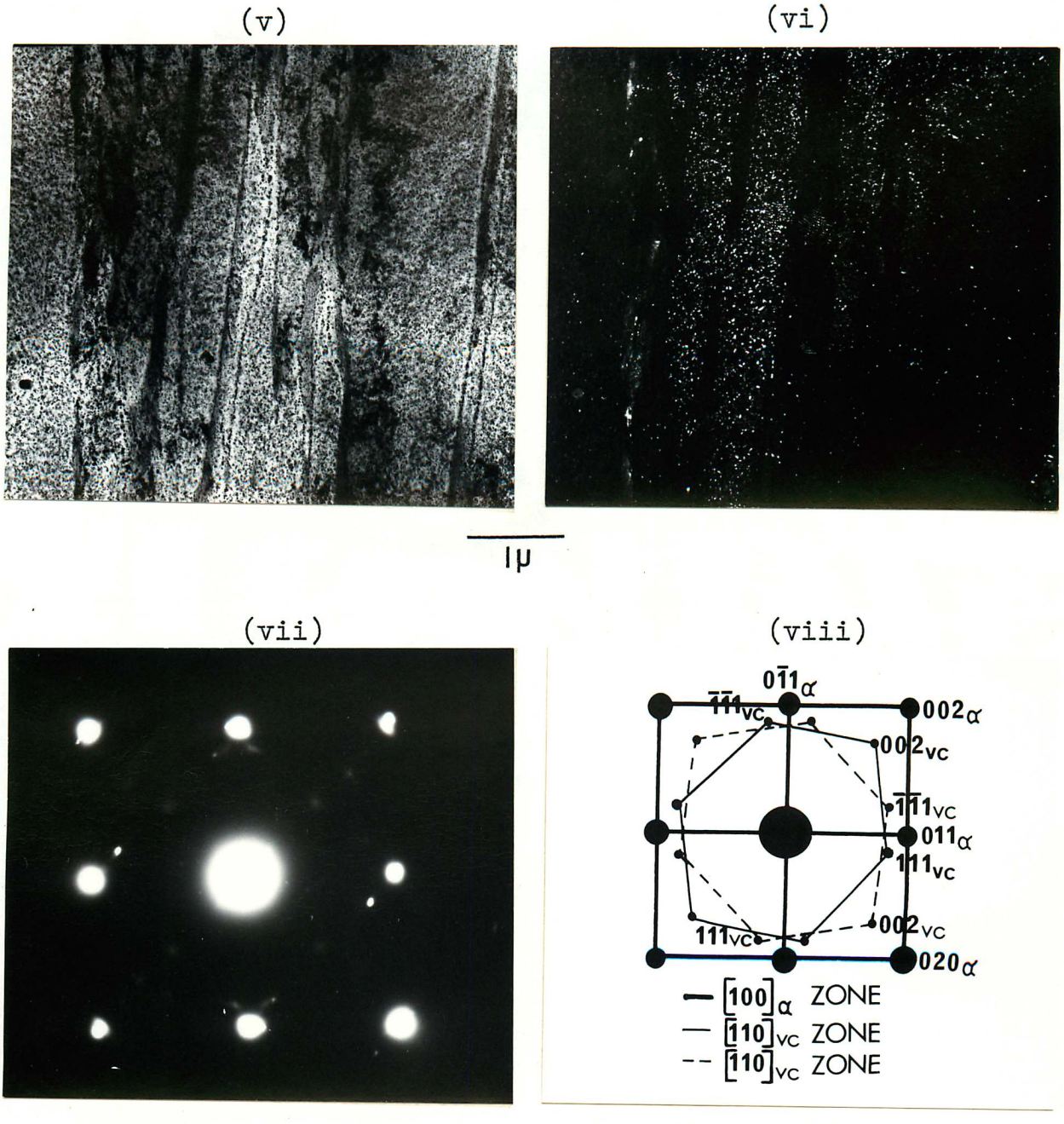

Fig. 4.15: (continued) Thin foil electron micrographs of the martensite structure held at 840°C for 15 secs. and iced brine quenched.
(v) Bright field.
(vi) Centred dark field using the (111) vanadium carbide reflection.
(vii) Diffraction pattern.
(viii) Analysis of (vii).

are shorter than for the ferrite structure and is consistent with the optical investigation, which revealed qualitatively that the bainite and martensite structures displayed a higher nucleation rate. The times to complete the transformation vary in a similar manner.

Direct measurement of nucleation rates proved difficult owing to uncertainty in establishing the existence of a boundary between the nuclei. This is normally accomplished by a tempering treatment which results in segregation to these boundaries and renders them susceptible to certain etchants (Aaronson, Johnston and Schmatz, 1968). However, the low impurity content (Appendix 1.1) rendered this treatment unsuccessful. Growth rates could be measured however, and fig. 4.17 compares the rates of growth of austenite nuclei in the three microstructures. Under the high magnifications necessary to measure nodule sizes, it proved difficult to differentiate between grain boundary nucleated nodules and intragranular nodules; however, low magnification studies suggested that once site saturation had occurred, then there was no major difference between the two. A systematic method of measuring the nodule sizes was employed whereby for each measurement the largest ten nodule radii were measured over ten fields of view.

The growth rates were found not to differ significantly in the three starting microstructures, and was attributed to the fact that the austenite was growing through structures bearing essentially similar carbide dispersions, as shown in the electron microscopy investi-

(a)

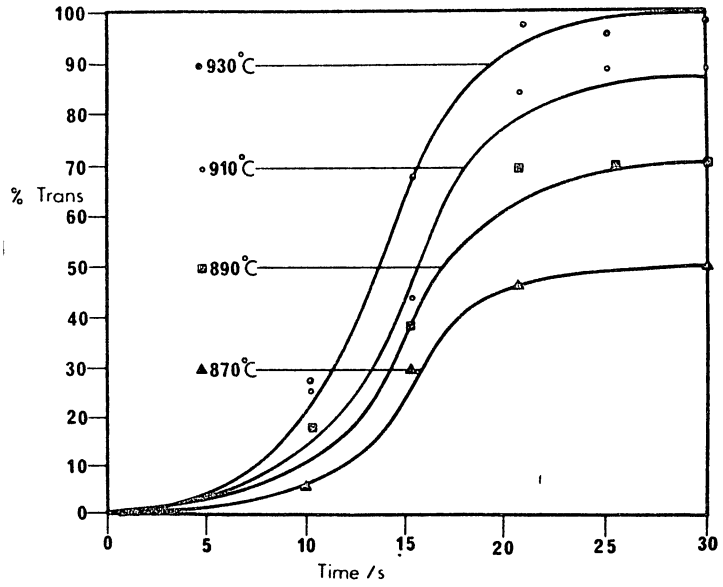

(b)

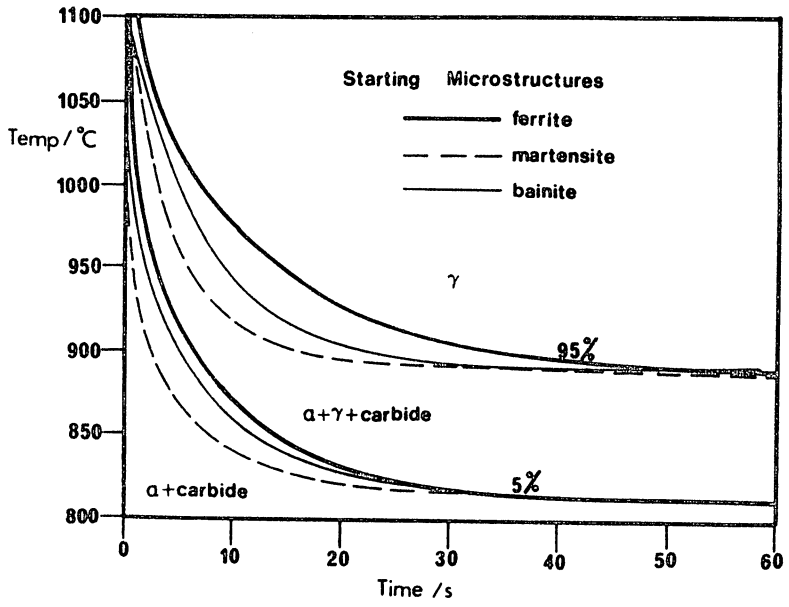

Fig. 4.16
(a) Isothermal austenitisation curves for Fe-IV-0.2C directly transformed at 700°C.
(b) The TTT curve for the austenitisation of Fe-IV-0.2C from ferritic, bainitic and martensitic microstructures.

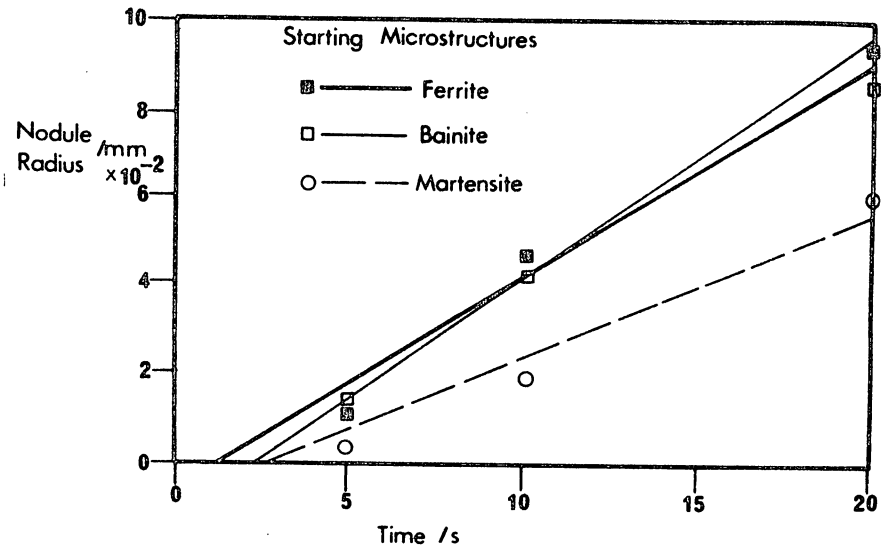

Fig. 4.17 Growth rates of austenite into ferrite, bainite and martensite at 925°C.

gation of fig. 4.15a and 4.15b.

By assuming that the austenite grows at an equal rate through the three starting microstructures, a comparison of the nucleation rates in the three alloys can be achieved through comparison of the grain sizes on retransforming to ferrite. At 950°C the relative nucleation rates of the ferrite, martensite and bainite are in the ratio 1:1.23:1.36 respectively.

(ii) Gradual Heating:

A dilatometer study, using a Theta Industries high speed dilatometer, was performed to investigate the influence of heating rate on the Ar_1 and Ar_3 temperatures for the martensite, bainite and ferrite structures.

The form of a typical dilatometer trace is shown in fig. 4.18 and the Ar_1 and Ar_3 temperatures were taken as the turnover points in the extension trace.

Fig. 4.19 compares the Ar_1 and Ar_3 temperatures for the starting microstructures as a function of heating rate varying from $50^{\circ}Cs^{-1}$ to $0.05^{\circ}Cs^{-1}$. In all cases the Ar_1 temperature decreases as the heating rate is reduced and the transformation proceeds more closely according to equilibrium conditions.

The results extrapolated to give an Ae_1 temperature between 820°C and 830°C and as such are in agreement with the prolonged heating results quoted earlier.

Throughout the range of heating rates, the Ar_1 temperature was lowest in the case of the martensite specimens. The temperature increased for the bainite structure and also the ferrite.

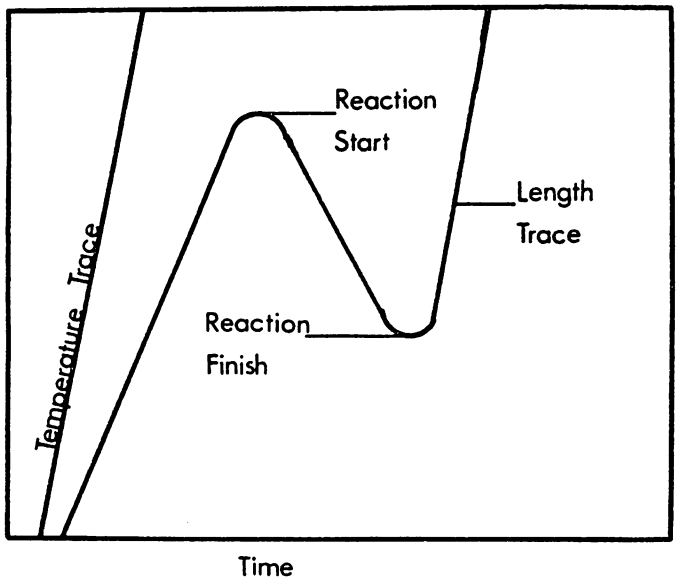

Fig. 4.18: A typical dilatometer trace of the ferrite to austenite transformation in Fe-IV-0.2C.

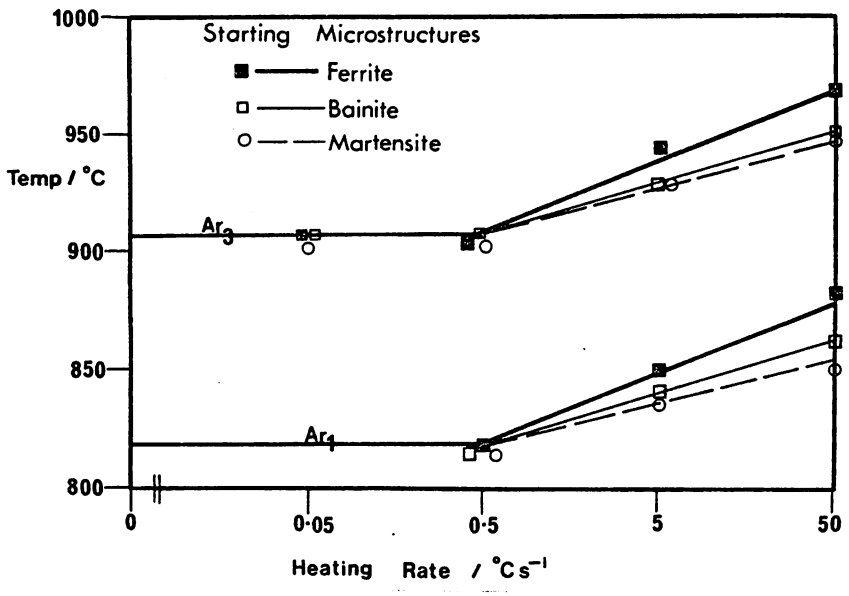

Fig. 4.19: The austenite transformation start (Ar_1) and finish (Ar_3) temperatures as a function of heating rate, from the ferrite, bainite and martensite structures.

These results can be compared with the nucleation behaviour observed in the isothermal transformation studies, where the martensite structure was found qualitatively to have the highest austenite nucleation rate, followed by the bainite and the ferrite structures.

It is more difficult to draw direct conclusions from variations in the Ar_3 temperature, as this will necessarily be influenced by the temperature at which the transformation began, the nucleation rate and the subsequent growth rate of the nodules. These were studied earlier using isothermal investigations and it is consistent that the transformation should be completed firstly in the martensite structure then in the bainite and ferrite structures.

4.5 Discussion and Conclusions

The reaustenitisation reaction in Fe-IV-0.2C has been studied from ferritic, bainitic and martensitic starting microstructures and has been found to occur exclusively by a nucleation and growth process. The growth morphologies of the austenite in all cases conformed to the Dubé classification describing allotriomorphic and idiomorphic growth of ferrite; the primary sideplate morphologies reported by Fong and Glover (1975) were not observed.

The distribution of austenite nuclei at low degrees of superheat was found to occur on the prior austenite grain boundaries in the martensite and bainite structures, and on the ferrite grain boundaries in the ferritic steel. At higher degrees of superheat, brought about by a high isothermal transformation temperature or a rapid heating

rate, intragranular nucleation also occurred at lath boundaries in the martensite and bainite strucutres and on subboundaries in the ferrite structure.

Thin foil examination by transmission electron microscopy, revealed that both the bainite and martensite dispersions tempered quickly on heating to produce fine dispersions of vanadium carbide. This poses two main points for discussion:

(a) The mechanism and feasability of tempering at elevated temperatures;

(b) The nucleation mechanism of austenite in low-alloy steels.

Tempering reactions in steels have been studied extensively and in the presence of a carbide forming element a cementite displacement reaction has been shown to occur (Baker and Nutting (1959), Davenport and Honeycombe (1975)). Thus, the alloy carbide forms on the sites of the pre-existing cementite, which may not be situated so as to act most efficiently to strengthen the steel; for example, at lath boundaries. The micrographs shown in fig. 4.15a and 4.15b do not display any appreciable lath boundary precipitation and this may well indicate that a more direct route to the equilibrium carbide has been adopted. The resulting precipitation is very fine and indicates that a rapid heat treatment at high temperatures may provide an alternative and more efficient method of tempering thin sections.

It has been noted that a prior austenite boundary in the martensite or bainite microstructures provides a more

efficient boundary for nucleation than a ferrite grain boundary in the directly transformed ferritic steel. It might be expected that in the presence of free cementite, localised regions of high carbon concentration would form easily and thereby provide a preferential site for austenite nucleation. However, there is no evidence that free cementite exists at elevated temperatures in any of these structures. Consequently, further work will be required to establish why one type of boundary nucleates the austenite phase more prolifically than another.

Replica and thin foil examination established that the passage of the austenite/ferrite interface, effected the dissolution of the alloy carbide dispersions followed by coarser reprecipitation of vanadium carbide in the austenite, with a cube/cube orientation relationship. The coarser precipitation was originally revealed as a zone of corser precipitates surrounding the austenite nodules. This was shown to result from the partial retransformation of the austenite nodule during quenching. The ferrite thus formed was of the same orientation as the parent ferrite indicating that recourse to a separate nucleation event was not necessary.

Austenite nucleated on sub-boundarious in the ferrite was found to be K-S related to the surrounding matrix, while grain boundary nucleation produced austenite which was K-S related to the grain into which the majority of growth did not occur. This situation can be compared to the ferrite reaction described in the last chapter. The grain boundary nucleated austenite clearly grows by move-

ment of an incoherent interface into the ferrite, however, the sub-boundary nucleated species is related to the surrounding ferrite and hence the possibility of coherent interfaces exists. No evidence was found however, to suggest that the reaction front adopts a facetted configuration and consequently it can be assumed to grow without the necessity to form ledges.

Although nucleation rates could not be measured directly, indirect evidence indicated that nucleation rates increased with increasing temperature and that the highest rates were observed in the martensite strucutres, decreasing through the bainite and ferrite structures. Growth rates were also found to increase with increasing temperature, although little variation in growth rate was observed between the martensite, bainite and directly transformed ferrite structures.

The nucleation and growth of austenite bears certain differences with its decomposition. Classically, the thermodynamic driving force for a reaction is dependent upon the temperature difference between the equilibrium temperature, and the temperature at which the reaction occurs. In the case of austenite decomposition this is hampered by a decrease in the diffusion rates as the temperature is lowered; this behaviour produces the characteristic C-curve. In the case of the austenitisation reaction, both driving force and diffusion rates increase with increasing temperature, and hence no nose is expected on the transformation curve. It can be seen to increase exponentically with increase in temperature in fig. 4.16b.

This means that both nucleation and growth rates increase as the temperature is raised. However, this behaviour is complicated by the fact that, in general, austenite is forming from more than one phase; usually a carbide phase is present, which itself is coarsening and dissolving as a function of both temperature, and microstructural condition. This phase can both assist nucleation, and impede growth. It is thus likely that optimum conditions will exist to produce a minimum austenite grain size, and this is discussed more fully in the next chapter.

CHAPTER FIVE

GRAIN REFINEMENT BY RAPID HEAT TREATMENT AND THE RESULTING INFLUENCE ON MECHANICAL PROPERTIES IN Fe-IV-0.2C

5.1 Introduction

The previous chapter has considered the processes involved in the formation of austenite from a number of starting microstructures. Investigations included studies of the microstructural changes occuring during transformation and examination of the nucleation and growth phenomena governing the reaction kinetics. The austenite grain size produced after transformation is dependant largely upon the interaction of these processes and this chapter investigates the conditions under which small austenite grain sizes can be achieved.

The literature describing the rapid heat treatment of steel is reviewed, together with some of the related techniques for producing grain refinement by heat treatment processes.

The results largely describe an investigation into the grain refinement of ferritic structures and the resulting influence on mechanical strength and toughness. Despite the superior nucleation characteristics of the martensite and bainite structures, experiments using such microstructures to produce retransformed ferritic structures were considered inconsistent with the heat treatment philosophy proposed for directly trans-

formed interphase steels. This was discussed more fully in chapter one, where it was pointed out that the advantages of using directly transformed ferritic steels included the avoidance of quenching to acicular structures followed by a tempering treatment.

The results are discussed in section 5.5 on the basis of the viability of rapid heat treatment cycles for producing fine grained structures in low-alloy ferritic steels.

5.2 Literature Survey

The dependence of mechanical strength and toughness upon grain size was first rationalised in the Hall (1951)-Petch (1953) relationships. These show that the yield stress (σy) and the cleavage fracture stress (σc) vary with grain size (d) according to the expressions:

$$\sigma y = \sigma_1 + k_1 d^{-\frac{1}{2}}$$
$$\sigma c = \sigma_2 = k_2 d^{-\frac{1}{2}}$$

σ_1, σ_2, k_1 and k_2 are constants

It is clear that a refinement in grain size results not only in an increase in strength but also an improvement in the cleavage fracture stress. Grain refinement is therefore a desirable route to high strength levels, as all other strengthening mechanisms, such as precipitation hardening or solid solid solution strengthening, adversely affect toughness.

Much work has therefore been directed towards the development of grain refinement techniques, particularly in steels, and has been reviewed by Gladman (1973), but

it has only been in recent years that rapid heat treatment has been recognised as a viable method of producing fine grained structures (Grange, 1966). Rapid heat treatment relies on two main aspects of austenite formation to produce fine grain sizes:

(a) Rapid heating enables the transformation to austenite to occur at a higher temperature, encouraging a high rate of nucleation.

(b) By holding above the Ac_3 for no longer than is sufficient to effect complete austenitisation, austenite grain growth is minimised.

Any subsequent transformation will be greatly influenced by the refined austenite grain size, in that the number of high energy nucleation sites (i.e. grain boundaries) will be increased, thereby encouraging a fine grained transformation product.

Grange (1971) emphasised the importance of the starting microstructure in rapid heat treatment schedules. Fine dispersions of carbide in ferrite, as encountered in martensite and tempered martensite, were found more conducive to grain refinement than coarser structures, such as ferrite/pearlite aggregates. Grange does not speculate as to the reason for this but it can be noted that apart from the relatively greater abundance of nucleation sites in the martensite structure, the temperature required to complete austenitisation is higher in the coarser structures. The austenite formed from coarser structures will therefore be subjected to higher temperatures and grain growth will be more rapid. In conven-

tional heat treatments such grain growth would prove insignificant because of the relatively low holding temperature. However, in steels which have undergone a rapid austenitisation treatment, the austenite grains are far smaller and less stable, and may grow rapidly because of the high energy associated with the extensive grain boundary area.

Grange reports that the effect of rapid heat treatment can be optimised by cycling. This relies on the fact that formation of a fine grained transformation product provides a more suitable microstructure for a further rapid reaustenitisation cycle, as there will be a greater abundance of nucleation sites. In turn, reaustenitisation will occur more quickly, transformation being complete at a lower temperature. However, the effect soon saturates as the austenite grain structure becomes so unstable, because of the small grain size, and rarely are more than four cycles worthwhile. Grain growth of the austenite is therefore the limiting factor in such treatments.

Grange (1971) used a range of steels for his investigation ranging from a 0.18%C steel to a high carbon cutlery steel. The treatment proved effective in all cases, but it was also reported that in the high carbon range of steels a unique microstructure was developed consisting of a uniform dispersion of fine carbides in an ultrafine martensitic matrix. This was a result of incomplete dissolution of the carbides on heating, but was not considered deleterious to the subsequent mechanical behaviour of the steel, as the particles were suf-

ficiently fine not to crack under an applied stress, while providing an added strength.

The principles laid down by Grange have been applied to commercial strip steels. Wallbridge and Parr (1967) used a resistance heating method to rapidly austenitise low carbon strip. This was quenched to martensite with a very fine prior austenite grain size and produced enhanced strength and toughness of the strip.

More recent work by Mahajan, Venkataraman and Mallik (1973), on a commercial medium carbon steel, reports that ultrafine grain sizes (4 μm) were produced after a four cycle rapid reaustenitisation treatment and that corresponding improvements were experienced in both the strength, ductility and the fracture behaviour of the steel. This was attributed mainly to the decrease in grain size, but also to a fine dispersion of carbides which were evident in the quenched specimens. In agreement with the work of Grange (1971) it was claimed that this dispersion is inherited from an inhomogeneous austenite; a consequence of the reduced hold time providing insufficient opportunity for complete carbide dissolution.

Work on higher alloy steels (Miller, 1972) achieved ultrafine grain sizes by an alternative route. By annealing cold worked steels in the two-phase ($\alpha+\gamma$) region, grain sizes in the range 0.3-1.1 μm were achieved. The technique depends on the high alloy content of the steel producing an extended austenite phase field so that annealing in the austenite/ferrite region can be effected between about 450°C-650°C. Growth rates of the austenite

are consequently low while the cold worked steel provides an abundance of nucleation sites. Subsequent grain growth of the austenite is minimised by the surrounding ferrite and ultrafine grain sizes are retained after holds of up to 4,000 hours. General improvement in the mechanical properties is reported and examination of the yield behaviour revealed that the yield stress was dependent on the grain size according to the Hall-Petch relationship, even at ultrafine grain sizes.

A treatment which also involves annealing in the austenite/ferrite phase field has been developed by Jin, Morris and Zackay (1975). They commented on the undesirability of cold working in the final stages of alloy processing and showed that this could be eliminated, while still achieving grain sizes of between 0.5-2 μm. The treatment involves intermediate anneals in the austenite and austenite/ferrite phase fields and optimum properties are achieved by repeating until the effect saturates. Employing the treatment on an Fe-12Ni-0.26Ti cryogenic alloy, the ductile brittle transition temperature was suppressed to below 4K and can be attributed entirely to the ultrafine grain size.

Since the early work of Hall and Petch, the influence of other parameters on the yield stress has been incorporated into a modified Hall-Petch relationship (Pickering and Gladman, 1963). Here, the yield stress is expressed in the form of a vector equation in terms of the contributions from the friction stress (σ_o), solid solution strengthening (σ_{ss}), precipitation hardening (σ_{ph})

and grain size ($kyd^{-\frac{1}{2}}$).

$$\sigma_y = \sigma_o + \sigma_{ss} + \sigma_{ph} + kyd^{-\frac{1}{2}}$$

Increments in the yield stress can therefore be achieved by a number of strengthening mechanisms. However, comparable increases in the cleavage fracture stress do not occur unless the improved strength is achieved by grain refinement.

This is because an increased contribution to yield stress by solid solution hardening or precipitation hardening is not generally accompanied by a significant change in the cleavage stress. Cleavage failure generally occurs through the inability of the material to accommodate an applied stress by plastic deformation and hence a decrease in the ratio of cleavage stress to yield stress encourages brittle behaviour. The adverse influences of solid solution strengthening and precipitation hardening upon toughness are adequately described by this explanation but the beneficial effect of grain refinement is not explained.

The cleavage fracture of crystalline materials has been known for some time to be related to the mechanisms of slip within the particular system considered. Fracture normally occurs along crystallographic planes where dislocation movement has a high activation energy. Thus, cleavage normally occurs along the basal plane of the hexagonal structure in zinc, while in iron, cleavage usually occurs on a $\{100\}_\alpha$ plane.

If a cleavage crack is considered to propagate through a polycrystal, then renucleation of the crack is necessary when the crack is confronted by a grain of

differing orientation. This is an energy consuming process and consequently a higher stress is required to promote cleavage failure in a fine grained material.

Work has attempted to define empirical relationships to predict the impact transition temperature resulting from a combination of structural variables (Gladman, Dulieu and McIvor, 1975). Thus, the impact transition temperature (ITT), can be expressed in terms of the grain size (d), and the precipitate dispersion characteristics

$$ITT = C_1 - k_1(d^{-\frac{1}{2}}) + k_2 \text{ (dispersion)}$$

C_1, k_1 and k_2 are constants

The contribution from the precipitation hardening is dependent upon the nature of the dispersion itself and consequently its effectiveness in impeding the propagation of dislocations.

5.3 Results

5.3.1 Alloys and Heat Treatment

The alloy used for this study was of nominal composition Fe-IV-0.2C (Appendix 1.1) and was initially solution treated at 1,200°C for 30 mins., then isothermally transformed at 700°C for 2 mins. This produced a ferritic steel containing a banded dispersion of vanadium carbide, as described in chapter three.

The specimens used were 3 mm. rod cut into 15 mm. lengths and provided samples for both optical and electron microscopy, and hardness tests. Specimens for tensile and impact testing are described in Appendix 1.4 and 1.5 respectively.

5.3.2 Isothermal Austenitisation

In order to minimise austenite grain growth, Grange (1971) has advised that heating should be prolonged only for sufficient time to allow complete austenitisation to occur. The austenitisation kinetics must therefore be accurately determined. These were established in the previous chapter (fig. 4.14), and consequently specimens were heated in a salt pot until austenitisation was complete. They were then retransformed in a tin bath at 700°C and the structures examined using optical and electron metallography.

(i) Optical Microscopy:

(a) Structural Examination

The retransformed structure consisted of fine grained ferrite which differed morphologically from the ferrite starting microstructure in two main ways. Firstly, the ferrite grains conformed more closely to a classical equiaxed structure, and secondly, there did not appear to be any marked sub-grain formation (fig. 5.1). The possibility that the fine-grained structure transformed by a different mechanism was examined in the light of these results. Partial transformation studies of the ferrite reaction were performed and similar morphologies to those encountered in chapter three were observed (fig. 5.2). Consequently it was concluded that the mechanism of ferrite formation had not changed. However, as might be expected, the number of ferrite nuclei per austenite grain had decreased because of the reduced boundary area per austenite grain. Thus, there is a greater probabi-

lity that any particular boundary between two austenite grains is consumed before further nucleation events on the same boundary take place. There is consequently less chance of low-angle boundaries caused by the impingement of grains of similar orientation as a result of nucleation on the same boundary. Also a reduction in grain size reduces the potential for sub-grain formation caused by growth faults, as impingement with neighbouring grains occurs before substantial growth has taken place.

Further investigation of structures retransformed after austenitisation between 915°C and 925°C, revealed areas where the parent ferrite had not responded to the rapid heat treatment cycle. Fig. 5.3 shows such an area composed of large ferrite grains surrounded by the finer, equi-axed structure. Austenitisation at higher temperatures eliminated the effect.

(b) Grain Size Measurements

Measurement of the grain size formed on austenitisation proved unsuccessful because of the inability to segregate impurities to the austenite grain boundaries, which would thereby provide sites for preferential attack by an etchant. However, measurements of the ferrite grain size were considered to provide some idea of the effectiveness of the heat treatments and to afford comparison between heat treatment cycles.

Ferrite grain sizes were measured using a calibrated graticule which gave values of the mean linear intercept grain size. Problems were encountered in measuring the grain size of the ferrite starting microstructure as the

(i) 100μ (ii)

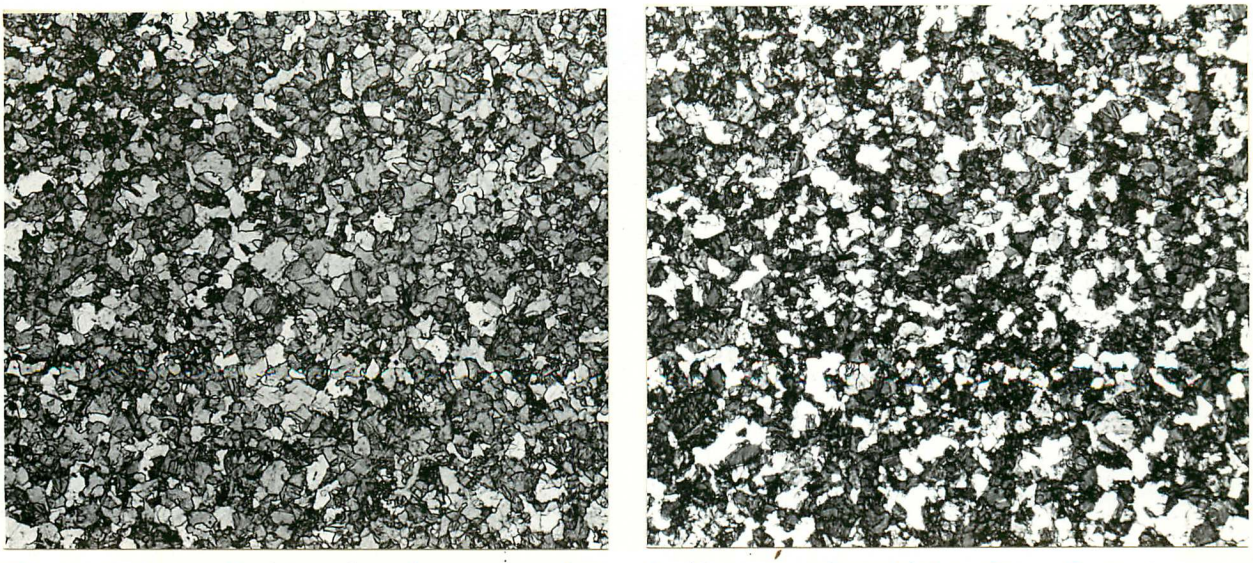

Fig. 5.1: Optical micrographs of the austenitised and retransformed structures.
(i) Austenitised at 1200°C for 5 secs. and retransformed at 700°C
(ii) Austenitised at 950°C for 30 secs. and retransformed at 700°C

(i) 10μ (ii)

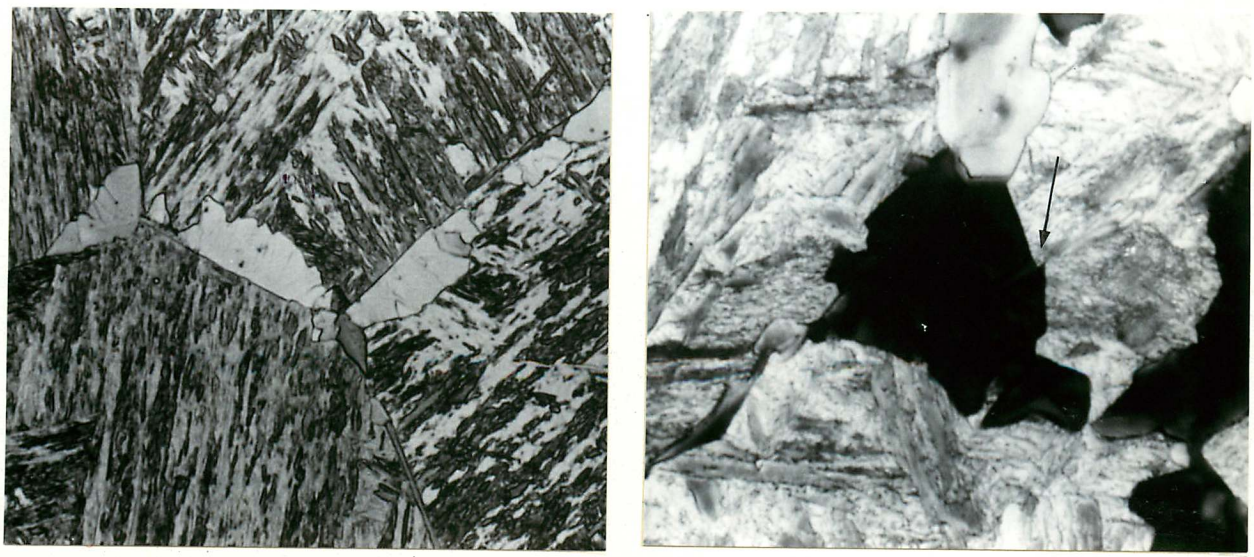

Fig. 5.2: Optical micrographs of the austenitised and partially retransformed structures.
(i) Austenitised at 1200°C for 5 secs. and partially transformed at 700°C for 5 secs. and quenched.
(ii) Austenitised at 1000°C for 20 secs. and partially transformed at 700°C for 10 secs. and quenched. (Phase contrast micrograph)

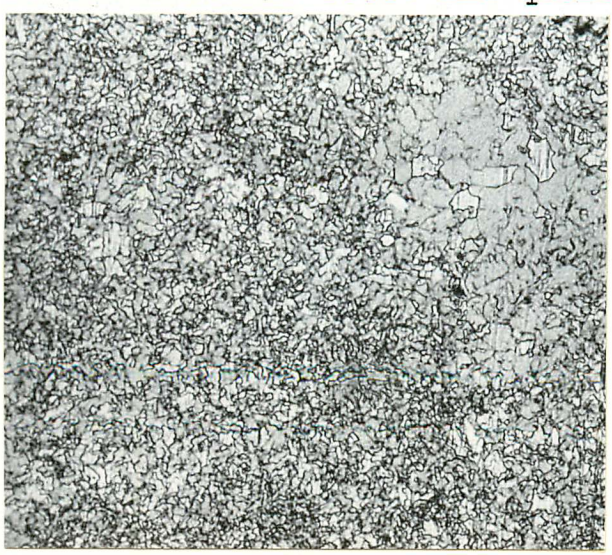

Fig. 5.3: Optical micrograph of Fe-IV-0.2C after austenitising at 925°C for 1 min. and retransforming at 700°C.

15μ

high sub-grain density caused confusion in establishing the boundary types in the optical microscope. For this reason the initial ferrite grain size was measure after partially austenitising at 840°C and quenching. This procedure helped to outline the ferrite grain boundaries, as they presented preferential sites for austenite nucleation and are then defined by a rim of martensite on quenching.

An initial ferrite grain size of 55 μm (standard deviation, $\sigma = 22$) after isothermal transformation to ferrite at 700°C was measured. This is larger than those encountered by either Batte (1970), Benson (1976) or Wilyman (1976) but can be explained by the minor diferences in heat treatment, these workers having used an intermediate quench after homogenisation, followed by a lower temperature solution treatment.

Fig. 5.4 shows the variation in ferrite grain sizes after rapid heat treatment to various austenitising temperatures. The curve appears to display two minima. As the temperature is lowered from 925°C, the mean grain size increases as a result of retransformation to large ferrite grains in some areas (fig. 5.3). This is reflected in large error bars at these temperatures, where there is a broad grain size distribution. A minimum is present at around 940°C and represents the point at which the large grained areas are eliminated. A second minimum is evident at approximately 1050°C and is thought to be the result of the interaction of processes occurring during austenitisation, as discussed in the previous chapter.

This minimum is thought to represent the point at which the nucleation rate of the austenite is high enough to produce a small grain size, despite the high austenite growth rate and subsequent grain growth of the austenite. It is possible that the precipitates in the virgin ferrite are presenting the greatest hindrance to the advancing austenite/ferrite interface at this particular temperature, thereby enabling nucleation to be more profuse. Further increase in austenitising temperature results in an increase in grain size, as grain growth of the unstable austenite becomes more rapid.

(ii) Electron Microscopy Examination:

The electron microscopy of fully retransformed specimens was consistent with the partial transformation studies of the previous chapter. It was shown that austenite nodules consumed the ferrite matrix and that dissolution of the interphase precipitation occurred at the austenite/ferrite interface, followed by reprecipitation of the alloy carbide as a coarser dispersion in the austenite. Retransformation to ferrite revealed this uniform dispersion of coarse carbides but also showed that a second dispersion of aligned precipitates had formed, as shown in fig. 5.5.

Single surface trace analysis showed that the aligned rows occupied a {110} ferrite habit and diffraction analysis confirmed that the precipitates obeyed the B-N orientation relationship. It was concluded that the aligned precipitation had occurred by the interphase precipitation reaction described in chapter three, and consequently,

that some dissolution of the alloy carbide had occurred during austenitisation. Fig. 5.6 shows a complete grain which has transformed to produce rows of aligned vanadium carbide and is seen to conform to the classical interphase precipitation structure. It is worthy of note that the boundary between the adjacent ferrite grains is of a stepped nature and is therefore consistent with the results presented in chapter three, where a ledge mechanism was shown to be responsible for the development of aligned precipitation structures.

Closer examination of fig. 5.5 reveals that the coarsened vanadium carbide precipitates are surrounded by a precipitate free zone. This could be a result either of solute depletion, which occurs during the formation and growth of the coarse carbides, or of further Ostwald coarsening of these carbides in retransformed ferrite at the isothermal transformation temperature, or a combination or both effects.

(iii) Hardness Measurements:

The variation in hardness with reheat temperature (fig. 5.7) is seen at low temperatures to correspond inversely to the grain size variation (fig. 5.4). At low reheating temperatures (below 925^{o}C) the lower hardness values are thought to reflect directly the coarser ferrite grain size and is seen to increase correpondingly as the coarse grained areas are eliminated. The hardness decreases again as the ferrite grain size increases at above 1000^{o}C, but a further increase in reaustenitising temperature results in a significant increase in hardness

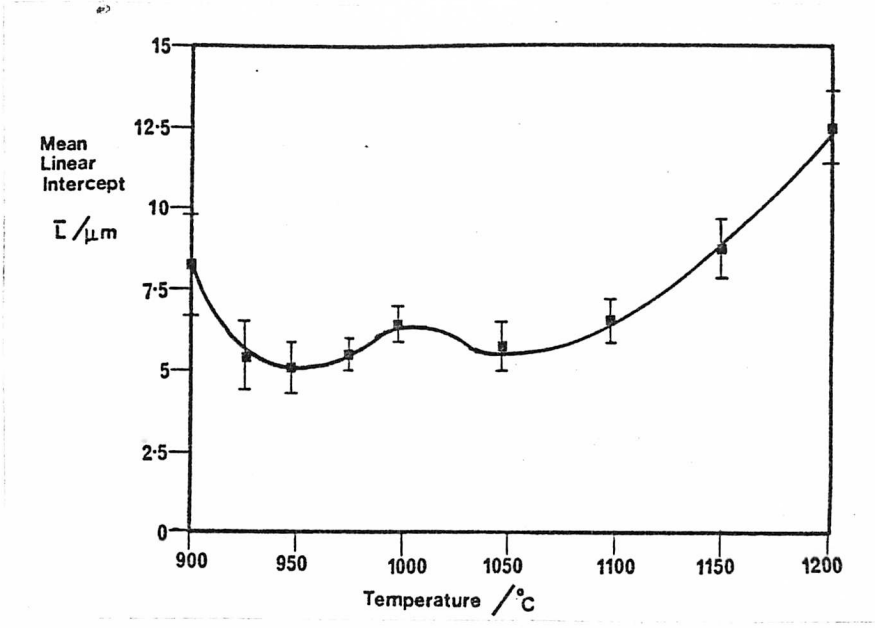

Fig. 5.4: Variation in ferrite grain size with austenitising temperature. Retransformed at 700°C for 2 mins.

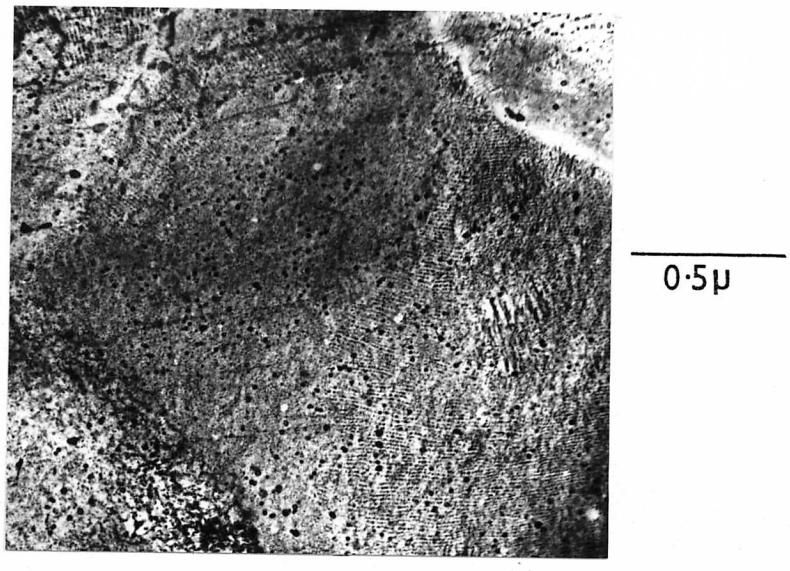

Fig. 5.5: Bright field, thin foil electron micrograph of Fe-IV-0.2C austenitised at 1050°C for 15 secs. and retransformed at 700°C.

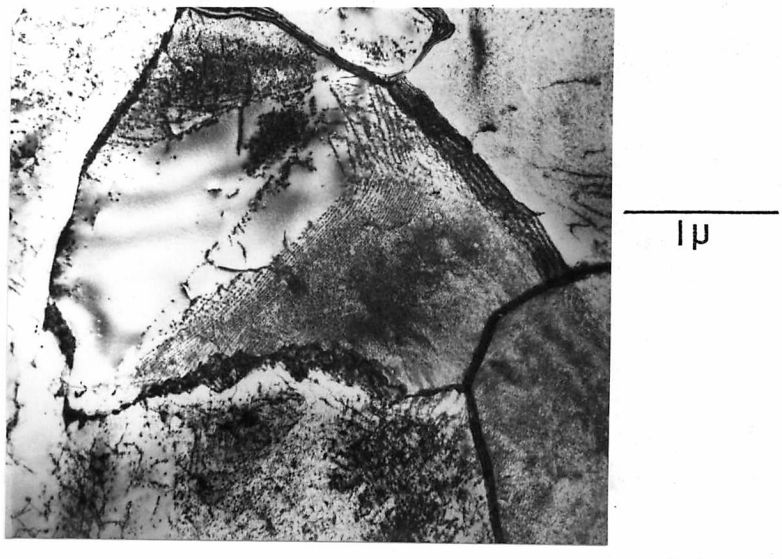

Fig. 5.6: Bright field, thin foil electron micrograph of Fe-IV-0.2C austenitised at 950°C for 30 secs. and retransformed at 700°C.

values. The latter behaviour is attributed to the higher dissolution kinetics of the alloy carbide at elevated temperatures, which results in a higher volume fraction of fine interphase precipitation on retransformation to ferrite.

The overall hardness variations are complex but can be partly explained by the variations in ferrite grain size and partly by the coarsening and dissolution kinetics of the vanadium carbide precipitates. The coarsened particles provide a less effective means of strengthening than do the fine precipitates produced on retransformation to ferrite. Consequently, complete dissolution of the vanadium carbide is advantageous for achieving high strength levels as a higher volume fraction of aligned precipitation is produced on retransformation.

5.3.3 Cyclic Rapid Reaustenitisation

The limitations of the rapid heat treatment process were investigated by repeating the austenitisation cycle up to six times. The specimens were heated to 950°C for 30 secs. followed by retransformation at 700°C. The resulting microstructures were examined optically and corresponding hardness values were measured. These results are shown in fig. 5.8, where a decrease in grain size is apparent as the number of cycles is increased, but beyond approximately four cycles, the process has minimal effect.

In apparent conflict with the Hall-Petch relation-

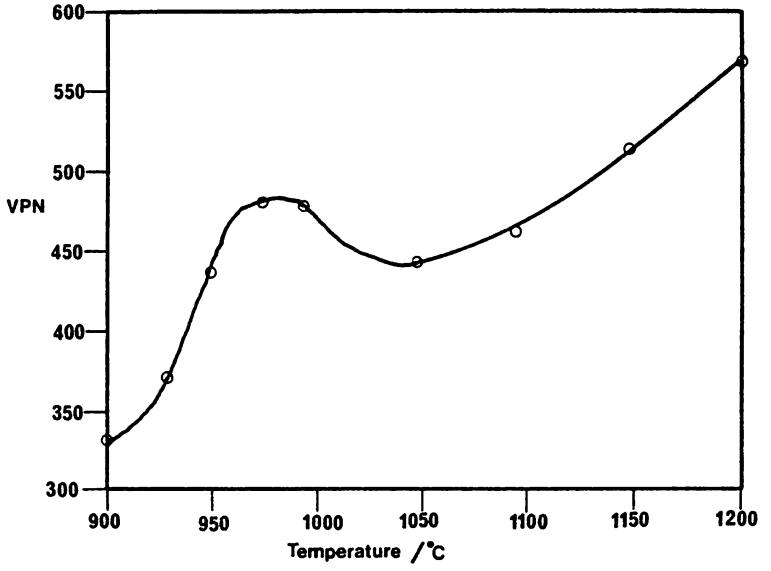

Fig. 5.7: Variation in hardness with reheat temperature.

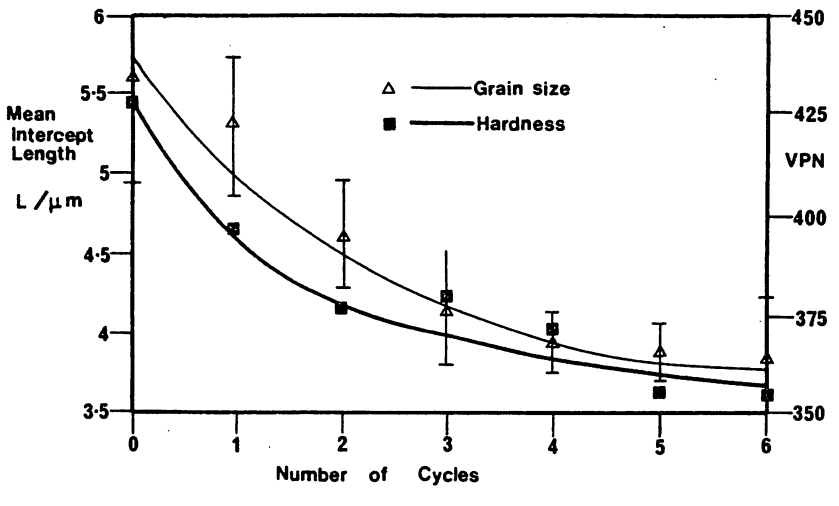

Fig. 5.8: Variation of grain size and hardness with the number of rapid heat treatment cycles.

ship, the hardness decreases with decreasing grain size. This is readily explained, however, in terms of the vector yield strength equation of Pickering and Gladman (1963) where the influence of precipitation hardening and solid solution strengthening are also taken into account. During the first reaustenitisation cycle the precipitate dispersion in the ferrite is of a very fine nature and consequently dissolution occurs readily. However, on subsequent cycles the precipitate dispersion contains a significant volume fraction of coarser particles, which dissolve less rapidly. The amount of solute available for reprecipitation, therefore, decreases to lower the precipitation hardening contribution to the yield stress. Thus, despite the decrease in grain size, the hardness falls owing to the diminished influence of the precipitation.

5.3.4. Gradual Heating

In the last chapter, a number of ferrite specimens were austenitised in a dilatometer to determine the influence of starting microstructure upon the temperature range of the transformation. The ferrite specimens, which had initially been transformed at 700°C, were also cooled at a constant rate of $20^{\circ}Cs^{-1}$ to enable measurement of the transformation temperature on cooling (Ac_3 and Ac_1). This enabled the influence of differences in the asutenite structure, as a result of various heating rates, upon the subsequent transformation kinetics to be measured. The specimens were also used to investigate the influence of heating rate upon the grain size and hardness of the

retransformed ferrite, and the size of the coarsened particles.

(i) Variation of Retransformation Temperatures (Ac_3 and Ac_1) with Heating Rate:

The range of temperatures over which the specimens retransformed to ferrite showed little variation over the range of heating rates. The transformation start temperature (Ac_3) was fixed at 803°C (standard deviation σ= 4) and the transformation finish temperature (Ac_1) at 747°C (standard deviation σ= 6.5). It was therefore concluded that the austenite structures formed on reheating did not differ significantly in any manner which would influence the subsequent transformation kinetics.

(ii) Influence of Heating Rate on Grain Size:

This is represented graphically in fig. 5.9a. As demonstrated in the previous chapter, the transformation temperatures to austenite decreased as the heating rate was lowered; consequently the transformation occurs at a lower temperature. This was shown to result in a reduction in the nucleation rate. The grain size measurements in fig. 5.9c confirm this behaviour, the fastest heating rates producing a grain size of approximately 8.5 μm. This is larger than those produced by isothermal treatments not only because of the reduced rate of heating, but also because retransformation to ferrite occurs on a continuous cool rather than isothermally.

(iii) Influence of Heating Rate on Carbide Particle Size:

From fig. 5.9b the mean diameter of the coarsened particles is seen to increase in a similar way to the grain

size variation. The factors which control the final particle size are complex but the velocity of the advancing austenite/ferrite interface is probably an important consideration, as this determines the time period over which the grain boundary is available for the transport of solute.

(iv) Influence of Heating Rate on Hardness:

Despite the variations in grain size and coarse particle diameter, the hardness of the retransformed ferrite does not vary appreciably over the range of heating rates used (fig. 5.9c). If the solid solution strengthening increment of the strength is assumed to be the same for each heating rate, then the results suggest that the precipitation hardening contribution to strength is similar over the range of heating rates. This implies that the volume fraction of precipitate is the same in all cases and therefore, that the equilibrium concentration of vanadium carbide in solid solution in the austenite is reached very quickly.

5.3.5 Mechanical Testing of Rapidly Reaustenitised Specimens

Specimens for mechanical testing were reheated isothermally using the salt bath described in Appendix 1.2 and were then retransformed in a molten tin bath at 700°C.

(i) Tensile Behaviour:

In order to afford comparison between the various heat treatments used, and also to determine their effectiveness, the standard structure of ferrite transformed

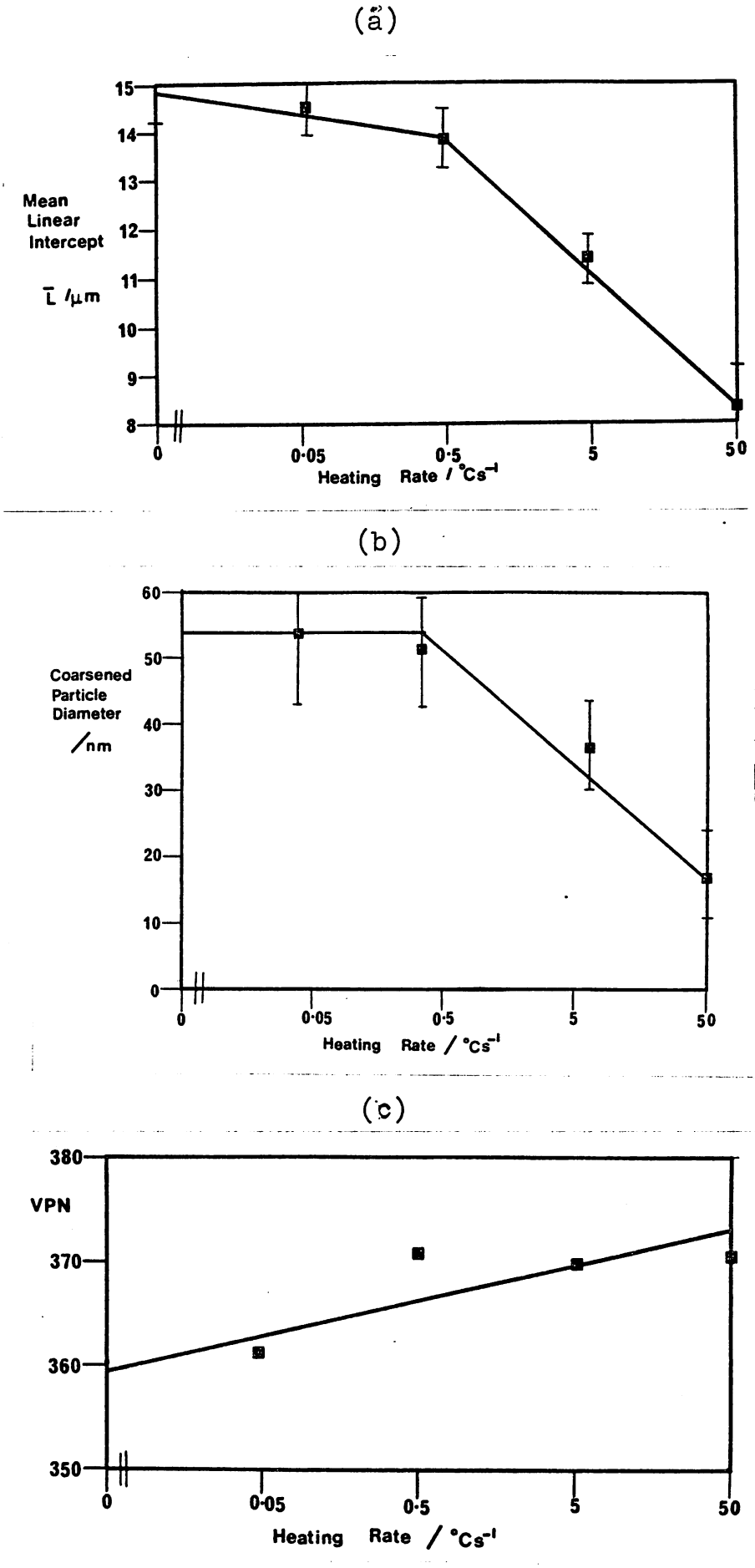

Fig. 5.9: Influence of heating rate on:
(a) Grain size.
(b) Coarsened particle diameter.
(c) Hardness.

at 700°C after solution treatment at 1200°C for 30 mins., was tested as a control. However, despite accurate machining of the specimen and careful polishing to remove any surface flaws, attempts to measure the yield stress and the tensile stress in this material proved unsuccessful, as cleavage failure invariably occurred before the specimens yielded. The results of Wilyman (1976), however, have been used to provide comparison. He successfully tested similar material, though of a smaller grain size, and quotes a yield stress of approximately 1100MNm^{-2}.

Fig. 5.10 shows the variation of yield stress and tensile stress with isothermal reheat temperature and displays a similar form to the hardness curve shown in fig. 5.9c, with a notable minimum at approximately 1050°C.

The ratio of tensile stress to yield stress decreases as the reheat temperature is increased and this is plotted in fig. 5.11. This is an important parameter as it describes the general shape of the stress strain curve. Clearly the high temperature reaustenitisation treatments produce a very "flat" stress/strain curve, while the lower temperature treatments require a significant increase in stress before necking occurs.

Fig. 5.12 demonstrates corresponding variations in elongation and reduction in area with reheat temperature, the curves tending to zero as the ratio of tensile stress to yield stress tends to zero.

The fractography of the specimens was studied using both optical and scanning electron microscopy. Fig. 5.13 shows a series of scanning electron micrographs of speci-

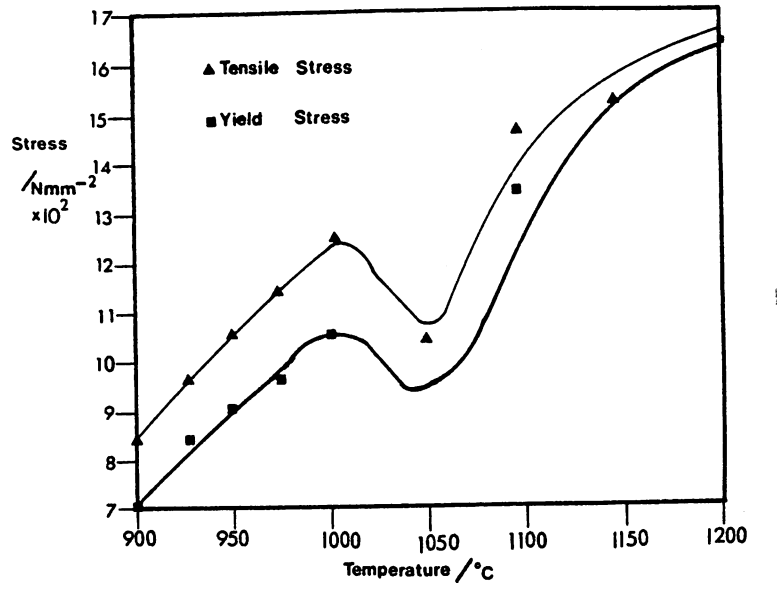

Fig. 5.10: Variation of the tensile and yield stresses with austenitisation temperature.

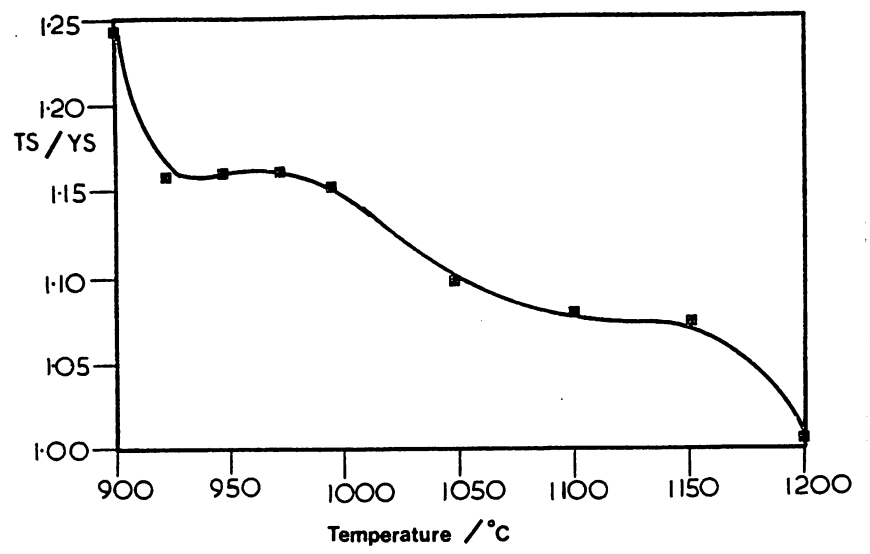

Fig. 5.11: Variation of the ratio of tensile to yield stress with austenitisation temperature.

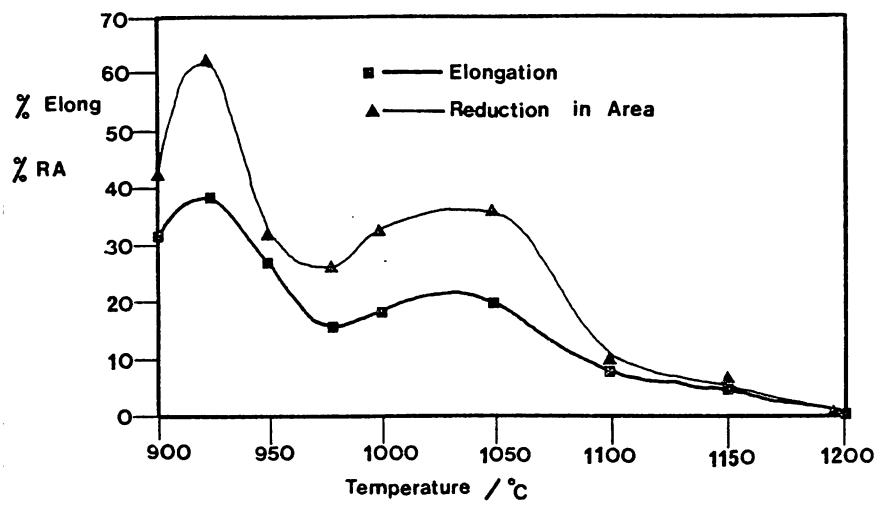

Fig. 5.12: Variation of the elongation and reduction in area with austenitisation temperature.

mens tested over the range of reheat temperatures. At low reheat temperatures the fracture surface is heavily deformed suggesting a classical ductile failure by a mechanism of microvoid coalescence. Close examination of the fracture surface reveals that some of the dimples contain small particles.

Fig. 5.13a, representing a specimen reheated to a temperature of 925°C, displays a typical cup and cone fracture, often observed in tensile specimens, and occurs when the stress increase, caused by necking and the formation of microvoids, promotes a shear mode of fracture at the free surfaces of the neck.

As the reheat temperature is increased the fracture surface becomes more facetted and the classical "river patterns" which accompany cleavage failure can be seen.

The results are supported by the optical examination shown in fig. 5.13b where extensive deformation is evident in the specimen treated at 950°C, while the specimen treated at 1200°C shows no reduction in cross-section at the fracture surface and no microstructural evidence of deformation.

(ii) Impact Behaviour:

Impact transition curves were plotted for reheat temperatures of 952°C, 950°C, and 1200°C, as described in Appendix 1.5. Testing at other temperatures was precluded by a shortage of material.

The results are shown in fig. 5.14, where the specimens reheated to 950°C are shown to display both a superior

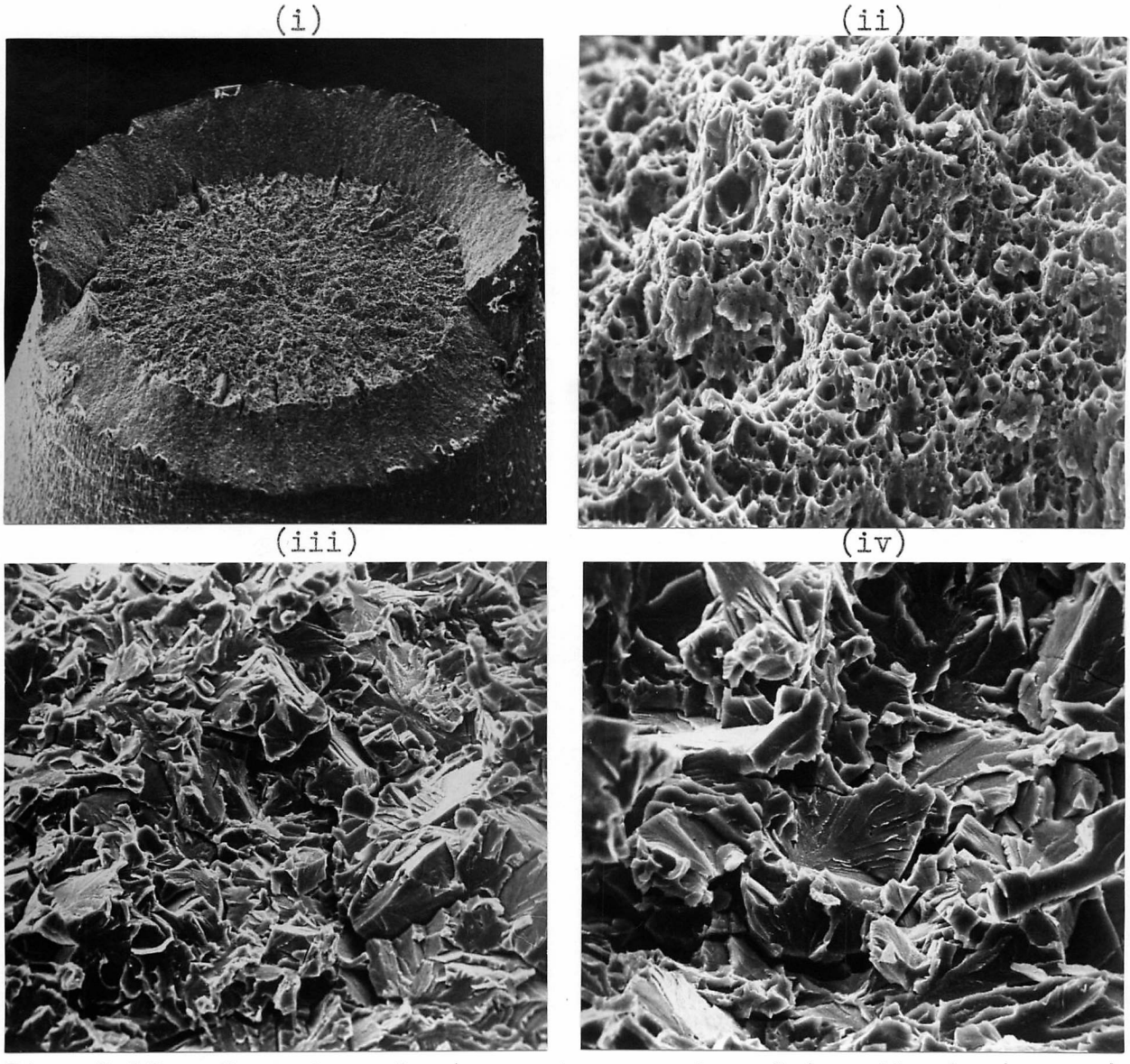

Fig. 5.13a Scanning electron micrographs of tensile test specimen fracture surfaces.
(i) Austenitised at 925°C and retransformed at 700°C.——100μ
(ii) Austenitised at 950°C and retransformed at 700°C.—— 5μ
(iii) Austenitised at 1100°C and retransformed at 700°C.——10μ
(iv) Austenitised at 1200°C and retransformed at 700°C.—— 3μ

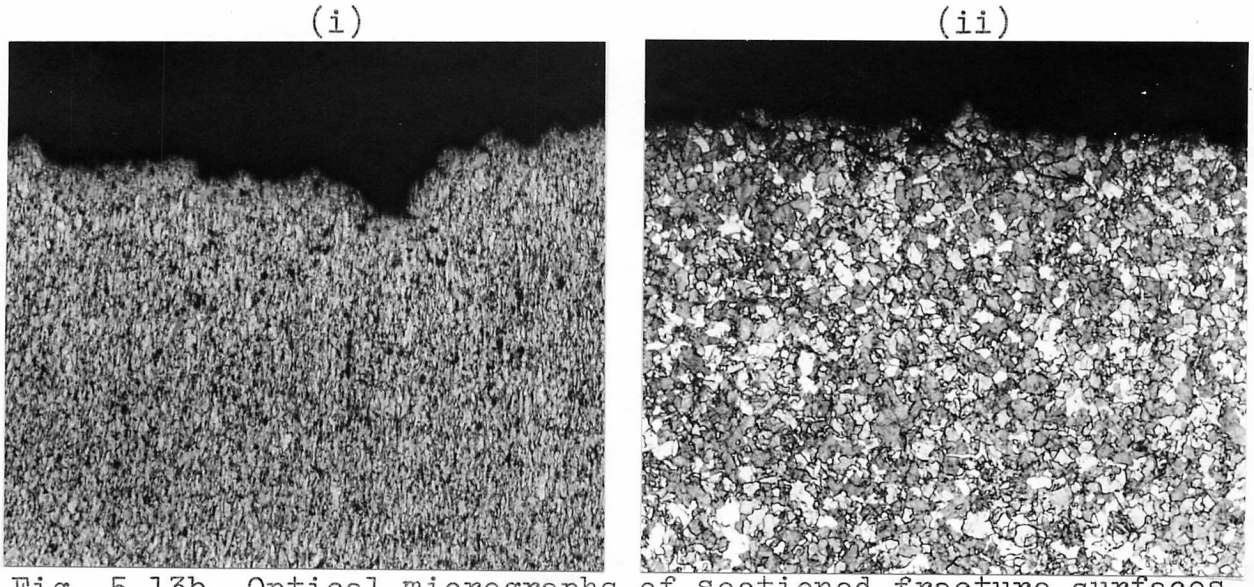

Fig. 5.13b Optical micrographs of sectioned fracture surfaces.
(i) Austenitised at 950°C and retransformed at 700°C.
(ii) Austenitised at 1200°C and retransformed at 700°C. ——100μ

upper shelf energy and also a lower impact transition temperature. The specimens reheated to 925°C and 1200°C show a more gradual transition from brittle to ductile behaviour and show a decrease in upper shelf energy as the test temperature is raised.

A specimen transformed to ferrite at 700°C, which had not undergone a rapid heat treatment cycle, was also tested as a control. Even at elevated testing temperatures (400°C) the fracture surface indicated that failure occurred exclusively by a cleavage mechanism (fig. 5.15). The fractography of specimens reaustenitised to 925°C, 950°C and 1200°C are shown in fig. 5.16. In each case the transition from cleavage to ductile behaviour can be seen as the temperature is increased. The specimens heated to 950°C and 1200°C pass through an intermediate region where the two fracture modes can be seen to be intimately mixed. However, the specimens heated to 925°C, while also displaying these regions of mixed fracture, appear to contain more extensive regions of brittle failure.

The regions exhibiting ductile behaviour, for the three reheat temperatures, can be seen to contain a mixed dimple size. The origin of the two varieties of dimples is clearly different as the morphologies are quite distinct. It is possible that the smaller variety correspond to the coarsened particles, documented in the electron microscopy study of the reaustenitisation process (fig. 5.5), as their spacing of approximately 100 nm corresponds roughly to the dimple spacing.

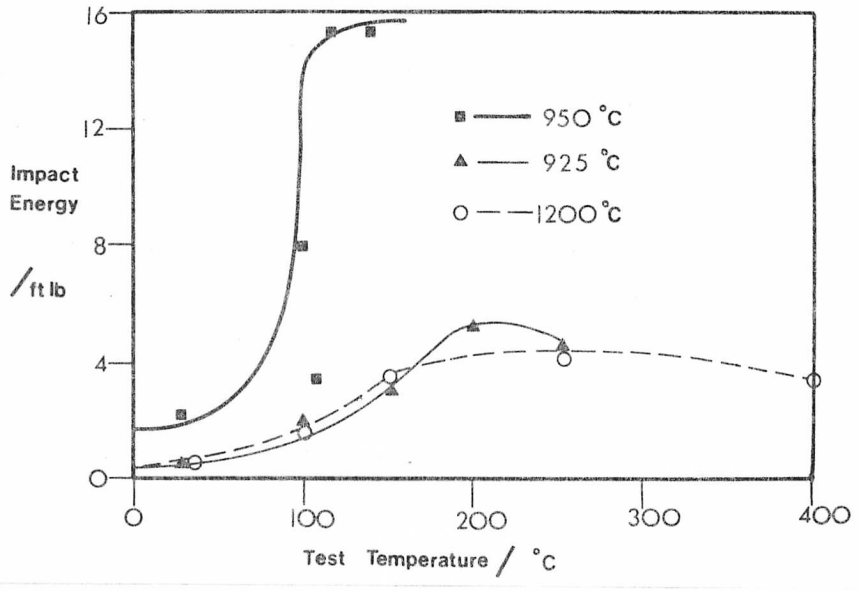

Fig. 5.14 Variation of impact energy with temperature for specimens austenitised at 925°C, 950°C and 1200°C.

Fig. 5.15 Scanning electron micrograph of Fe-IV-0.2C solution treated at 1200°C for 30 mins., isothermally transformed at 700°C and impact tested at 400°C.

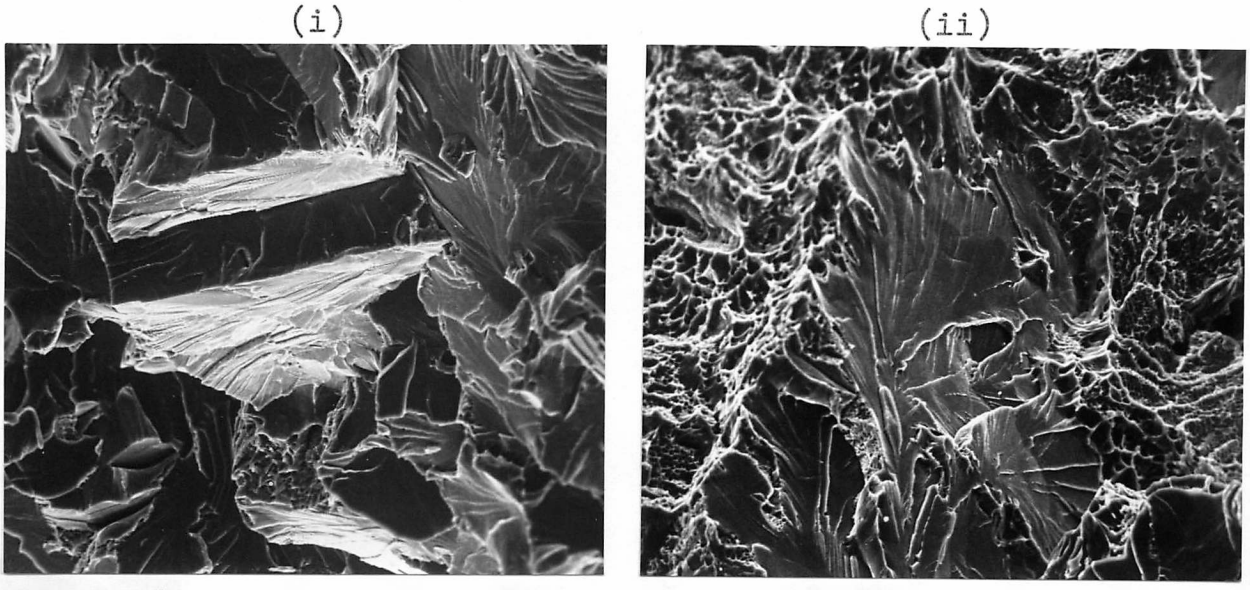

Fig. 5.16 Scanning electron micrographs of Fe-IV-0.2C; impact test fracture surfaces.
(a) Austenitised at 925°C and retransformed at 700°C.
(i) Tested at 20°C.
(ii) Tested at 125°C.

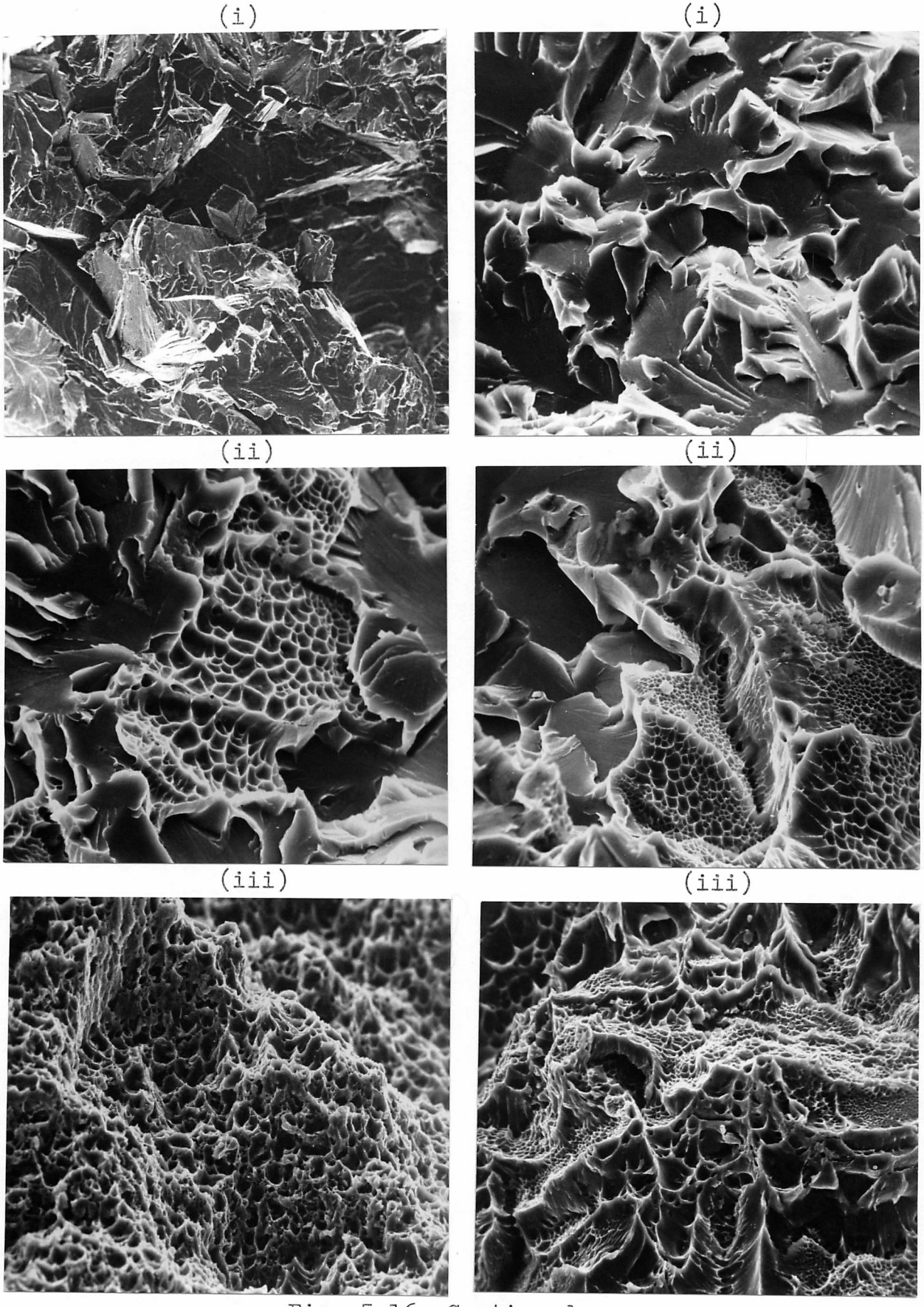

Fig. 5.16 Continued

(b) Austenitised at 950°C and retransformed at 700°C.
(i) Tested at 20°C. ——3μ
(ii) Tested at 100°C. ——1μ
(iii) Tested at 110°C. ——4μ

(c) Austenitised at 1200°C and retransformed at 700°C.
(i) Tested at 20°C. ——1μ
(ii) Tested at 125°C. ——1μ
(iii) Tested at 250°C. ——3μ

(iii) Mechanical Behaviour of Cycled Specimens:

A reheat temperature of 950°C was selected for cycling experiments, as this eliminated the large regions of brittle behaviour encountered in the specimens impact tested at 925°C. Specimens were cycled up to a maximum of six times and the tensile results are presented in fig. 5.17. Both the yield stress and tensile stress decrease as the number of cycles is increased and this correlates directly with the hardness curve shown in fig. 5.8. Coresponding increases in elongation, reduction in area, and tensile to yield stress ratio can also be seen.

The impact behaviour of the cycled specimens is shown in fig. 5.18. An increase in the number of cycles is reflected in an increase in upper shelf energy and also a decrease in impact transition temperature.

5.4 Discussion

This part of the research programme has investigated the grain size response of dispersion strengthened ferritic structures to rapid heat treatment and has studied the resulting influence on mechanical properties.

Using a single cycle rapid heat treatment, grain sizes of the order of 5 μm were produced under optimum conditions. This represents a considerable refinement in grain size and as a result, corresponding changes in the mechanical behaviour of the steel were observed. However, the heat treatment conditions most conducive to producing high strength levels differed from those most suitable for improving toughness. The highest tensile strength (1635MNm^{-2})

(i)

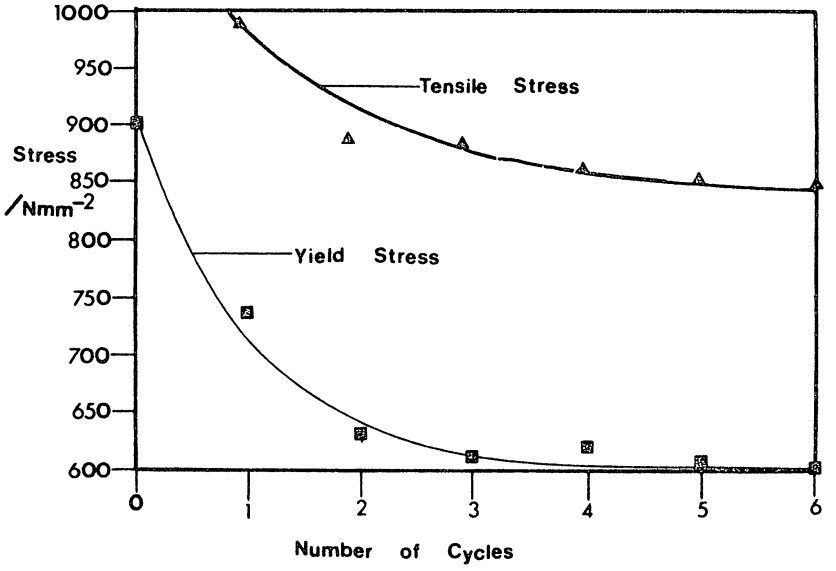

(ii)

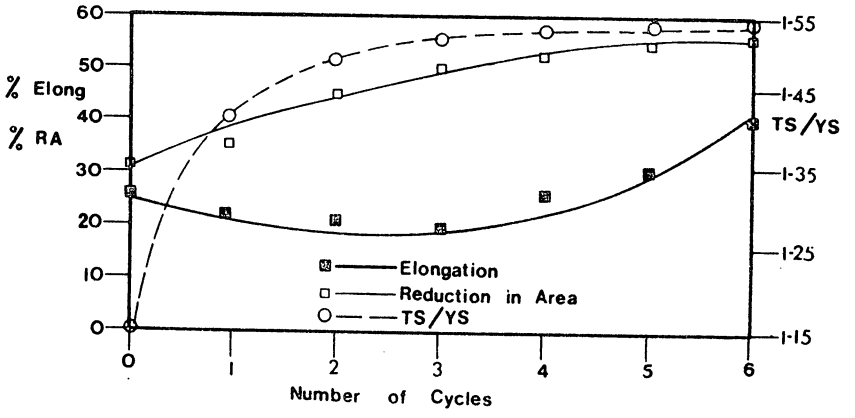

Fig. 5.17 Variation of tensile properties with the number of rapid heat treatment cycles.
(i) Tensile and yield stress.
(ii) Elongation, reduction in area and tensile to yield stress ratio.

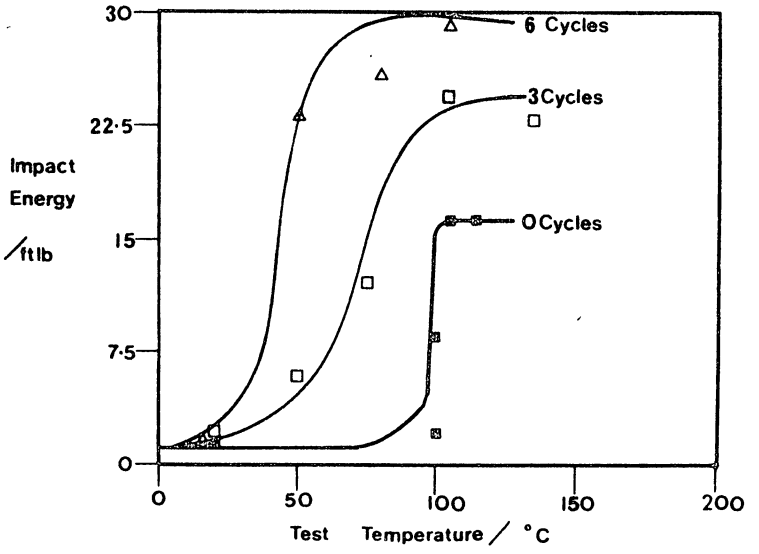

Fig. 5.18 Variation of impact energy as a function of the number of heat treatment cycles.

was produced after rapidly austenitising at 1200°C, but this particular treatment resulted in poor toughness. However, reheating to 950°C reduced the impact transition temperature by more than 300°C, but produced a reduced tensile strength of 1040MNm^{-2}.

Clearly a combination of grain size effects and precipitation hardening effects are responsible for the variation in mechanical properties resulting from different austenitising temperatures, and it has not been possible from the results of the present investigation to assign absolute values to the contribution from each effect. The inherent difficulties of such an analysis are evident in the elctron microscopy study of the structures, which revealed that the rapid heat treatment process provides insufficient opportunity for complete carbide dissolution in the austenite phase and consequently coarse carbides are present in the retransformed product. These provide a less effective strengthening increment than the finer precipitates, and consequently the dispersion parameters of these coarse particles would have to be quantified to enable the influence of grain refinement on the mechanical properties to be determined. This would require an extensive statistical analysis to be made, but in this case it can only produce an approximate solution, as the dispersion parameters of the aligned precipitation vary according to the solute concentration in solid solution (Batte, 1970).

A possible means of eliminating the coarse particles, and hence enabling the improved mechanical proper-

ties to be attributed purely to grain size variations, might be effected by using a more dilute alloy. The dissolution kinetics of the vanadium carbide ought to be more rapid in a matrix which contains a lower solute concentration and hence complete dissolution might be effected without impairing the grain refining effects produced by rapid heat treatment.

However, despite the difficulties in acquiring quantitative information on the grain size and dispersion parameters which influence mechanical properties, it was shown conclusively that very high strength levels and much improved toughness values can be achieved by rapid heat treatment. This reflects favourably on rapid heat treatment techniques in general as a means of improving the mechanical behaviour of dispersion strengthened ferritic steels. However, in considering the viability of the process as applied to Fe-IV-0.2C, which has been directly transformed at 700°C, certain limitations must be recognised. Recent calculations by Benson (1977) have used the dispersion parameters for interphase precipitation , derived by Batte (1970), to give the grain size necessary to lower the impact transition temperature to 20°C (N.B. This analysis is purely general, in that it does not refer to material which has undergone a specific heat treatment cycle. Thus, the vanadium carbide is assumed to be entirely arranged as an aligned dispersion). It can be shown that the precipitation hardening contribution to strength is so great that a grain size of 0.64 μm is required to reduce the impact transition tem-

perature to room temperature. This is clearly unobtainable by conventional heat treatment and a reduction in alloy content to reduce the potency of the precipitation strengthening seems necessary, if directly transformed steels are to provide adequate toughness for commercial applications.

Thermal cycling experiments were performed to investigate the response of the refined structures to additional rapid heat treatments. Some further refinement of the grain size was achieved with continued cycling although this was accompanied by a decrease in strength and hardness. However, cycling improved the impact properties and again these effects can be explained by considering the independent contributions of grain size and precipitation hardening to strength and toughness. Rapid heat treatment has been shown to produce a coarse dispersion of vanadium carbide in Fe-IV-0.2C, and consequently the dissolution kinetics will be reduced during further heat treatment cycles. Thus, despite the refinement in grain size, the precipitation hardening component will be reduced and hence strength levels may decrease while toughness will be improved. The overall structural changes produced by repeated cycling are small compared to the initial cycle, yet can produce added increments of toughness provided high strength levels are not at a premium.

CHAPTER SIX

CONCLUSIONS AND SUGGESTIONS FOR FUTURE WORK

6.1 Introduction

This dissertation has been concerned largely with transformation studies in alloys based upon Fe-IV-0.2C, yet has involved four independent areas of ferrous physical metallurgy. Chapter two dealt with the metallographic structure of lath martensite and the occurrence of interlath and interpacket films of retained austenite. Chapter three investigated the mechanisms of formation of proeutectoid ferrite, as modified by the discontinuous precipitation of vanadium carbide. Chapter four dealt with the austenitisation reaction from ferritic, bainitic and martensitic microstructures, while chapter five extended this to examine heat treatment schedules for the production of fine grained ferritic structures and to investigate their influence on mechanical properties.

Thus, despite the fact that the chapters are interrelated, they form autonomous units in themselves and will be discussed individually.

6.2 Retained Austenite

The retention of austenite in the quenched alloy was considered to be associated with the formation of lath martensite and consequently the martensite structure was examined in detail.

(i) The martensite was shown to have a lath morphology and these laths were shown to occupy a {110} martensite

habit plane. The problems of identifying a discrete growth direction by single surface trace analysis were discussed.

(ii) Three martensite morphologies were observed. Packets of "interwoven" and regular martensite are described while large independent laths were also seen. The larger laths contained an autotempered cementite dispersion which was shown to obey the Bagaryatski relationship with the martensite.

(iii) The laths within a particular martensite packet were found to be of similar orientation in most cases. However, groups of laths were observed, where the laths themselves were of similar orientation but the groups twin related.

(iv) Films of interlath and interpacket austenite were observed and shown to obey either the Kurdjumov-Sachs or Nishiyama-Wassermann relationship with the martensite. In general, the austenite was found to be of single orientation over large areas and in some cases encompassed many martensite packets.

(v) The stability of the retained austenite was studied when subjected to deformation, refrigeration and tempering. Thirty percent deformation resulted in the decomposition of the austenite films but cooling to liquid nitrogen temperatures for 30 mins. left them unaffected. Tempering at 700^{o}C for 30 mins. induced their complete decomposition and resulted in a martensite structure of large, twin related laths. These were considered to be equivalent to the twin related groups of laths in the untempered structure.

The study of lath martensites revealed two fundemental areas where further work is necessary. Firstly, the investigation demonstrated that in low-carbon martensites, the shape of the martensite unit cannot be unambiguously defined, and secondly, the studies of the relative orientations of adjacent laths and adjacent groups of laths showed that further work is necessary to establish the mechanisms by which various lath orientations occur.

The morphology and distribution of retained austenite was described for this particular steel but a complete characterisation must include a study of the influence of other alloy additions. This may also affect the mechanism of formation of the martensite and therefore provide a deeper insight into the manner in which films of austenite are retained.

Thomas (1973) has suggested that films of retained austenite can enhance toughness in low-alloy steels. This also requires further investigation.

6.3 The Proeutectoid Ferrite Reaction and Interphase Precipitation

The ferrite reaction, as modified by the precipitation of aligned and fibrous carbide dispersions, was studied, particular emphasis being given to relating morphological aspects of the transformation to the observed crystallography, by using the films of retained austenite to identify the parent austenite orientation. The results show that:

(i) The aligned and fibrous vanadium carbide precipitates

were found to obey the Baker-Nutting orientation relationship with the ferrite.

(ii) The sheets of aligned precipitates were found to occupy a {110} ferrite habit plane, and partial transformation studies revealed that these sheets were parallel to the transformation front.

(iii) Ferrite containing aligned precipitation was shown to obey the Kurdjumov-Sachs orientation relationship with the austenite grain into which it was growing.

(iv) High-resolution studies of a chromium-vanadium steel revealed growth ledges, whose height corresponded with the intersheet spacing of the aligned dispersion. It was concluded that growth of ferrite associated with the precipitation of aligned vanadium carbide, occurred by a ledge mechanism.

(v) The single habit plane selected by the vanadium carbide was explained in terms of the three phase crystallography operating at the austenite/ferrite interface.

(vi) Ferrite containing fibrous precipitation was found to obey a Kurdjumov-Sachs orientation relationship with the austenite grain on the opposite side of the nucleating prior austenite boundary. Consequently, it was concluded that growth occurred by the movement of an incoherent interface.

(vii) At low transformation temperatures, growth was accompanied by aligned precipitation, while at higher temperatures fibrous growth became more significant. A single ferrite nucleus tended to grow into one austenite grain, bearing aligned precipitation and into the adjacent grain

bearing fibrous precipitation.

Much has now been established concerning the interphase and fibrous precipitation reactions in low-alloy steels, but certain observations can be noted which deviate from ideal behaviour. The occurrence of curved sheets of aligned carbide, for instance, is not entirely consistent with the strict crystallography described for the reaction. In some cases, these can be attributed to sub-grain formation but other observations remain inconsistent with this explanation. Areas of intermixed fibrous and aligned precipitation have also been seen and it seems likely that a modification to the proposed mechanisms of growth may be necessary to explain these occasional observations.

6.4 The Austenitisation Reaction in Low-Alloy Steels

The austenitisation reaction from ferritic, bainitic and martensitic starting microstructures was investigated, particular attention being paid to morphological, kinetic and crystallographic features. The results show that:

(i) At low degrees of superheat, the austenite nuclei were concentrated at the prior austenite grain boundaries in the bainitic and martensitic structures and at the ferrite grain boundaries in the ferrite structure.

(ii) At high degrees of superheat, more extensive nucleation occurred on the interlath and interpacket boundaries in the bainite and martensite structures and on the subgrain boundaries in the ferrite structure.

(iii) Nucleation of austenite was found to be most pro-

fuse in the martensite structure, followed by the bainite and finally the ferrite structure.

(iv) In the ferrite structure, grain boundary nucleated austenite was found to bear a Kurdjumov-Sachs orientation relationship with the austenite grain into which significant growth did not occur.

(v) Sub-grain boundary nucleated austenite in the ferrite structure, bore a Kurdjumov-Sachs orientation relationship with the surrounding matrix.

(vi) As the austenite grew through the dispersion of vanadium carbide in the ferrite structure, it was observed to cause dissolution of the alloy carbide at the transformation interface. This was followed by reprecipitation of a coarser dispersion in the austenite, with the precipitates related to the austenite by a cube/cube orientation relationship.

Further work is necessary to establish the factors which control nucleation at boundaries within steels and thereby explain the different nucleation rates observed in the three structures. As the martensite and bainite structures both contain free cementite, it is possible that this has a major bearing on the free energy of formation of austenite and requires further investigation to establish the exact nature of these microstructures at the point when austenite nucleation occurs.

The influence of alloying elements on the austenitisation reaction, from both nucleation and growth considerations, is an area where little evidence of a fundamental nature has been established. Clearly this is a fruitful

area for further investigation.

6.5 Rapid Heat Treatment and Grain Refinement

The response of the ferrite microstructure to rapid heat treatment and the resulting influence on mechanical properties was studied. The results show that:

(i) Ferrite grain sizes of approximately 5 μm could be produced using a single heat treatment cycle, and of approximately 3.5 μm using a multi-cycle treatment.

(ii) Under specific conditions tensile strengths of approximately 1600MNm^{-2} were achieved using single cycle, rapid heat treatment.

(iii) The impact transition temperature was lowered by over 300°C with a single cycle treatment, and further reductions were produced using multi-cycle treatments.

These results were explained in terms of grain size and precipitation effects, as quantified by a modified Hall-Petch orientation relationship.

Further work is required to investigate the response of other microstructures to rapid heat treatment. In this way, it may be possible to assess the microstructural parameters which influence the response of an alloy to such cycles and thereby to tailor alloy contents and heat treatments to produce fine grained transformation products.

An important aspect of rapid heat treatment as a means of processing large sections, is the ability to heat a component sufficiently rapidly to produce an adequate response. This is an engineering problem and may well prove to be an important consideration in any wide-

spread commercial application of rapid heat treatment as a means of producing fine grained structures in steels.

APPENDIX I

EXPERIMENTAL TECHNIQUES

1.1 Preparation of Alloys

The basic alloy, of nominal composition Fe-IV-0.2C, was received in the form of 1.5 cm. diameter bar having been prepared from an induction melt. Any additions were made using a standard Edwards Argon Arc Melting Furnace. The contents for the melt were placed on a water-cooled copper hearth and the furnace chamber was evacuated to 5×10^2 torr. Melting was performed under a partial pressure of argon and was repeated four times to ensure homogeneity.

The ingots produced were about 10 cm. long and weighed approximately 70 g. A homogenisation treatment was given before the specimens were sampled for analysis. Table A.1 provides the actual compositions in wt.%. The homogenisation treatment was carried out at 1250°C for approximately 50 hours and was given to all materials prior to analysis or specimen preparation. The ingots were sealed in a silica tube under a partial pressure of argon to prevent oxidation and decarburization.

The ingots were worked down to size by a combination of hot rolling and cold swaging. Intermediate anneals were given if necessary.

1.2 Salt Pot Heating

Isothermal reaustenitisation experiments were performed in a carbon salt pot, as shown in fig. A.1, the

Chemical Analysis of the Alloys used

Basic Alloy A1:

V	1.08
C	0.25
Mn	0.019
Si	0.07
Ni	0.028
Cr	0.034
Mo	0.002
Nb	0.038
Cu	0.011
S	0.012
P	0.004

Alloy A2:

Basic Alloy + 1.68Ni

Alloy A3:

Basic Alloy + 1.83Mn

pot being heated by radio frequency induction using a Radyne machine. Partial transformation studies were effected by quenching into iced brine.

1.3 Controlled Radiation Heating

For reaustenitisation experiments at various controlled heating rates, an infra-red, focussed radiation furnace was used (fig. A.2). The apparatus was arranged so that the bottom specimen support and the specimen could be readily dropped from the furnace into a quench bath. For slower heating rate experiments, where prolonged holding at elevated temperatures could promote oxidation and decarburisation, provision was made for an argon atmosphere in the specimen chamber.

1.4 Tensile Testing

Tensile specimens were made to a Hounsfield No. 11 design by a two stage machining process (fig. A.3). The first lug was machined followed by the necessary heat treatment. Final machining of tne second lug was then carried out to the tolerances shown. This procedure was adopted for a number of reasons:

(i) Initial machining reduced the specimen cross-section along the gauge length by 42%, thereby ensuring a more uniform microstructure during heat treatment.

(ii) Some distortion of the specimen occurs during heat treatment and hence the final gauge length, along the thrust faces, must be finish machined in order to produce

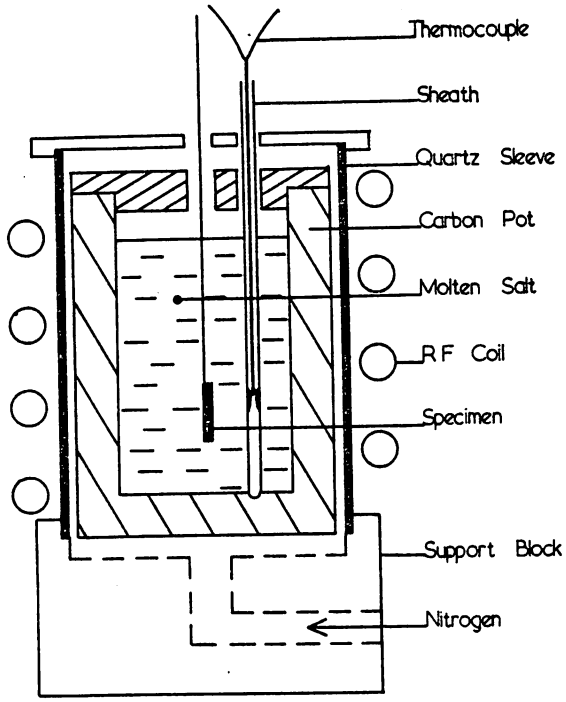

Fig. A.1: The salt pot arrangement used for isothermal austenitisation.

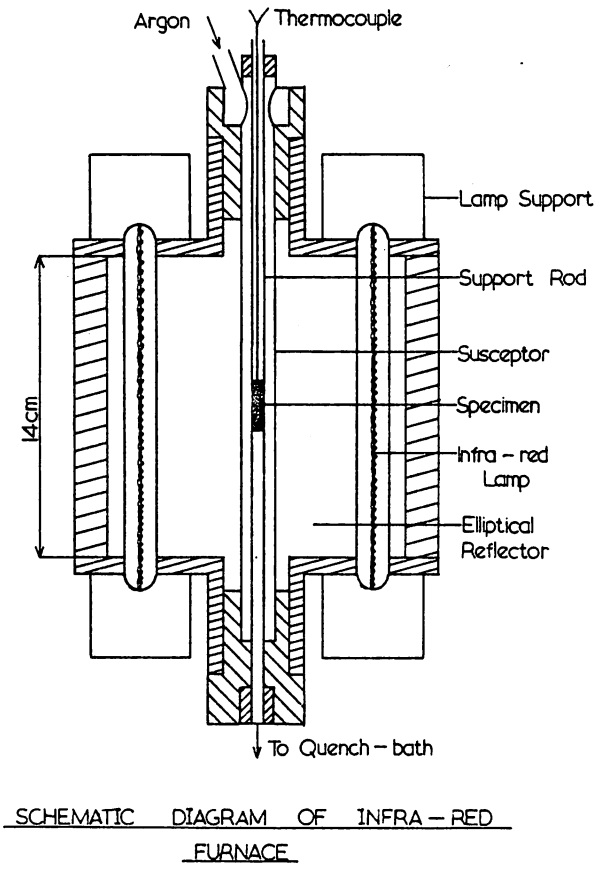

Fig. A.2: The focussed, infra-red radiation furnace.

a specimen of accurate dimensions.

(iii) Final machining removes any unrepresentative surface layers.

The tests were carried out on an Instron TM-CML tensile testing machine with a cross-head speed of .05cm./min.

1.5 Impact Testing

A shortage of material precluded the use of standard Charpy or Izod notched specimens and a specimen design was adopted which permitted the production of an adequate number of specimens and which was compatible with the Hounsfield Impact Testing Machine. The specimens used were of 6mm. diameter rod, 4.5cm. in length with a 2mm. deep notch (fig. A.4). The notch was inserted using a standard Hounsfield notching tool but with the specimen supported in a jig with an eccentricity of 3.5cm.

The brittle nature of many of the specimens at room temperature necessitated the use of high temperature impact testing. This was carried out on a standard Hounsfield machine but with a facility to enable the specimen to be heated from both sides by a stream of hot air.

1.6 Hardness Testing

Hardness measurements were made on a Vickers Hardness Machine using a diamond pyramid indentor and a load of 20kg. The mean of five hardness values per specimen were taken.

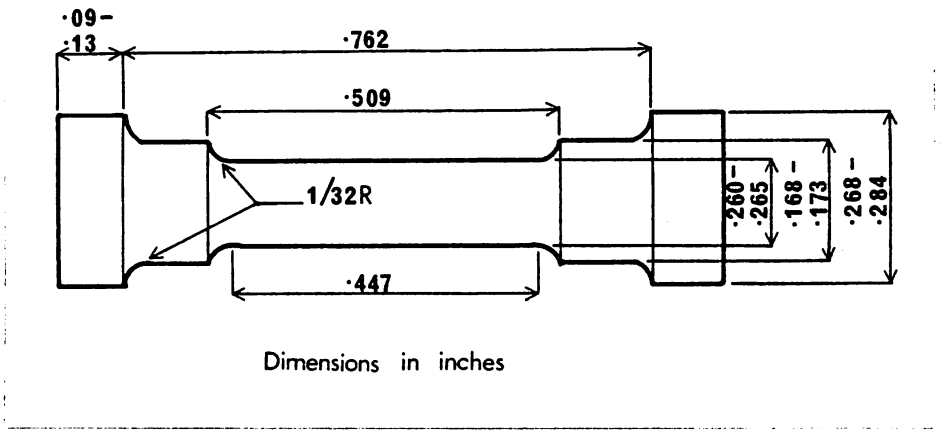

Fig. A.3: The Hounsfield No. 11 tensile test specimen.

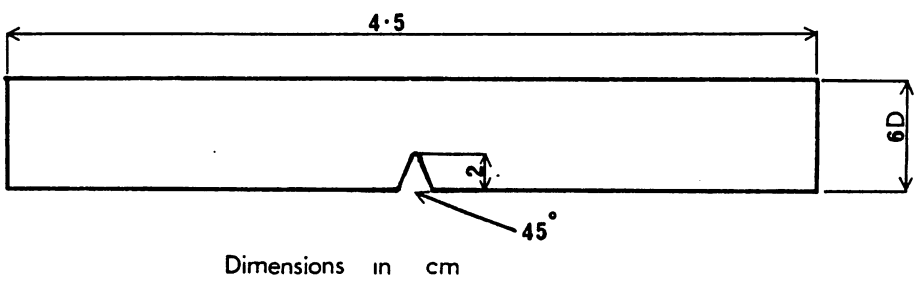

Fig. A.4: The impact test specimen.

1.7 Optical Microscopy

Specimens for optical examination were mounted in perspex using a standard hot mounting technique and were ground to a polish of 0.25 μm. The specimens were etched in 3% nital (3 vol. % nitric acid in alcohol) and were photographed using a Zeiss Neophot 2 or a Zeiss Universal optical microscope.

Quantitative measurements of grain size and growth rates were measured using a graticule, inserted into the microscope eyepiece. This was calibrated for the particular magnification used, by means of a standard scribed graticule.

Grain sizes were measured by a mean intercept method, fifty fields of view being used for each measurement. Growth rates were measured as a nodule radius, the largest ten nodules being measured for each of ten fields of view.

1.8 Electron Microscopy

1.8a Replica Examination

This was carried out on an AEI EM6G microscope and employed a standard carbon extraction replica technique. The specimens for examination were polished to 0.25 μm. and lightly etched in 3% nital. Carbon was then evaporated onto the surface using an Edwards 3AM Evaporator. The specimens were scribed to segment the carbon film into 1mm. squares and were then etched further in 3% nital. The replicas were removed on distilled water and examined between copper grids.

1.8b Thin Foil Examination

This was performed mainly on a Phillips EM 300 though some work was carried out using a Jeol, Jem 200A and a Phillips EM 301. The thin foils were prepared from 3mm. rod specimens. The rod was slit into 0.2mm. discs, which were subsequently ground to approximately .05mm. Thinning was accomplished using a Fischione, Twin-Jet Electropolisher, thinning being discontinued on the appearance of a small hole in the centre of the specimen. Two electropolishing solutions were found to be adequate for the range of specimens used, the polishing conditions being as follows:

(i) 5% perchloric acid in 2-butoxyethanol at a potential of 70 volts and a temperature of $-20^{o}C$;

(ii) 5% perchloric acid and 25% glycerol in ethanol at a potential of 35 volts and at a temperature of $-5^{o}C \pm 5^{o}C$.

1.9 Scanning Electron Microscopy

Fracture surfaces of tensile and impact specimens were examined using a Cambridge Scientific Instruments "Stereoscan Mk. II". Specimens were mounted on aluminium stubs using conducting glue to prevent charge build up at the specimen.

APPENDIX II

Stereographic projections of the standard orientation relationships used in this thesis.

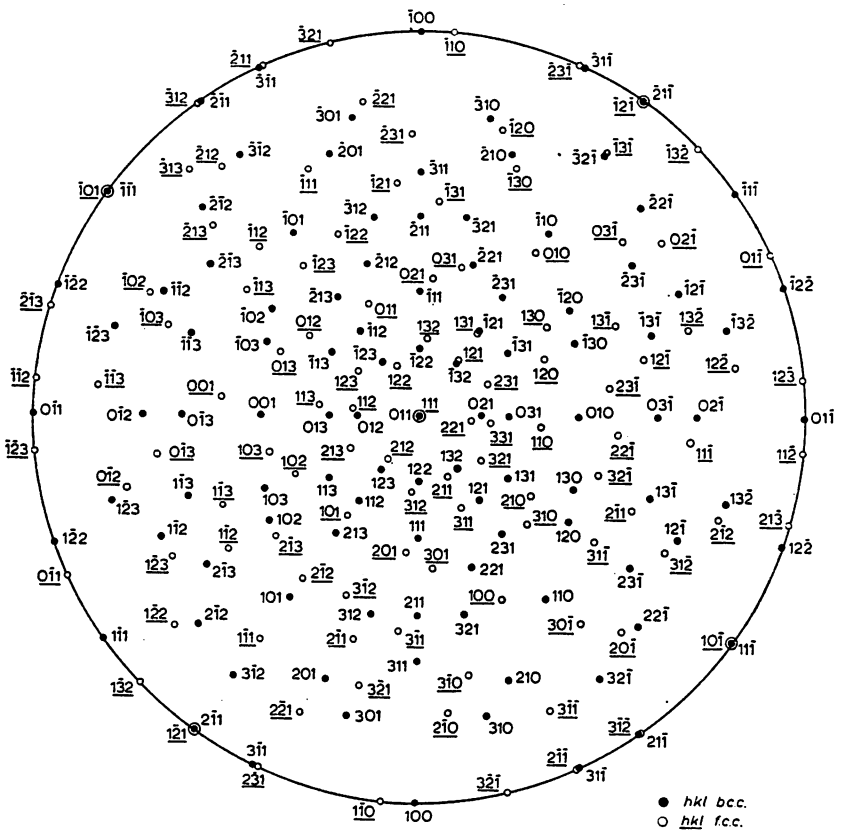

Fig. A2.1: The Kurdjumov-Sachs orientation relationship.

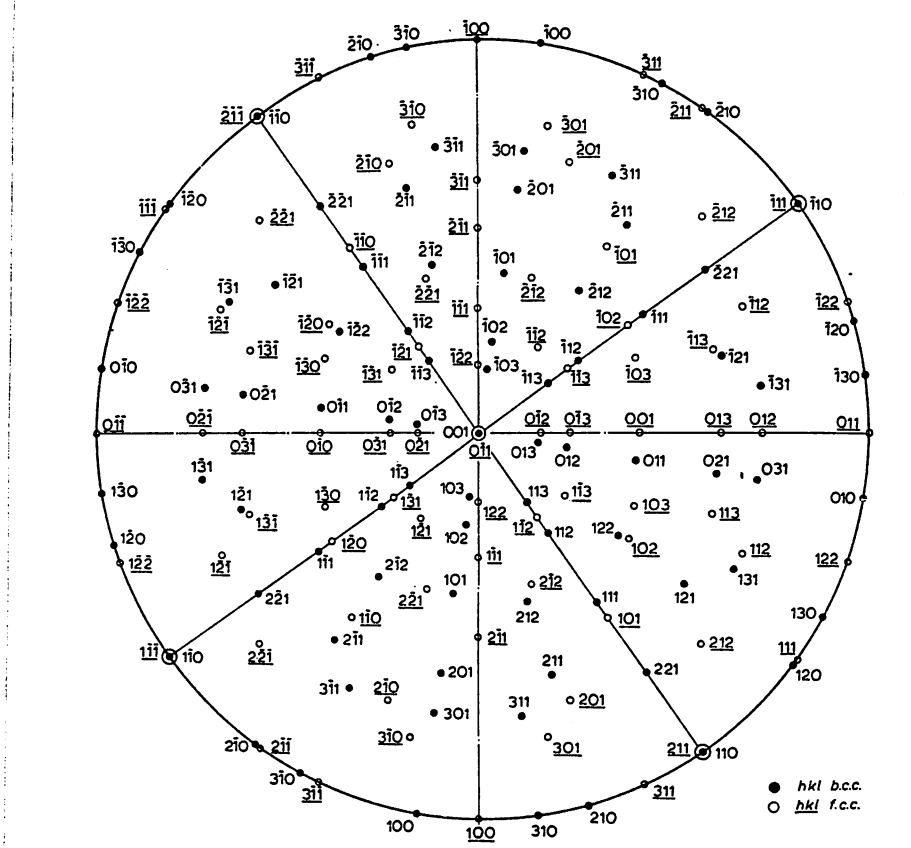

Fig. A2.2: The Nishiyama-Wassermann orientation relationship.

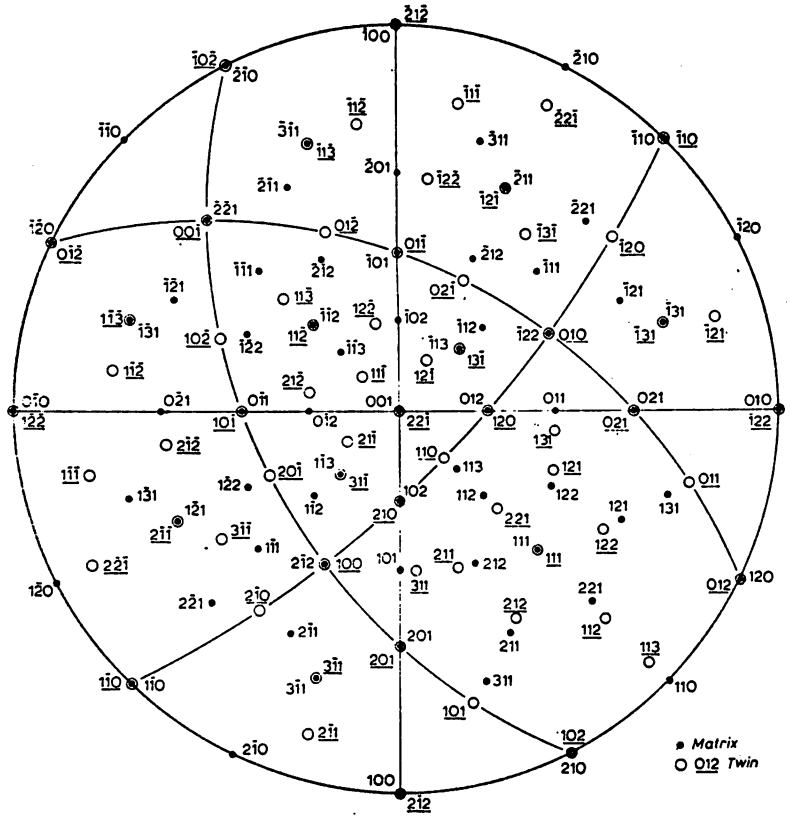

Fig. A2.3: Twin orientation for face-centred cubic and body-centred cubic crystals. (After Kelly, 1965)

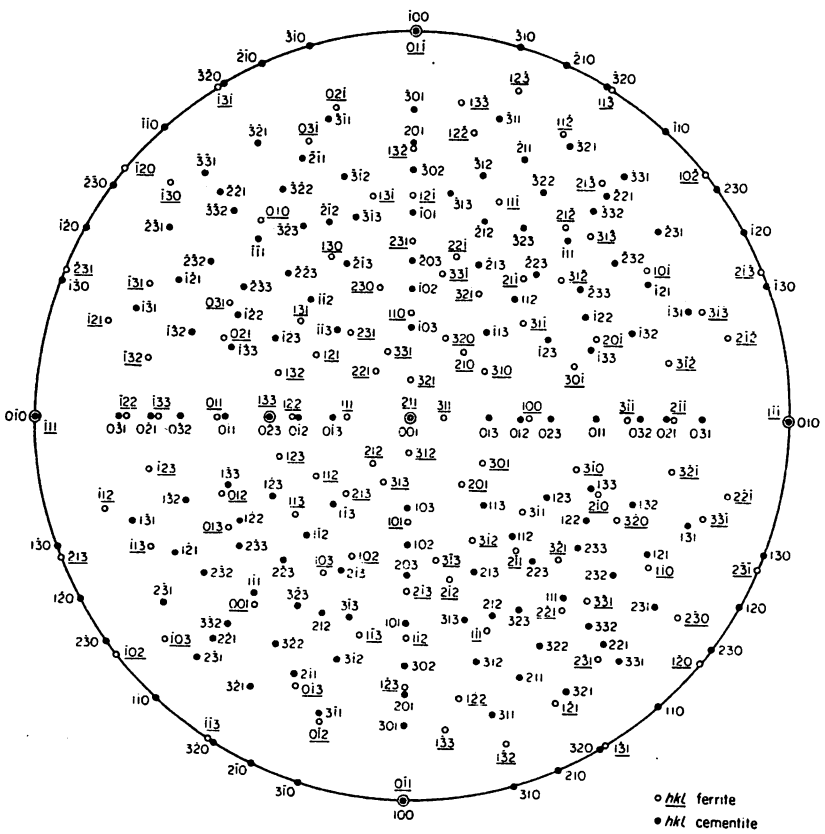

Fig. A2.4: The Bagaryatski orientation relationship.

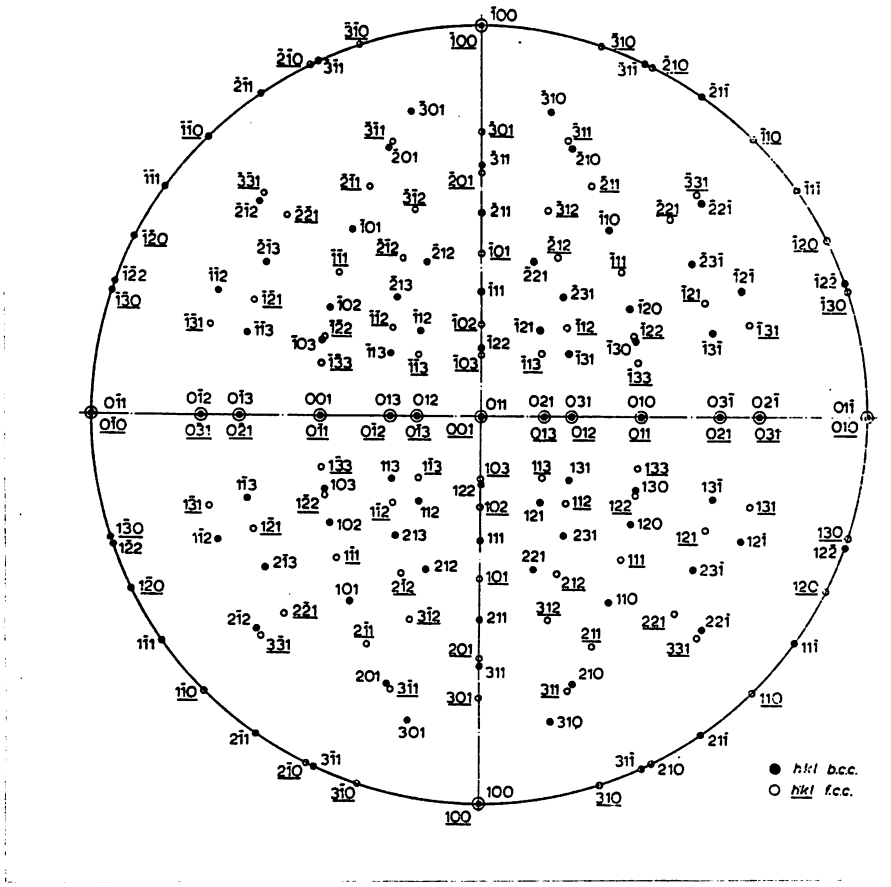

Fig. A2.5: The Bain orientation relationship.

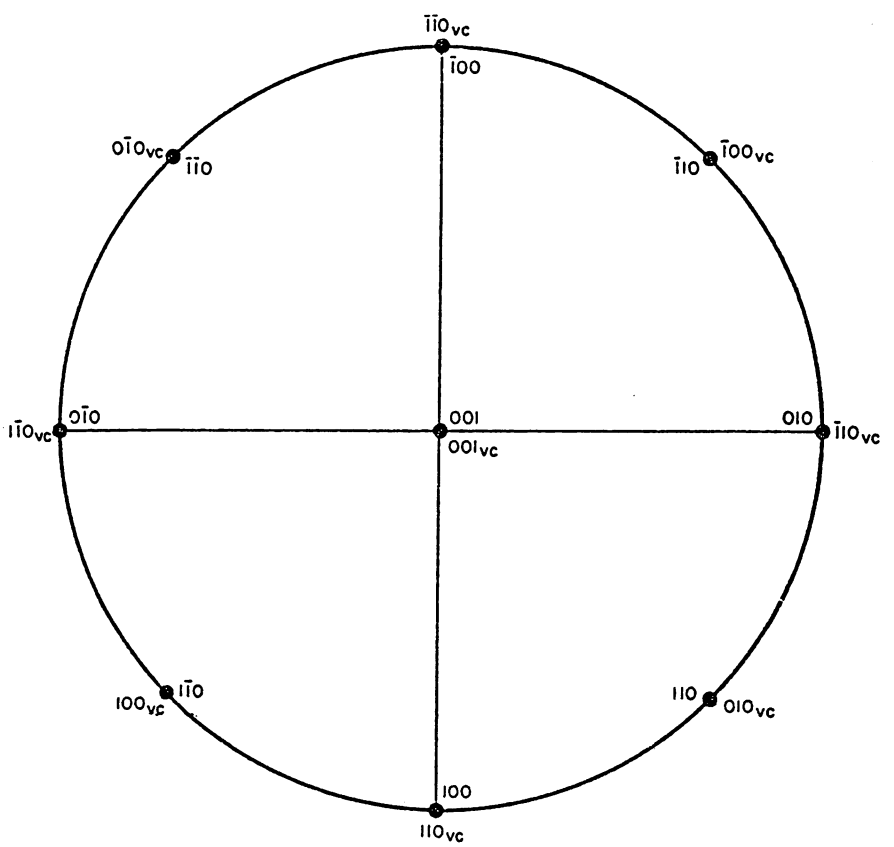

Fig. A2.6: The Baker-Nutting orientation relationship.

REFERENCES

1 Aaronson, H.I., "Decomposition of Austenite by Diffusional Processes", (1962), Interscience Publishers, New York.

2 Aaronson, H.I., Johnston, T.L. and Schmatz, D.J.,(1968), Trans. A.S.M., 61, p. 349.

3 Aaronson, H.I. and Laird, C., Trans. A.I.M.E., 242, (1968), p. 1437.

4 Aaronson, H.I., Laird, C. and Kinsman, K.R., "Phase Transformations", (1970), A.S.M. Cleveland, p. 313.

5 Amity, I., Rosen, A. and Bar 'Or, A., J.I.M., (1967), 95, p. 48.

6 Bagaryatski, Y.A., Dokl. Akad. Nauk. S.S.S.R., (1950), 73, p. 1161.

7 Baker, R.G. and Nutting, J., I.S.I., Report no. 64, (1959), p. 1.

8 Batte, A.D., Ph.D. Thesis, (1970), University of Cambridge.

9 Batte, A.D. and Honeycombe, R.W.K., J.I.S.I., (1973), p. 283.

10 Beaven, P.A., Unpublished work, (1975).

11 Belaiew, N.T., J.I.M., (1923), 29, p. 379.

12 Benson, J.P., Ph.D. Thesis, (1976), University of Cambridge.

13 Berry, F.G., Ph.D. Thesis, (1968), University of Cambridge.

14 Berry, F.G. and Honeycombe, R.W.K., Met. Trans., (1970), 1, p. 3279.

15 Bhadesia, H.K.D., Private Communication, (1977).

16 Biswas, M.G.A. and Codd, I., J.I.S.I., (1968), 206, p. 494.

17 Bollmann, W., referenced by Smith, D.A. and Pond, R.C., Int. Met. Rev., (1976), 205, p. 61.

18 Bozic, B.I. and Lucic, R.J., J. Mat. Sci., (1977), 12, p. 751.

19 Campbell, K. and Honeycombe, R.W.K., J. Mat. Sci., (1974), 8, p. 197.

20 Chilton, J.M., Barton, C.J. and Speich, G.R., J.I.S.I., (1970), 208, p. 184.

21 Chilton, J.M. and Speich, G.R., Met. Trans., (1970), 1, p. 1019.

22 Christian, J.W., I.S.I. Special Report, (1965), 93, p. 1.

23 Darbyshire, J.M., Referenced in J.I.S.I., (1972), p. 284.

24 Das, S.K. and Thomas, G., Trans. A.S.M., (1969), 62, p. 659.

25 Davenport, E.S. and Bain, E.C., Trans. A.I.M.E., (1930), 90, p. 117.

26 Davenport, A.T., Berry, F.G. and Honeycombe, R.W.K., Met. Sci. J., (1968), 2, p. 104.

27 Davenport, A.T. and Honeycombe, R.W.K., Met. Sci. J., (1975), 9, p. 201.

28 Davenport, A.T. and Honeycombe, R.W.K., Proc. Roy. Soc., (1971), A322, p. 191.

29 Davies, R.G. and Magee, C.L., Met. Trans., (1971), 2, p. 1939.

30 De Ardo, A.J., Unpublished work, (1972).

31 Debuyschere, M., Trait. Therm., (1975), 98, p. 59.

32 Dubé, C.A. and Aaronson, H.I., Rév. Met., (1958), 55, p. 201.

33 Dunlop, G.L., Ph.D. Thesis, (1974), University of Cambridge.

34 Dunlop, G.L. and Honeycombe, R.W.K., Phil. Mag., (1975), 32, p. 61.

35 D'Yackenko, S.S. and Fedorov, G.V., Phys. Met. Metallog., (1964), 18, p. 68.

36 Edmonds, D.V., J.I.S.I., (1972), p. 363.

37 Edmonds, D.V. and Honeycombe, R.W.K., J.I.S.I., (1973), p. 209.

38 Fisher, J.C., Trans. A.I.M.E., (1953), 197, p. 918.

39 Flewitt, P.E.J. and Towner, J.M., J.I.M., (1967), 95, p. 273.

40 Fong, H.S. and Glover, S.G., Trans. J.I.M., (1975), 16, p. 115.

41 Freeman, S., Conf. on "The Effect of Second Phase Particles on the Mechanical Properties of Steels", B.S.C./I.S.I., (1971), p. 68.

42 Gardner, F.S., Cohen, M. and Antia, D.P., Trans. A.I.M.E., (1943), 154, p. 306.

43 Gladman, T., Conf. on "Recrystallisation in the control of microstructure", I.S.I./I.O.M., (1973).

44 Gladman, T., Dulieu, D. and McIvor, I.D., Micro. Alloying, (1975), p. 25.

45 Goodenow, R.H. and Hehemann, R.F., Trans. A.I.M.E., (1965), 233, p. 1777.

46 Grange, R.A., Trans. A.S.M., (1966), 59, p. 26.

47 Grange, R.A., Met. Trans., (1971), 2, p. 65.

48 Gray, J.M. and Yeo, R.B.G., Trans. A.S.M., (1968), 61, p. 255.

49 Greday, T., Prec. 3rd European Conference on Electron Microscopy, (1964), Prague.

50 Greninger, A.B. and Troiano, A.R., J. Met., (1949), p. 590.

51 Hall, E.O., Proc. Phys. Soc., (1951), B64, p. 747.

52 Heckel, R.W. and Paxton, H.W., Trans. A.S.M., (1961), 53, p. 539.

53 Heikkinen, V.K., Trans. I.S.I.J., (1973a), 13, p. 78.

54 Heikkinen, V.K., Scand. Journ. Met., (1973b), 2, p. 109.

55 Hehemann, R.F., Kinsman, K.R. and Aaronson, H.I., Met. Trans., (1972), 3, p. 1077.

56 Hillert, M., Nilsson, K. and Törndahl, L.E., J.I.S.I., (1971), p. 49.

57 Homma, R., Trans. I.S.I.J., (1974), 14, p. 434.

58 Honeycombe, R.W.K., Climax Molybdenum Publication, "Structure and Strength of Alloy Steels", (1973).

59 Honeycombe, R.W.K., Met. Trans., (1976), 7A, p. 915.

60 Hultrgren, A., Trans. A.S.M., (1947), 39, p. 915.

61 Jin, S., Morris, J.W. and Zackay, V.F., Met. Trans., (1975), 6A, p. 141.

62 Kelly, P.M., Acta. Met., (1965), 13, p. 635.

63 Kelly, P.M., Trans. A.I.M.E., (1965), 233, p. 264.

64 Kelly, P.M. and Nutting, J., Proc. Roy. Soc., (1960), A259, p. 45.

65 Kelly, P.M. and Nutting, J., J.I.S.I., (1961), 197, p. 199.

66 King, A.D. and Bell, T., Met. Trans., (1975), 6, p. 1419.

67 Kinoshita, S. and Ueda, T., Trans. I.S.I.J., (1974), 14, p. 411.

68 Kinsman, K.R. and Aaronson, H.I., "Transformation and Hardenability in Steels", Climax Molybdenum, (1967), p. 39.

69 Kinsman, K.R., Eichen, E. and Aaronson, H.I., Met. Trans., (1965), 6A, p. 303.

70 Ko, T. and Cottrell, S.A., J.I.S.I., (1952), 172, p. 307.

71 Krauss, G. and Marder, A.R., Met. Trans., (1971), 2, p. 2343.

72 Kula, E. and Cohen, M., Trans. A.I.M.E., (1954), 46, p. 727.

73 Kurdjimov, G.V. and Sachs, G., Z. Physik, (1930), 64, p. 325.

74 Laird, C. and Aaronson, H.I., Acta. Met., (1967), 15, p. 73.

75 Laird, C. and Aaronson, H.I., Trans. T.M.S.-A.I.M.E., (1968), 242, p. 1393.

76 Laird, C, and Aaronson, H.I., Acta. Met., (1969), 17, p. 505.

77 Leslie, W.C., "The Relation between Structure and Mechanical Properties", H.M.S.O., (1963), p. 334.

78 Liu, Y.C., Aaronson, H.I., Kinsman, K.R. and Hall, M.G., Met. Trans., (1972), 3, p. 1318.

79 Lyman, T. and Traiano, A.R., Trans. A.I.M.E., (1945), 162, p. 196.

80 Magee, C.L., "Phase Transformations", (1970), A.S.M. Cleveland, p. 115.

81 Mahajan, S.W., Venkataraman, G. and Mallik, A.K., Metallography, (1973), 6, p. 337.

82 Maksimova, O.P. and Nikonorova, A.I., Prob. Metallored Fiz. Metal., (1955), 4, p. 125.

83 Mannerkoski, M., Acta. Polytech. Scand., (1964), Ch. 26.

84 Matsuda, S. and Okamura, Y., Trans. I.S.I.J., (1974a), 14, p. 363.

85 Matsuda, S. and Okamura, Y., Trans. I.S.I.J., (1974b), 14, p. 444.

86 Marder, A.R. and Krauss, G., Trans. A.S.M., (1967), 60, p. 651.

87 Marder, J.M. and Marder, A.R., Trans. A.S.M., (1969), 62, p. 1.

88 McIvor, I.D., J.I.S.I., (1969), 207, p. 106.

89 Mehl, R.F., Barret, C.S. and Smith, D.W., Trans. A.I.M.E., (1933), 105, p. 215.

90 Mehl, R.F. and Van Winkle, D.M., Rev. Met., (1953), 50, p. 465.

91 Menter, J.W., Tsou, A.L. and Nutting, J., Proc. Phys. Soc., (1952), 65, series 13, p. 305.

92 Miller, R.L., Trans. A.S.M., (1964), 57, p. 892.

93 Miller, R.L., Met. Trans., (1972), 3, p. 905.

94 Morrison, W.B., J.I.S.I., (1963), 201, p. 317.

95 Nemoto, M., Met. Trans., (1977), 8A, p. 431.

96 Nishiyama, Z., Sci. Rep. Tohoku Univ., (1934), 23, p. 637.

97 Nutting, J., J.I.S.I., (1969), 207, p. 872.

98 Owen, W.S., Schoen, F.J. and Srinivasan, G.R., "Phase Transformations", (1970), A.S.M. Cleveland, p. 157.

99 Paetke, S., Beavan, P.A. and Edmonds, D.V., Unpublished research work, (1965).

100 Pascover, J.S. and Radcliffe, S.V., Trans. A.I.M.E., (1968), 242, p. 673.

101 Paxton, H.W., "Transformation and Hardenability in Steels", Climax Molybdenum, (1967), p. 3.

102 Petch, N.J., J.I.S.I., (1953), 174, p. 25.

103 Pickering, F.B. and Gladman, T., I.S.I. Spec. Report, (1963), No. 81, p. 10.

104 Pickering, F.B., "Transformation and Hardenability in Steels", Climax Molybdenum, (1967), p. 109.

105 Pitsch, W., Arch. Eisenhültenw, (1963), 34, p. 381.

106 Roberts, G.A. and Mehl, R.F., Trans. A.S.M., (1943), p. 613.

107 Ryder, P.L., Pitsch, W. and Mehl, R.F., Acta. Met., (1967), 15, p. 1431.

108 Seal, A. and Honeycombe, R.W.K., J.I.S.I., (1958), 188, p. 9.

109 Shackleton, D.N. and Kelly, P.M., I.S.I. Spec. Report, (1965), 93, p. 126.

110 Shimizu, K. and Nishiyama, Z., Mem. Inst. Sci. Ind. Res., Osaka Univ., (1963), 20, p. 43.

111 Smith, C.S., Trans. A.S.M., (1953), 45, p. 533.

112 Smith, H. and West, D.R.F., J. Mat. Sci., (1973), 8, p. 1413.

113 Southwick, P.D., Howell, P.R. and Honeycombe, R.W.K., Research work to be published.

114 Speich, G.R. and Leslie, W.C., Met. Trans., (1972), 3, p. 1043.

115 Speich, G.R. and Swann, P.R., J.I.S.I., (1965), 203, p. 480.

116 Speich, G.R., Szirmae, A., Trans. A.I.M.E., (1969), 245, p. 1063.

117 Spretnack, J.W. and Speiser, R., Trans. A.S.M., (1954), 46, p. 1089.

118 Srinivason, G.R. and Wayman, C.M., Acta. Met., (1968), 16, p. 621.

119 Tanino, M., Suzuki, M.G. and Aoki, K., Trans. Japan Inst. Metals, (1968), p. 393.

120 Thomas, G., Iron and Steel International, (1973), p. 451.

121 Tsou, A.L., Nutting, J. and Menter, J.W., J.I.S.I., (1952), 172, p. 163.

122 Unwin, P.N.T. and Nicholson, R.B., Acta. Met., (1969), 17, p. 1379.

123 Wallbridge, J.M. and Parr, J.G., J.I.S.I., (1967), p. 750.

124 Wassermann, G., Mit. Kaiser-Wilhelm Inst. Eisenforsch, (1935), 17, p. 149.

125 Watanabe, S. and Kunitaki, T., Trans. I.S.I.J., (1976), 16, p. 29.

126 Wilyman, P.R., Ph.D. Thesis, (1976), University of Cambridge.

127 Yajima, E., Miyazaki, T., Sugiyama, T. and Tenajima, H., Trans. J.I.M., (1974), 15, p. 173.

128 Yershov, V.M., Phys. Met. Metallog., (1973), 35, p. 119.